

Mechanical properties of solid polymers : constitutive modelling of long and short term behaviour

Citation for published version (APA):

Klompén, E. T. J. (2005). *Mechanical properties of solid polymers : constitutive modelling of long and short term behaviour*. [Phd Thesis 1 (Research TU/e / Graduation TU/e), Mechanical Engineering]. Technische Universiteit Eindhoven. <https://doi.org/10.6100/IR583394>

DOI:

[10.6100/IR583394](https://doi.org/10.6100/IR583394)

Document status and date:

Published: 01/01/2005

Document Version:

Publisher's PDF, also known as Version of Record (includes final page, issue and volume numbers)

Please check the document version of this publication:

- A submitted manuscript is the version of the article upon submission and before peer-review. There can be important differences between the submitted version and the official published version of record. People interested in the research are advised to contact the author for the final version of the publication, or visit the DOI to the publisher's website.
- The final author version and the galley proof are versions of the publication after peer review.
- The final published version features the final layout of the paper including the volume, issue and page numbers.

[Link to publication](#)

General rights

Copyright and moral rights for the publications made accessible in the public portal are retained by the authors and/or other copyright owners and it is a condition of accessing publications that users recognise and abide by the legal requirements associated with these rights.

- Users may download and print one copy of any publication from the public portal for the purpose of private study or research.
- You may not further distribute the material or use it for any profit-making activity or commercial gain
- You may freely distribute the URL identifying the publication in the public portal.

If the publication is distributed under the terms of Article 25fa of the Dutch Copyright Act, indicated by the "Taverne" license above, please follow below link for the End User Agreement:

www.tue.nl/taverne

Take down policy

If you believe that this document breaches copyright please contact us at:

openaccess@tue.nl

providing details and we will investigate your claim.

Mechanical properties of solid polymers

Constitutive modelling of long and short term behaviour

CIP-DATA LIBRARY TECHNISCHE UNIVERSITEIT EINDHOVEN

Klompen, Edwin T.J.

Mechanical properties of solid polymers : constitutive modelling of long and short term behaviour / by Edwin T.J. Klompen. - Eindhoven : Technische Universiteit Eindhoven, 2005.

Proefschrift. - ISBN 90-386-2806-4

NUR 971

Trefwoorden: glasachtige polymeren / constitutieve modellering / post-yield deformation / strain softening / strain hardening / moleculaire transitities / fysische veroudering / lange duur falen

Subject headings: polymer glasses / constitutive modelling / post-yield deformation / strain softening / strain hardening / molecular transitions / physical ageing / long-term failure

Reproduction: University Press Facilities, Eindhoven, The Netherlands.

Cover design: Jan-Willem Luiten (JWL-Producties).

Cover illustration: surface representing the intrinsic response of a glassy polymer at different strain rates; the red line is the response to a constant rate of deformation, while the blue line is the response to a constant stress.

Mechanical properties of solid polymers

Constitutive modelling of long and short term behaviour

PROEFSCHRIFT

ter verkrijging van de graad van doctor aan de
Technische Universiteit Eindhoven, op gezag van de
Rector Magnificus, prof.dr. R.A. van Santen, voor een
commissie aangewezen door het College voor
Promoties in het openbaar te verdedigen
op donderdag 3 februari 2005 om 16.00 uur

door

Edwin Theodorus Jacobus Klompen

geboren te Roggel

Dit proefschrift is goedgekeurd door de promotoren:

prof.dr.ir. H.E.H. Meijer

en

prof.dr.ir. F.P.T. Baaijens

Copromotor:

dr.ir. L.E. Govaert

Voor mijn ouders

Contents

Summary	xi
1 Introduction	1
1.1 Motivation	1
1.2 Intrinsic deformation behaviour	2
1.3 Molecular background	4
Temperature-activated mobility: time dependence	4
Stress activated mobility: nonlinear flow	7
Influence of history: physical ageing and mechanical rejuvenation	9
Consequences for modelling	10
1.4 Scope of the thesis	11
References	12
2 Deformation of thermorheological simple materials	15
2.1 Introduction	15
2.2 Experimental	16
Materials	16
Mechanical testing	17
2.3 Deformation behaviour	17
Linear viscoelastic deformation	17
Plastic deformation	19
Nonlinear viscoelastic deformation	22
2.4 Results	25
Applicability of time-stress superposition	25
Linear viscoelastic behaviour	27
Model verification	28
2.5 Conclusions	30
References	30
2.A Appendix: retardation time spectrum	32
2.B Appendix: relaxation time spectrum	33

3	Deformation of thermorheological complex materials	35
3.1	Introduction	35
3.2	Experimental	36
	Materials	36
	Mechanical testing	37
3.3	Deformation behaviour	37
	Linear viscoelastic deformation	37
	Plastic deformation	40
	Nonlinear viscoelastic deformation	43
3.4	Numerical investigation	45
	Model parameters	45
	Numerical creep simulations	47
	Consequences for characterization	52
3.5	Conclusions	53
	References	53
3.A	Appendix: numerical spectra	55
4	Post-yield response of glassy polymers: influence of thermorheological complexity	57
4.1	Introduction	57
4.2	Experimental	58
	Materials	58
	Mechanical testing	59
4.3	Thermorheological simple materials	59
	Constitutive modelling	59
	Application to polycarbonate	62
4.4	Thermorheological complex materials	64
	Constitutive modelling	64
	Application to polymethylmethacrylate	66
	Deformation induced heating	70
4.5	Conclusions	73
	References	75
5	Post-yield response of glassy polymers: influence of thermomechanical history	77
5.1	Introduction	77
5.2	Experimental	79
	Materials	79
	Thermo-mechanical treatments	80
	Mechanical testing	81
5.3	Numerical modelling	81

Constitutive model	81
Incorporation of ageing kinetics	84
5.4 Results	86
Characterization of intrinsic behaviour	86
Validation of intrinsic behaviour	91
Characterization of ageing kinetics	92
Validation of ageing kinetics	98
5.5 Conclusions	99
References	100
5.A Appendix: ageing kinetics	104
6 Quantitative prediction of long-term failure of polycarbonate	107
6.1 Introduction	107
6.2 Experimental	110
Materials	110
Thermo-mechanical treatments	111
Mechanical testing	111
6.3 Time-dependent ductile failure: relation to intrinsic behaviour	111
6.4 Constitutive modelling	114
6.5 Application to time-dependent ductile failure	116
Influence of loading geometry	116
Influence of thermal history	117
Influence of molecular weight: a tough-to-brittle transition	120
6.6 Conclusions	124
References	124
7 Conclusions and recommendations	129
7.1 Main conclusions	129
7.2 Recommendations	131
References	132
Samenvatting	135
Dankwoord	139
Curriculum Vitae	141

Summary

Rather than time-consuming experiments, numerical techniques provide a fast and cost-effective means to analyze and optimize the mechanical performance of polymer materials and products. One of the pre-requisites for a reliable analysis is an accurate constitutive model describing the materials' true stress-strain behaviour. The intrinsic deformation, however, depends on the molecular structure of the polymer, and is influenced by the thermal and mechanical history, e.g. due to processing. This implies that a constitutive model that is applicable for a polymer material with a specific processing history, can not be readily used for another polymer material, or one with a different processing history. In this work, an attempt is made to solve this problem by establishing a relationship between, on the one hand, the intrinsic deformation, and on the other, the molecular structure and processing history.

The ability of a polymer material to deform is determined by the mobility of its molecules, characterized by specific molecular motions and relaxation mechanisms, that are accelerated by temperature and stress. Since these relaxation mechanisms are material specific and depend on the molecular structure, they are used here to establish the desired link with the intrinsic deformation behaviour.

In Chapter 2, a material, polycarbonate, with only a single (active) molecular mechanism is selected as a model material. Using this thermorheological simple material, a constitutive model based on time-stress superposition is derived. This principle states that all relaxation times are equally influenced by the total stress applied, comparable to the time-temperature superposition principle where all relaxation times are the same function of temperature. The influence of stress is quantitatively described by the Eyring theory of nonlinear flow. For polycarbonate, the applicability of time-stress superposition is demonstrated, showing an excellent agreement between the stress nonlinearity obtained from time-stress superposition and that obtained from yield experiments. Furthermore, it is demonstrated that

the complete deformation up to yield is determined by the linear relaxation time spectrum combined with a single nonlinearity parameter, which is governed by the activation volume V^* .

Since the majority of polymers exhibits at least two molecular processes, the approach is extended to account for an additional process in Chapter 3. Based on linear viscoelastic theory, this extension could be achieved, either by adding a process in parallel, or in series. Experiments in the range of plastic deformation suggested, however, an approach based on stress additivity, that is, a parallel arrangement of two molecular processes. The resulting model consists of two linear relaxation time spectra in parallel, each with its own characteristic stress and temperature dependence. While in the case of a single process the influence of stress and temperature was comparable, this does not hold for two processes since the molecular processes only depend on a part of the total stress rather than on the total stress itself. A numerical study employing the extended representation shows that the model correctly describes the yield observed in practice, while calculated creep experiments at various stress levels and temperatures show a good qualitative agreement with experimental observations reported in literature.

In the post-yield range, the approaches based on stress activated spectra of relaxation times predict a constant flow stress, whereas in reality the stress changes due to intrinsic strain softening and hardening. Both these post-yield phenomena play a crucial role in strain localization, and thus in the resulting macroscopic failure behaviour, and are, therefore, addressed in Chapter 4. For a thermorheological simple material, polycarbonate, the post-yield behaviour is not influenced by strain rate, which is characterized by a constant yield-drop. On the other hand the yield drop for polymethylmethacrylate, a thermorheological complex material, displays a clear strain-rate dependence. This strain-rate dependence coincides with the occurrence of the contribution of the secondary relaxation mechanism to the yield stress. From a study employing an extended large strain model which accounts for two relaxation processes, two mechanisms for the strain-rate dependence observed in the post-yield range could be identified: intrinsic strain-rate dependence due to additional softening in the secondary contribution, and thermal softening due to an increase in the deformation induced heating. Although the strain-rate induced increase in yield drop appears to fit the classical concept that a low temperature secondary transition is required for ductile deformation at impact rates, there are more variables that influence the post-yield deformation, such as the strain hardening modulus and processing history.

The processing history (thermal and mechanical) determines the current state of the material, which will generally be a non-equilibrium state. As a consequence the material attempts to attain equilibrium in the course of time at the expense of a decreasing molecular mobility; physical ageing. The reduced mobility leads to changes in the material's intrinsic deformation, which can be reversed by applying large deformations, or re-quenching the material: mechanical or thermal rejuvenation. To capture the influence of physical ageing on the intrinsic deformation, in Chapter 5 a large strain constitutive model is modified and enhanced by including a state parameter that evolves with time. The model parameters are determined for polycarbonate, resulting in a validated constitutive relation that is able to describe the deformation over a large range of molecular weights and thermal histories, with one parameter set only. In this approach the entire prior history, which is generally unknown, is captured in a single parameter, S_a , which can be easily determined from a single tensile or compression test.

An area where ageing can be expected to play an important role is long-term loading of polymers. For long-term static loading the time-to-failure and the actual failure mode are influenced by stress, temperature and processing history, while molecular weight only affects the failure mode. It is shown in Chapter 6 that long-term ductile failure under a constant load is governed by the same process as short-term ductile failure at a constant rate of deformation. Failure proves to originate from the polymer's intrinsic deformation behaviour, more particularly the true strain softening after yield, which inherently leads to the initiation of localized deformation zones. It is demonstrated that the large strain constitutive relation including physical ageing derived in Chapter 5 is capable of numerically predicting plastic instabilities under a constant load. Application of this model the ductile failure of polycarbonates with different thermal histories, subjected to constant loads, is accurately predicted, also for different loading geometries. Even the endurance limit, observed for quenched materials, is predicted, and it is shown that this originates from the structural evolution due to physical ageing that occurs during loading. For low molecular weight materials this same process causes a ductile-to-brittle transition. A quantitative prediction thereof is outside the scope of this thesis and requires a more detailed study, including the description of the local stress state.

The thesis ends in Chapter 7 with some conclusions and recommendations for further research.

CHAPTER ONE

Introduction

1.1 Motivation

Due to the favorable combination of easy processability and attractive mechanical properties, the use of polymer materials in structural applications has assumed large proportions over the last decades. To ensure proper operation under heavy duty conditions, these applications have to meet specific requirements regarding quality, safety, and mechanical performance (e.g. stiffness, strength and impact resistance). Mechanical performance is generally optimized by trial-and-error until the functional demands of the design are satisfied. This, however, implies by no means that the final result is fully optimized.

The main problem in designing optimized structural products is that their mechanical performance is determined by three factors:

- *molecular structure*, which for polymers is characterized by their chemical configuration, stereoregularity, and chain length (distribution);
- *processing*, constituting the entire chain of processes that transforms the raw material to the final product, thereby modifying microstructural characteristics such as e.g. molecular orientation and crystallinity;
- *geometry*, the product's final functional macroscopic shape obtained as a result of processing.

An optimal performance of a product would require an optimization of these three factors. Considering the large amount of parameters involved (at all levels, molecular, microstructural, macroscopic), it is virtually impossible to realize this in a purely experimental setting. A promising way to simplify the problem is

the employment of numerical tools. A direct numerical approach from ab-initio calculations is still out of reach, given the impossibility to successfully bridge the large length and time scales involved. Therefore, in most cases, alternative routes based on continuum mechanics are followed, where phenomenological approaches are applied to analyze macroscopic deformation. Using a finite element method (FEM) combined with a suitable constitutive equation that properly captures the deformation behaviour, it is possible to optimize the application's final geometry for working conditions.

A full optimization, however, fails due to lack of information concerning the underlying molecular structure and the influence of processing. This relation can, though, be implemented by systematically investigating the influence of molecular properties and processing on the deformation behaviour [1–4], and incorporating these aspects in the constitutive model. Ultimately, this would provide a constitutive model with a proper physical basis that correctly describes the phenomena experimentally observed.

1.2 Intrinsic deformation behaviour

Intrinsic deformation is defined as the materials' true stress-strain response during homogeneous deformation. Since generally strain localization phenomena occur (like necking, shear banding, crazing and cracking), the measurement of the intrinsic materials' response requires a special experimental set-up, such as a video-controlled tensile [5] or an uniaxial compression test [6,7]. Although details of the intrinsic response differ per material, a general representation of the intrinsic deformation of polymers can be recognized, see Figure 1.1.

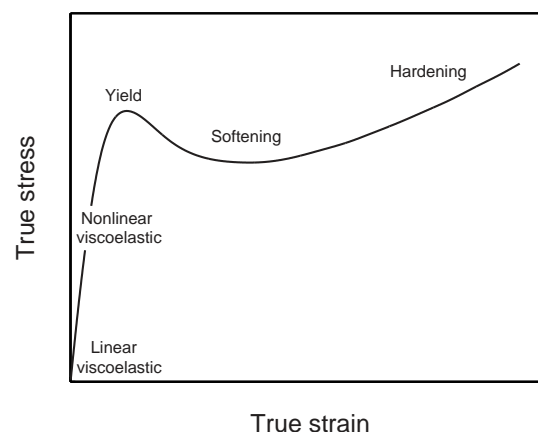


Figure 1.1: Schematic representation of the intrinsic deformation behaviour of a polymer material.

Initially we find a viscoelastic, time-dependent, response that is considered to be fully reversible. For small loads the material behaviour is linear viscoelastic, while with increasing load the behaviour becomes progressively nonlinear. At the yield point the deformation becomes irrecoverable¹ since stress-induced plastic flow sets in leading to a structural evolution which reduces the material's resistance to plastic flow: *strain softening*. Finally, with increasing deformation, molecules become oriented which gives rise to a subsequent increase of stress at large deformations: *strain hardening*.

Linear viscoelasticity is commonly described using linear response theory, which results in a Boltzmann single integral representation. The characteristic viscoelastic functions are supplied either as continuous or discrete spectra of relaxation times [10, 11]. For short times the approach reduces to time-independent Hookean elasticity (linear elasticity).

For the nonlinear viscoelastic range an abundance of different constitutive relations is available. Most of them are generalizations of the linear Boltzmann integral, employing higher order stress or strain terms (multiple integral representation [12]), nonlinear stress/strain measures (factorizability [13]), reduced-time approaches (stress [14], strain [15]) or combinations of the aforementioned approaches [16]. An extensive survey of these nonlinear viscoelastic theories can be found in the monograph by Ward [17].

Due to its strong strain-rate and temperature dependence, the yield stress of polymers can not be described using classical yield criteria such as a critical flow stress. Instead, (molecular) flow theories regarding polymers as high-viscosity stress-activated fluids are used, of which the Eyring theory [18], and Argon's double kink theory [19] are probably the most commonly known. Although they accurately capture the influence of both strain rate and temperature, their applicability is limited since they do not account for strain softening and strain hardening. Most present approaches to capture the large strain (post-yield) response originate from the work of Haward and Thackray [20], who proposed the addition of a finite extendable rubber spring placed in parallel to an Eyring dashpot in order to model strain hardening. Their approach was later extended to finite strain 3D constitutive equations by several authors [21–23]. In all cases strain hardening was modelled using a rubber elastic spring, whereas softening was introduced by basically adding a (plastic) strain dependence to the flow behaviour.

¹Although this component is generally considered irreversible, heating above T_g leads to a full recovery of plastic deformation [8, 9]

1.3 Molecular background

Independent of the stress level or amount of deformation involved, the origin of the deformation of polymer materials lies in their ability to adjust their chain conformation on a molecular level by rotation around single covalent bonds in the main chain. This freedom of rotation is, however, controlled by intramolecular (chain stiffness) and intermolecular (inter-chain) interactions. Together these interactions give rise to an energy barrier that restricts conformational change(s) of the main chain. The rate of conformational changes, i.e. the molecular mobility, is determined totally by the thermal energy available in the system. Increasing the thermal energy increases the rate of change which, on a fixed time scale, allows for larger molecular rearrangements and, thus, accommodation of larger deformations. Since thermal energy is determined by temperature, there will be a relatively strong relation between temperature and mobility, and thus also with macroscopic deformation (in fact polymers are known for their pronounced temperature dependence). In addition to this, there is also a strong influence of stress on molecular mobility since polymers allow for "mechanical" mobility when secondary bonds are broken by applying stress (rather than by increasing the thermal mobility). In the following sections the relation between temperature, stress, molecular mobility, and aspects of the deformation behaviour, will be discussed in somewhat more detail.

Temperature-activated mobility: time dependence

Molecular mobility is determined by the molecules' thermal energy, which is constant for a given temperature. Under a small constant load or deformation (linear range) this mobility gives rise to a pronounced time dependence, as illustrated schematically in Figure 1.2(a) and (b), respectively.

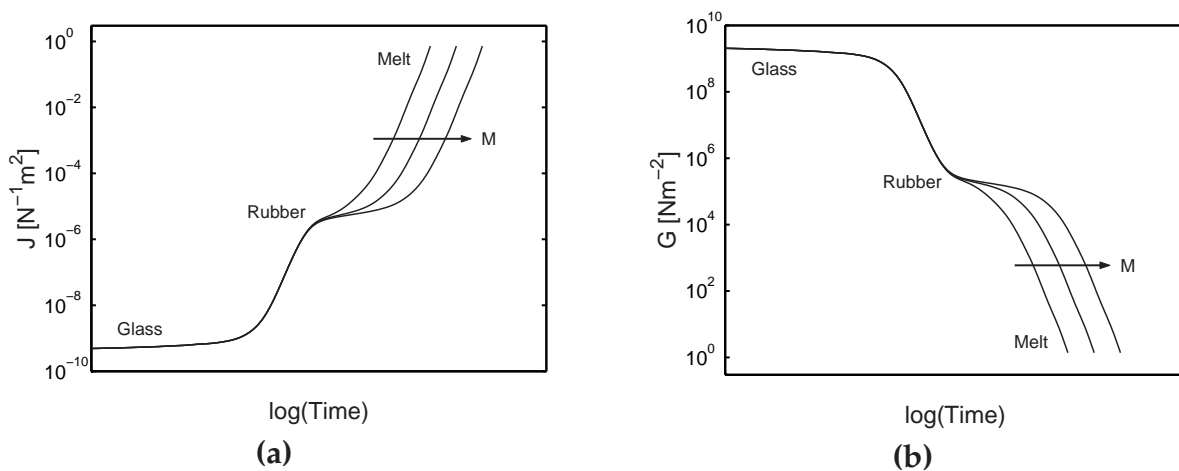


Figure 1.2: Schematic representation of the linear shear creep compliance (a) and shear modulus (b) versus time for an amorphous polymer at a constant temperature.

The behaviour is governed by two characteristic relaxation mechanisms: the glass transition and the reptation process. On short time scales the response is solid-like since only limited molecular rearrangements are possible. With increasing (logarithmic) time scale, the size of the conformational changes increases, ultimately resulting in unbounded segmental diffusion at the glass-rubber transition. Large scale motion of polymer chains is, however, inhibited by physical entanglements that can be envisaged as temporary cross-links. At this stage the polymer effectively behaves like a rubber, whereas at even longer times, reptation enables main-chain diffusion (entanglements are dissolved), and the polymer behaves as a fluid (melt).

The glass transition of a polymer is determined by its molecular structure, including the chemical configuration and stereoregularity. Covering multiple decades in time, and compliance and modulus, the associated relaxation mechanism has a marked influence on the (linear) deformation behaviour. Consequently, the relaxation mechanism provides a link between the spectrum of relaxation times used to describe the macroscopic deformation, and the underlying molecular structure. The influence of other molecular parameters such as molecular weight (chain length) is mainly restricted to the rubber region, where it determines the width of the rubber plateau. The height of the plateau compliance and modulus is related to the molecular weight between entanglements.

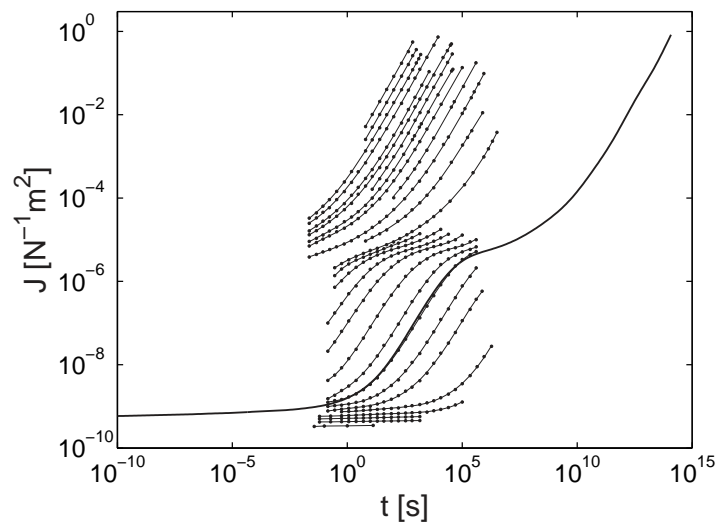


Figure 1.3: Linear shear creep compliance versus time for polystyrene ($M_w = 3.85 \cdot 10^5$), measured at different temperatures, and the master curve constructed using time-temperature superposition. Data reproduced from Schwarzl and Staverman [24].

Raising the temperature increases the thermal energy and hence the molecular mobility. An increased mobility implies that more, or larger, conformational changes can take place in the same time interval. This is illustrated by Figure 1.3 showing the linear shear creep compliance of polystyrene over a wide range of temperatures. On

the same experimental time scale, elevated temperatures allow for larger deformations (higher compliance).

Whereas a change in temperature does not seem to affect the shape of the curve, it clearly changes the position on the (logarithmic) time axis. This indicates that all relaxation times associated with the relaxation mechanism are equally influenced by temperature, i.e. the material behaves *thermorheological simple* [25], Figure 1.4(a). The resulting *time-temperature equivalence* was already observed by Leaderman [13], and led him to formulate a so-called reduced time, ϕ :

$$\phi(t) = \int_0^t \frac{dt'}{a_T[T(t')]} \quad (1.1)$$

where a_T is the ratio of the relaxation times at temperatures T and T_0 . From this it follows that a higher temperature accelerates the material's time scale and hence the relaxation.

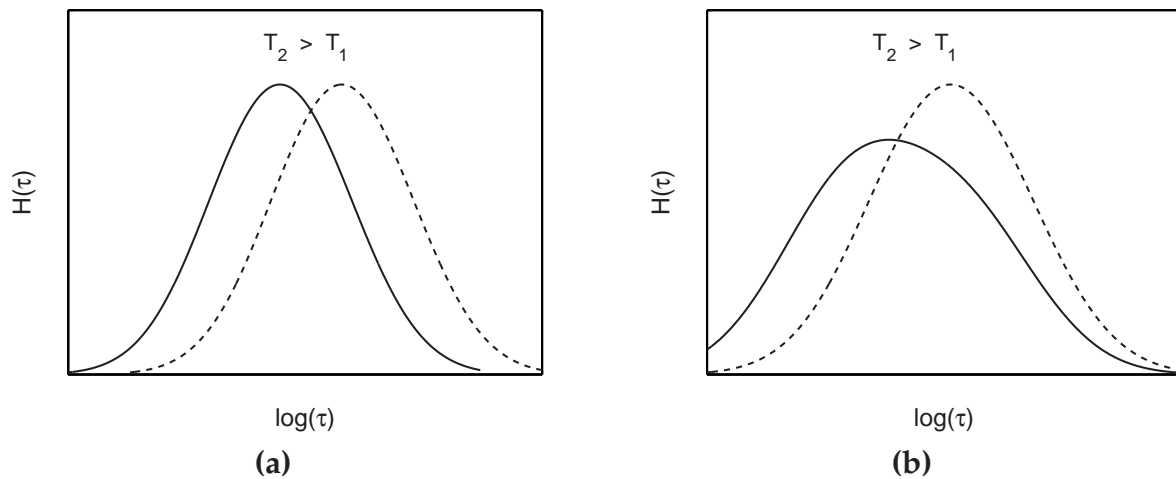


Figure 1.4: Schematic representation of the total relaxation time spectrum at a temperature T_1 and $T_2 > T_1$ for a material behaving (a) *thermorheological simple*, and (b) *thermorheological complex*.

Although it can be stated that main-chain segmental motion is the most important deformation mechanism, it should be noted that it is not the only source of mobility. Whereas the glass, or primary, transition involves large scale segmental motions of the main chain, there exist so-called secondary transitions originating from side-group motions (e.g. in PMMA), or mobility of a small part of the main chain (e.g. in PC) [26]. Similar to the primary glass transition these secondary relaxation mechanisms give rise to a spectrum of relaxation times, which are activated by temperature as well. Because of differences in the temperature dependencies, this leads to a change in the shape of the total spectrum, see Figure 1.4(b), which in its turn affects the deformation behaviour of the material. This type of behaviour is termed

thermorheological complex, and the magnitude of the effect is mainly determined by the relative position of the transitions on the time scale. Due to the shape change, experimental data of a viscoelastic function at different temperatures are generally no longer superimposable, like in Figure 1.4(a), by pure horizontal shifting and, therefore, a direct application of the principle of time-temperature superposition is no longer possible.

It was already observed by Schapery [16] and Nakayasu *et al.* [27], that semi-crystalline materials also show signs of thermorheological complex behaviour. In these materials the crystalline phase gives rise to a relaxation mechanism at temperatures above the glass transition temperature (in contrast to the sub- T_g secondary transitions). The strength and magnitude of these transitions depends on the degree of crystallinity and the size of the lamellae, and therefore is influenced by the thermal history (i.e. processing). Due to the composite nature of semi-crystalline materials, changes in the crystalline phase lead to changes in the amorphous mechanism as well. Any secondary relaxations are generally not affected by the presence of a crystalline phase. A detailed survey regarding relaxation processes in crystalline polymers is provided by Boyd [28,29].

Stress activated mobility: nonlinear flow

It was shown that the characteristic, time-dependent, material behaviour, generally observed for polymer materials, is caused by molecular transitions, and that these are activated by temperature. Application of stress has a similar effect as temperature, increasing mobility with increasing load. In contrast to temperature, however, stress preferentially promotes mobility in the direction of the load applied. This is the basis of the Eyring flow theory, which is schematically illustrated in Figure 1.5(a). An initially symmetric potential energy barrier with magnitude ΔU is biased by a load σ . The magnitude of this bias is determined by the parameter V^* , the (segmental) activation volume. This volume is characteristic for a particular flow process associated with a relaxation mechanism. It has been shown that this theory adequately describes both strain rate and temperature dependence of polymers [30].

As an example, the tensile yield stress of polycarbonate at different temperatures as function of strain rate, shown in Figure 1.5(b), is known to be governed by a single relaxation mechanism in the range of temperatures and strain rates of interest. A linear dependence of yield stress as a function of log strain rate can be observed over a large interval of strain rates and temperatures, which are described well using the Eyring theory (solid lines). Other flow theories, such as those of Argon [19], or Robertson [31], can be expected to describe the data equally well since, on a fitting level, they do not differ from the Eyring theory.

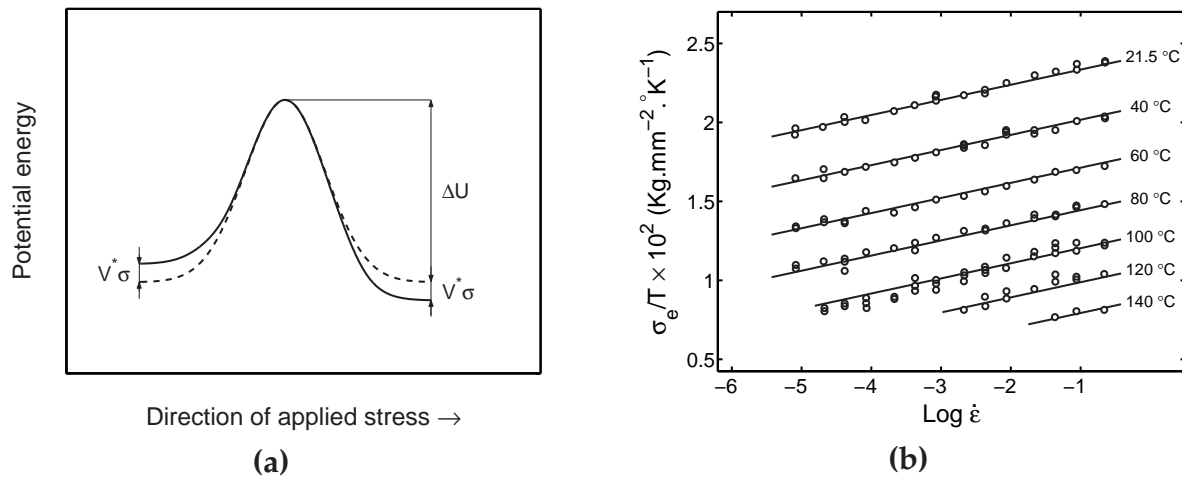


Figure 1.5: (a) Schematic representation of the Eyring flow theory. (b) Tensile yield stress versus strain rate at different temperatures for polycarbonate, symbols indicate experimental data and solid lines are fits using the Eyring-theory. Adapted from Bauwens-Crowet et al. [30].

It is known that, in the linear viscoelastic range, the time dependent behaviour can include contributions of secondary relaxation processes. It was shown by several authors that this also holds for the tensile yield stress of these materials [30,32].

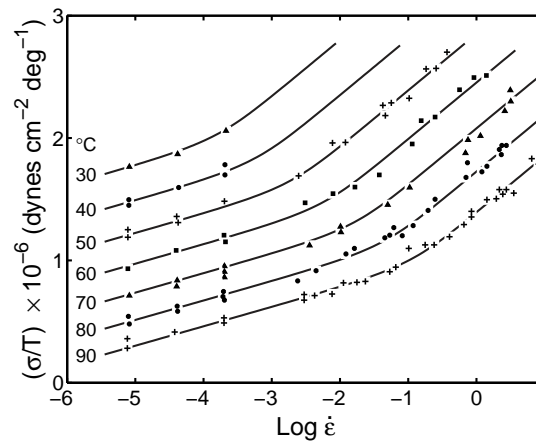


Figure 1.6: Tensile yield stress versus strain rate at different temperatures for polymethylmethacrylate, symbols are experimental data and solid lines are fits using the Ree-Eyring theory. Adapted from Roetling [32].

As an example, Figure 1.6 shows the yield stress of PMMA as function of strain rate for a large range of temperatures. With increasing strain rate $\dot{\epsilon}$ the yield stress shows a change in slope for all temperatures, the transition shifting to higher rates with increasing temperature. The additional contribution at the higher strain rates (i.e. shorter times, or a reduced time scale) is generally attributed to the secondary relaxation process.

To describe this yield behaviour, a Ree-Eyring modification of the Eyring flow theory is used. The modification consists of placing two Eyring flow processes in parallel. This approach was also shown to be applicable for semi-crystalline materials, such as e.g. isotactic polypropylene [33,34], while for some other materials an extra, third, process was necessary [35,36].

Influence of history: physical ageing and mechanical rejuvenation

Temperature and stress both increase the molecular mobility and, consequently, accelerate the time scale at which the material deforms. From this it might be concluded that when both are kept constant, the mobility and its resulting rate of deformation do not change. It was, however, shown by Struik that for many polymers this is not correct [37]. With increasing time elapsed after a (thermal) quench from above T_g , he observed a decrease in molecular mobility: the response to linear creep experiments at constant temperature shifts to longer loading times, see Figure 1.7(a).

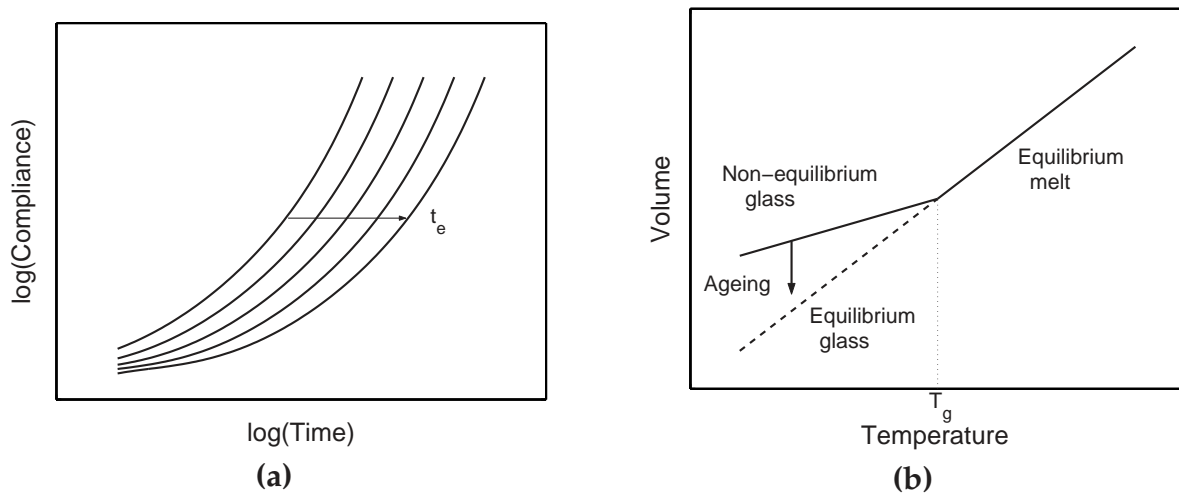


Figure 1.7: (a) Schematic representation of the influence of ageing time t_e on the linear creep compliance. (b) Schematic illustration of physical ageing: volume as a function of temperature.

This effect is generally referred to as *physical ageing* and can be explained in terms of the presence of a non-equilibrium thermodynamic state. When cooling a polymer melt that is in equilibrium, the mobility of the molecules decreases with decreasing temperature, thus increasing the time required to attain equilibrium. At a certain temperature, which depends on the cooling rate, the time required exceeds the experimental time available and the melt becomes a polymer glass. The temperature at which this occurs depends on the cooling rate and is termed the glass-transition temperature T_g . The material is now in a non-equilibrium state,

and thermodynamic variables such as volume and enthalpy deviate from their equilibrium value (Figure 1.7(b)). Although the mobility has decreased it does not become zero, which gives the material the opportunity to establish equilibrium after all. This gradual approach of equilibrium is termed physical aging, as to distinguish it from chemical aging (e.g. due to thermal degradation or photo-oxidation).

The influence of ageing is not restricted to the linear viscoelastic range but is also observed in the nonlinear viscoelastic and plastic range, increasing e.g. the yield stress. The effect of the increase in yield stress appears to be limited to a region of relatively small deformations, since the large strain behaviour remains unaffected [38], see Figure 1.8(a).

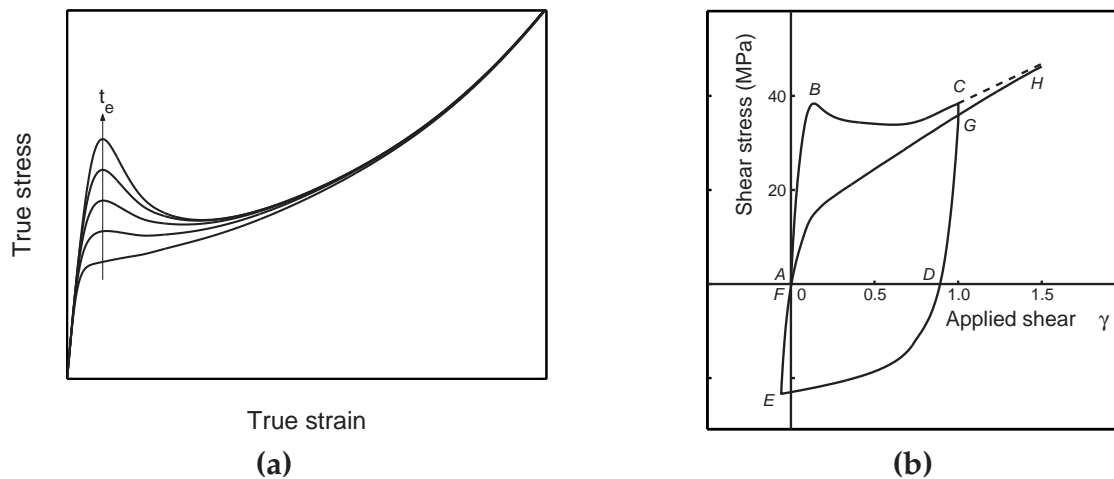


Figure 1.8: (a) Schematic representation of the influence of ageing time t_e on the yield stress and post-yield behaviour. (b) The effect of mechanical rejuvenation due to plastic cycling of polycarbonate in simple shear. Adapted from G'Sell [39].

It was suggested that the prior thermal history is erased by plastic deformation, *mechanical rejuvenation*, leading to a fully rejuvenated state independent of prior history (Figure 1.8(b)). Upon reloading a mechanically rejuvenated sample, the yield drop, initially present, has disappeared, and the material deforms macroscopically homogeneous (and “brittle” becomes “tough”). The effect of mechanical rejuvenation is, however, only of a temporary nature, as the material is still susceptible to ageing. Consequently, in due course ageing restores the higher yield stress and the associated intrinsic strain softening at a rate that depends on the polymer under consideration [1,40].

Consequences for modelling

The molecular structure is linked to deformation behaviour through (several) relaxation mechanisms, each representing specific molecular motions, giving rise

to a spectrum of relaxation times. Each relaxation mechanism is accelerated by the (momentary) temperature and stress, through specific shift functions which are characteristic for a specific relaxation mechanism. A model should, therefore, properly account for the contributions of the various relaxation mechanisms in the material, including time dependence, and temperature and stress dependence.

Not only the momentary values of temperature and stress are relevant, but the entire prior history is (i.e. stress and temperature during processing and service life). Two opposing mechanisms can occur simultaneously:

- physical ageing, that reduces the mobility through a continuous structural evolution after a quench and which is particularly relevant in long term loading situations,
- mechanical rejuvenation, that erases the prior history and appears to be inherently present at larger deformations in the form of intrinsic strain softening.

Depending on the working conditions and initial state of the material, both aspects should be accounted for.

Finally, at very large deformations, or very long times (depending on temperature), the presence of a rubber-like stress contribution is observed: strain hardening. For a proper description of large strain plasticity this last aspect should also be included in any model.

1.4 Scope of the thesis

In Chapter 2, a model is derived for thermorheological simple materials; model parameters are experimentally obtained, and the model is numerically verified.

The assumption of thermorheological simple behaviour is dropped in Chapter 3, and the previously derived model is extended to account for the contribution of an additional molecular process. Consequences of the resulting modification are numerically investigated.

Since both, Chapters 2 and 3, are limited to fairly small deformations, in Chapter 4 the consequences of the thermorheological behaviour for the post-yield deformation is investigated.

Thus far, the influence of an evolving structural state (physical ageing) was ignored. In Chapter 5, this issue is addressed for the large strain plasticity approach used in Chapter 4. A new approach is proposed, based on a modified viscosity definition, and also experimentally and numerically validated.

In Chapter 6, the enhanced model from Chapter 5 is used to predict ductile failure for polycarbonate with different initial states, under long-term static loading conditions.

Finally, in Chapter 7, overall conclusions are drawn and recommendations for further research are given.

References

- [1] van Melick, H.G.H., Govaert, L.E., Meijer, H.E.H. (2003). On the origin of strain hardening in glassy polymers. *Polymer*, **44**, 2493–2502.
- [2] Schrauwen, B.A.G., Janssen, R.P.M., Govaert, L.E., Meijer, H.E.H. (2004). Intrinsic deformation behaviour of semi-crystalline polymers. *Macromolecules*, **37**, 6069–6078.
- [3] van Melick, H.G.H., Govaert, L.E., Meijer, H.E.H. (2003). Localisation phenomena in glassy polymers: influence of thermal and mechanical history. *Polymer*, **44**, 3579–3591.
- [4] Schrauwen, B.A.G., van Breemen, L.C.A., Spoelstra, A.B., Govaert, L.E., Peters, G.W.M., Meijer, H.E.H. (2004). Structure, deformation and failure of flow-oriented semi-crystalline polymers. *Macromolecules*, **37**, 8618–8633.
- [5] G'Sell, C., Hiver, J.M., Dahoun, A., Souahi, A. (1992). Video-controlled tensile testing of polymers and metals beyond the necking point. *J. Mat. Sci.*, **27**, 5031–5039.
- [6] Arruda, E.M., Boyce, M.C. (1993). Large strain compression, tension, and simple shear of polycarbonate. *Int. J. Plast.*, **9**, 697–720.
- [7] Boyce, M.C., Arruda, E.M., Jayachandran, R. (1994). Large strain compression, tension, and simple shear of polycarbonate. *Pol. Eng. Sci.*, **34**, 716–725.
- [8] Gurevich, G., Kobeko, P. (1940). A study of polymers. III Technique of mechanical tests of vulcanizates of rubber and plastics. *Rubber Chem. Tech.*, **13**, 904–917.
- [9] Haward, R.N. (1942). Extension and rupture of cellulose acetate and celluloid. *Trans. Far. Soc.*, **38**, 394–403.
- [10] Ferry, J.D. (1980). *Viscoelastic Properties of Polymers*. John Wiley & Sons Inc., New York.
- [11] Tschoegl, N.W. (1989). *The Phenomenological Theory of Linear Viscoelastic Behaviour: An Introduction*. Springer Verlag, Berlin.
- [12] Findley, W.N., Lai, J.S., Onaran, K. (1976). *Creep and Relaxation of Nonlinear Viscoelastic Materials: With an Introduction to Linear Viscoelasticity*, Volume 18 of *Applied Mathematics and Mechanics*. North-Holland, Amsterdam.
- [13] Leaderman, H. (1943). *Elastic and Creep Properties of Filamentous Materials and Other High Polymers*. The Textile Foundation, Washington D.C.
- [14] Bernstein, B., Shokooh, A. (1980). The stress clock function in viscoelasticity. *J. Rheol.*, **24**, 189–211.

- [15] Valanis, K.C. (1971). A theory of viscoplasticity without a yield surface. *Arch. Mech.*, **23**, 517–533.
- [16] Schapery, R.A. (1969). On the characterization of nonlinear viscoelastic materials. *Pol. Eng. Sci.*, **9**, 295–310.
- [17] Ward, I.M. (1983). *Mechanical Properties of Solid Polymers*. John Wiley & Sons, Chichester.
- [18] Eyring, H. (1936). Viscosity, plasticity, and diffusion as examples of absolute reaction rates. *J. Chem. Phys.*, **4**, 283–295.
- [19] Argon, A.S. (1973). A theory for the low-temperature plastic deformation of glassy polymers, *Phil. Mag.*, **28**, 839–865.
- [20] Haward, R. and Thackray, G. (1968). The use of a mathematical model to describe isothermal stress-strain curves in glassy thermoplastics, *Proc. Roy. Soc. A*, **302**, 453–472.
- [21] Boyce, M.C., Parks, D.M., Argon, A.S. (1988). Large inelastic deformation of glassy polymers. Part I: Rate dependent constitutive model, *Mech. Mat.*, **7**, 15–33.
- [22] Buckley, C.P. and Jones, D.C. (1995). Glass-rubber constitutive model for amorphous polymers near the glass transition. *Polymer*, **36**, 3301–3312.
- [23] Govaert, L.E., Timmermans, P.H.M., Brekelmans, W.A.M. (2000). The influence of intrinsic strain softening on strain localization in polycarbonate: modeling and experimental validation, *J. Eng. Mat. Techn.*, **122**, 177–185.
- [24] Schwarzl, F.R. (1990). *Polymermechanik; Struktur und mechanisches Verhalten von Polymeren*. Springer, Berlin.
- [25] Schwarzl, F.R., Staverman, A.J. (1952). Time-temperature dependence of linear viscoelastic behavior. *J. Appl. Phys.*, **23**, 838–843.
- [26] Hutchinson, J.M. (1997). Relaxation processes and physical aging, In: R.N. Haward and R.J. Young, Eds., *The Physics of Glassy Polymers*, Chapman & Hall.
- [27] Nakayasu, H., Markovitz, H. and Plazek, D.J. (1961). The frequency and temperature dependence of the dynamic mechanical properties of a high density polyethylene. *Trans. Soc. Rheol.*, **5**, 261–283.
- [28] Boyd, R.H. (1985). Relaxation processes in crystalline polymers: experimental behaviour – a review. *Polymer*, **26**, 323–347.
- [29] Boyd, R.H. (1985). Relaxation processes in crystalline polymers: molecular interpretation – a review. *Polymer*, **26**, 1123–1133.
- [30] Bauwens-Crowet, C., Bauwens, J.-C., Homès, G. (1969). Tensile yield-stress behavior of glassy polymers. *J. Pol. Sci.: Part A-2*, **7**, 735–742.
- [31] Robertson, R.E. (1963). On the cold-drawing of plastics. *J. Appl. Pol. Sci.*, **7**, 443–450.
- [32] Roetling, J.A. (1965). Yield stress behaviour of polymethylmethacrylate. *Polymer*, **6**, 311–317.
- [33] Roetling, J.A. (1966). Yield-stress behavior of isotactic polypropylene. *Polymer*, **7**, 303–306.
- [34] Liu, Y., Truss, R.W. (1994). A study of tensile yielding of isotactic polypropylene. *J. Pol. Sci.: Part B: Pol. Phys.*, **32**, 2037–2047.

- [35] Truss, R.W., Clarke, P.L., Duckett, R.A., Ward, I.M. (1984). The dependence of yield behavior on temperature, pressure, and strain rate for linear polyethylenes of different molecular weight and morphology. *J. Pol. Sci.: Pol. Phys. Ed.* **22**, 191–209.
- [36] Govaert, L.E., de Vries, P.J., Fennis, P.J., Nijenhuis, W.F., Keustermans, J.P. (2000). Influence of strain rate, temperature and humidity on the tensile yield behaviour of aliphatic polyketone. *Polymer*, **41**, 1959–1962.
- [37] Struik, L.C.E. (1978). *Physical Aging in Amorphous Polymers and Other Materials*. Elsevier, Amsterdam, first edition.
- [38] Hasan, O.A., Boyce, M.C., Li, X.S., Berko, S. (1993). An investigation of the yield and postyield behavior and corresponding structure of poly(methyl methacrylate). *J. Pol. Sci.: Part B: Pol. Phys.*, **31**, 185–197.
- [39] G'Sell, C. (1986). Plastic deformation of glassy polymers: constitutive equations and macromolecular mechanisms, In: H.J. McQueen *et al.*, Eds. *Strength of metals and alloys*, Pergamon Press, Oxford, 1943–1982.
- [40] van Melick, H.G.H., Govaert, L.E., Raas, B., Nauta, W.J., Meijer, H.E.H. (2003). Kinetics of ageing and re-embrittlement of mechanically rejuvenated polystyrene. *Polymer*, **44**, 1171–1179.

Deformation of thermorheological simple materials¹

2.1 Introduction

In the introductory chapter, an outline of the deformation of glassy polymers was given in relation to the underlying molecular motions and structure. It was shown that the deformation up to and including the yield point is governed by at least one, but usually more, relaxation mechanisms. Each of these mechanisms finds its origin at the molecular level, and is activated by temperature and stress. Depending on the applied load level, a relaxation mechanism either manifests itself as a spectrum of relaxation times in the nonlinear viscoelastic regime before yield, or as a single stress-dependent relaxation time in the nonlinear regime of plastic flow at yield. For a correct description of the deformation up to yield a constitutive relation should include all of the features previously mentioned.

To achieve this, we will, in a first approximation, focus on materials that behave thermorheologically simple, which means that their deformation is governed by a single relaxation mechanism, generally the primary α , or glass, transition. To allow an experimental verification, polycarbonate (PC) is selected as a model material. Although polycarbonate displays a secondary relaxation mechanism, denoted by β in Figure 2.1, well below room temperature, this mechanism plays no role of importance at temperatures equal to, or above, room temperature provided that the rates of deformation are moderate. Under those conditions the deformation of polycarbonate is completely determined by the primary transition, denoted by α .

¹Reproduced in part from: Tervoort, T.A., Klompen, E.T.J., Govaert, L.E. (1996). A multi-mode approach to finite, nonlinear viscoelastic behavior of polymer glasses. *J. Rheol.*, **40**, 779–797.

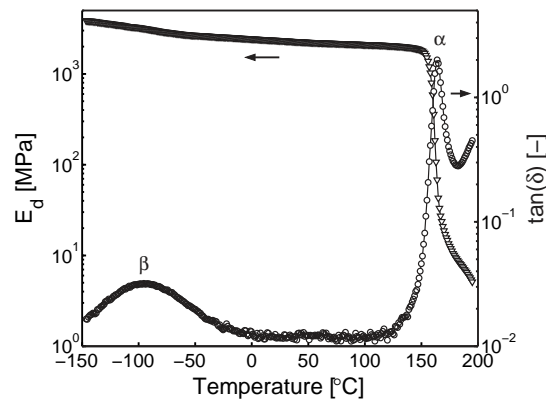


Figure 2.1: Dynamic modulus E_d and loss angle $\tan(\delta)$ versus temperature for Lexan 161R polycarbonate at a frequency of 1 Hz.

First, the deformation of polycarbonate in both the linear viscoelastic and nonlinear plastic range will be discussed and modelled using mechanical model analogies. Through comparison of similarities between the results for these two regions, a single model is proposed covering both regions including the intermediate nonlinear viscoelastic range. This model, which is based on time-stress superposition, correctly describes the deformation in monotone loading paths up to yield. Introduction of a stress-reduced time leads to a single integral stress-strain relation, with separated stress and time dependencies. Following an experimental verification of the time-stress superposition and determination of the material parameters, the stress-strain relation is numerically validated.

Although both physical aging and mechanical rejuvenation have a profound influence on both the viscoelastic and plastic deformation they are not considered here, but will be addressed in a later stage, see Chapters 4 and 5.

2.2 Experimental

Materials

Unless stated otherwise, all experiments were performed on injection moulded tensile bars, produced according to ISO R527, from General Electric polycarbonate Lexan 161R. Polycarbonate is selected as a model polymer since, at room temperature, it exhibits a single active relaxation mechanism: the glass transition, because the β -transition, situated around $-100\text{ }^\circ\text{C}$, is only relevant for very fast processes.

Mechanical testing

Dynamic experiments, using samples cut from 2 mm thick compression moulded sheets, were performed on a Rheometrics Scientific DMTA MK III in uniaxial extension at 1 Hz, and temperatures ranging from -150 to 200 °C.

Stress relaxation experiments were performed on a Frank 81565 tensile tester, while tensile and creep experiments were performed on a Zwick Rel servo-hydraulic tensile tester, equipped with an extensometer and a thermostatically controlled oven. In the latter case the extension was measured using an Instron (2620-602) strain gauge extensometer with a measure length of 50 mm and a range of ± 2.5 mm. The relative accuracy in the force and strain measurements was 1%.

Tensile tests, at various strain rates, were performed at 22 and 40 °C. Creep experiments, with loading times not exceeding 10^3 seconds, were performed in dead weight loading at loads of 15 to 50 MPa. The loads were applied within 0.1 seconds. Stress relaxation experiments with loading times not exceeding 10^4 seconds were performed at linear strains of 0.5 to 3%.

Each experiment used a new sample. All test samples had the same age, which exceeded by far the longest time in the experiments.

2.3 Deformation behaviour

Linear viscoelastic deformation

Linear viscoelastic deformation is commonly described using a Boltzmann single integral representation, either in its relaxation (i), or retardation (ii) form [1,2]:

$$(i) \sigma(t) = \int_{-\infty}^t E(t-t')\dot{\epsilon}(t')dt' \quad \text{and} \quad (ii) \epsilon(t) = \int_{-\infty}^t D(t-t')\dot{\sigma}(t')dt' \quad (2.1)$$

The information concerning time-dependent material behaviour is contained in the viscoelastic functions: the relaxation modulus $E(t)$ or the creep compliance $D(t)$. A characteristic example of the time dependent material response is shown schematically in Figure 2.2, representing the logarithm of the linear creep compliance against the logarithm of time.

After an initial elastic response, the material shows time dependent creep until gradually a constant rate of deformation is established, that is, the material is flowing. Due to the high molecular weight, this flow is stabilized by the presence of a physical entanglement network, resulting in a rubber plateau. The *apparent* flow occurring in the glass-rubber transition region can only be observed if the difference in compliance between the glassy and rubbery region is large enough. Because of the presence of entanglements this flow results in an ongoing molecular orientation within the material and it should not be confused with flow occurring beyond the rubber plateau, where deformation and orientation are no longer coupled.

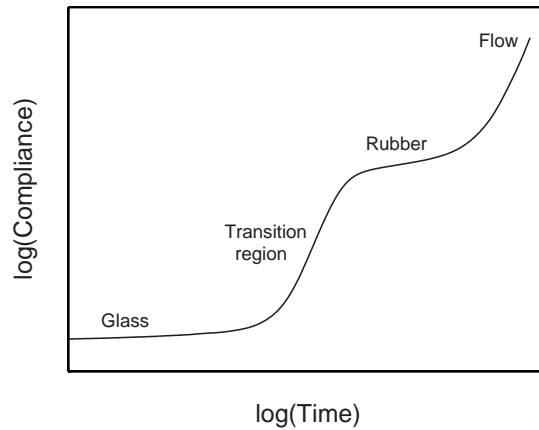


Figure 2.2: Schematic representation of the linear creep compliance versus time for a polymer glass at a fixed temperature.

The form of the time dependence of relaxation modulus and creep compliance can be captured by a mechanical model with a sufficient number of elastic and viscous elements [1, 2]. Here the influence of the rubber contribution is neglected, since it is only relevant at large deformations. As a consequence, the constitution of the mechanical analogies, shown in Figure 2.3(a), $E(t)$, and Figure 2.3(b), $D(t)$, is that of a linear viscoelastic liquid.

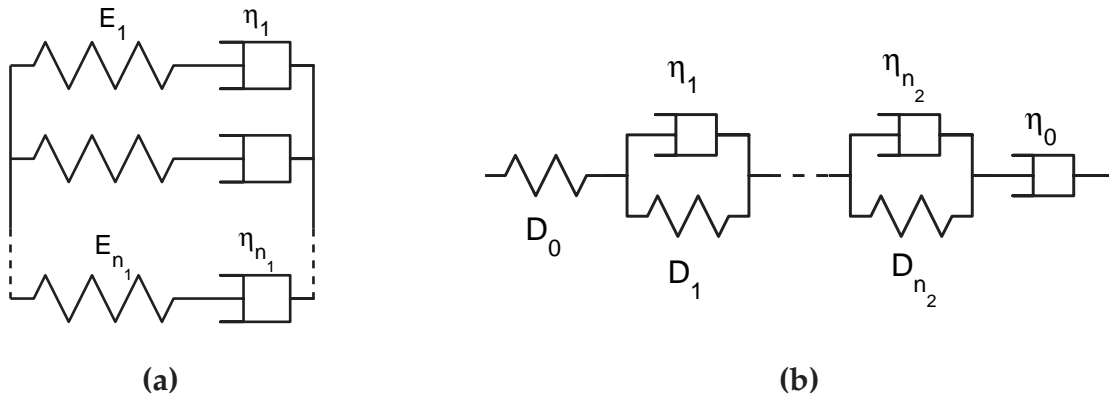


Figure 2.3: Schematic representation of the generalized linear Maxwell model (a) and the generalized Kelvin-Voigt model (b).

Besides graphically, the mechanical models can also be expressed in equations. For the generalized linear Maxwell model of Figure 2.3(a) this results in:

$$E(t) = \sum_{i=1}^{n_1} E_i \exp\left(-\frac{t}{\tau_i}\right) \tag{2.2}$$

where $\tau_i = \eta_i/E_i$; the index i refers to the i -th Maxwell element, while n_1 is the number of elements. For the generalized linear Kelvin-Voigt model from Figure 2.3(b) we find:

$$D(t) = D_0 + \sum_{i=1}^{n_2} D_i \left[1 - \exp\left(-\frac{t}{\tau_i}\right) \right] + \frac{t}{\eta_0} \quad (2.3)$$

where D_0 is the initial elastic response, η_0 represents the flow viscosity, and $\tau_i = \eta_i D_i$. The index i refers to the i -th Kelvin-Voigt element, while n_2 is the number of elements.

From both the figures and equations it should be clear that the generalized Maxwell and Kelvin-Voigt models represent the behaviour previously described: initially elastic, followed by time dependent deformation, and for times beyond the longest relaxation time, Newtonian flow. In practice, the latter condition is, however, seldom observed in a linear viscoelastic experiment at room temperature, since the longest relaxation/retardation time normally by far exceeds the time of the experiment.

Plastic deformation

Yield of polymer glasses is usually described using a fluid-like approach like that in Figure 2.3, thereby regarding the material as a strongly nonlinear fluid with a very high relaxation time. The most simple approach uses just a single nonlinear Maxwell element with one, temperature and stress-activated, relaxation time, Tobolsky and Eyring [3]. A schematic representation of such a model is given in Figure 2.4(a). The initial elastic response is described by the modulus E_0 , while plastic flow is determined by the stress dependent viscosity $\eta(\sigma)$.

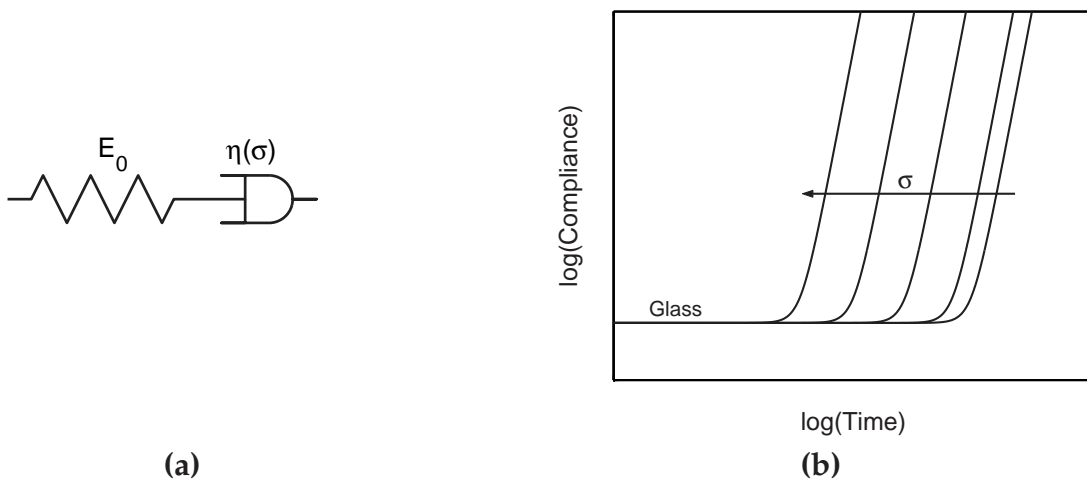


Figure 2.4: Schematic representation of a nonlinear Maxwell model (a), and its response to increasing levels of constant stress (b).

The stress dependence of the single relaxation time is best demonstrated in creep tests at different stress levels. At low stresses, the relaxation time of the element is constant, and the response is not influenced by stress (linear). With increasing stresses, the relaxation time decreases, resulting in a horizontal shift of the compliance curve along the logarithmic time axis towards shorter times (Figure 2.4(b)).

The stress dependence of the relaxation time is assumed to originate solely from the plastic flow process. For the viscosity an Eyring expression [4] is used, which is a semi-empirical relation that describes stress-activated flow of structural units in a material, such as segments of polymers [5]:

$$\dot{\epsilon} = \dot{\epsilon}_0 \exp\left(-\frac{\Delta U}{RT}\right) \sinh\left(\frac{\sigma V^*}{kT}\right) \quad (2.4)$$

where V^* is the activation volume, determining the stress dependence, ΔU the activation energy, determining the temperature dependence, $\dot{\epsilon}_0$ is a rate constant, R is the universal gas constant, k is Boltzmann's constant, and T the absolute temperature. Using the selected model material (polycarbonate) it can be demonstrated that this relation indeed gives a correct description of yield. Therefore the Eyring relation, Eq. (2.4), is rewritten in terms of strain rate:

$$\frac{\sigma}{T} = \frac{R}{V^*} \sinh^{-1}\left(\frac{\dot{\epsilon}}{\dot{\epsilon}_0^*}\right) \quad (2.5)$$

where

$$\dot{\epsilon}_0^* = \dot{\epsilon}_0 \exp\left(-\frac{\Delta U}{RT}\right) \quad (2.6)$$

For high stresses at yield, $\sinh(\sigma) \approx \frac{1}{2} \exp(\sigma)$ and a plot of σ_y/T against $\log(\dot{\epsilon})$ produces a series of straight lines, the slope of which is determined by the activation volume V^* . Figure 2.5 shows the results of the yield experiments on polycarbonate for various strain rates and two different temperatures.

Apparently Eq. (2.5) gives a good description of the rate dependence of the yield stress for both temperatures. The parameters that result from fitting the data using Eq. (2.5) are listed in Table 2.1.

Material	V^* [nm ³]	ΔU [kJ/mol]	$\dot{\epsilon}_0$ [s ⁻¹]
Polycarbonate	3.05	274.0	$1.118 \cdot 10^{27}$

Table 2.1: Eyring parameters for polycarbonate Lexan 161R obtained from fitting the yield data in Figure 2.5 with Eq. (2.5).

The value found for the activation volume is in good agreement with the values

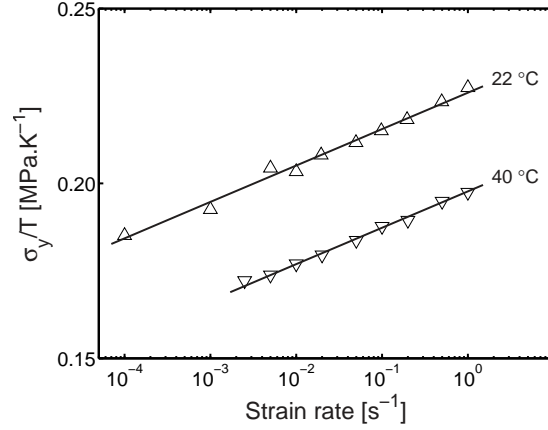


Figure 2.5: Ratio of yield stress to temperature as a function of strain rate for polycarbonate. Symbols represent experimental data and lines are fits using Eq. (2.5).

obtained by Robertson [6], 3.22 nm³, and Bauwens-Crowet *et al.* [7], 3.28 nm³ (both values were recalculated according to Eq. (2.5)).

To obtain an analytical expression for stress-dependent viscosity, Eq. (2.4) is substituted in:

$$\eta(\sigma) = \frac{\sigma}{\dot{\epsilon}(\sigma)} = \frac{\sigma}{\dot{\epsilon}_0 \exp\left(-\frac{\Delta U}{RT}\right) \sinh\left(\frac{\sigma V^*}{kT}\right)} \quad (2.7)$$

This can be written as:

$$\eta(\sigma) = \eta_0 \frac{(\sigma/\sigma_0)}{\sinh(\sigma/\sigma_0)} \quad (2.8)$$

where σ_0 is a characteristic stress:

$$\sigma_0 = \frac{kT}{V^*} \quad (2.9)$$

and η_0 the zero-viscosity at very small stresses:

$$\eta_0 = \frac{\sigma_0}{\dot{\epsilon}_0} \exp\left(\frac{\Delta U}{RT}\right) \quad (2.10)$$

Introduction of a stress dependent shift function a_σ , defined as

$$a_\sigma(\sigma) = \frac{(\sigma/\sigma_0)}{\sinh(\sigma/\sigma_0)} \quad (2.11)$$

further reduces Eq. (2.8) to

$$\eta(\sigma) = \eta_0 a_\sigma(\sigma) \quad (2.12)$$

For stresses below σ_0 , the stress shift function a_σ equals one and the material behaves Newtonian (albeit with a rather high viscosity, see Table 2.2), whereas for stresses above σ_0 , the stress shift function a_σ decreases exponentially and the material behaves strongly non-Newtonian.

Setting the temperature T equal to 22 °C, the characteristic stress σ_0 and the zero-viscosity η_0 can be calculated from the parameters in Table 2.1 using Eqs. (2.9) and (2.10), see Table 2.2.

Material	σ_0 [MPa]	η_0 [MPa s]
Polycarbonate	1.334	$4.15 \cdot 10^{21}$

Table 2.2: Parameters for the nonlinear viscosity function, Eq. (2.12), for a reference temperature of 22 °C.

The expression derived for the nonlinear viscosity can be used to obtain one-dimensional expressions for the relaxation modulus and creep compliance of the nonlinear Maxwell model. For the relaxation modulus the result is:

$$E(t) = E_0 \exp\left(-\frac{t}{\tau(\sigma)}\right) \quad (2.13)$$

where E_0 is the initial modulus and $\tau(\sigma) = \tau_0 a_\sigma(\sigma)$, with $\tau_0 = \eta_0/E_0$. While for the compliance we find:

$$D(t) = D_0 + \frac{t}{\eta(\sigma)} \quad (2.14)$$

where $D_0 = 1/E_0$. Eqs. (2.13) and (2.14) illustrate the characteristic behaviour of the model, a single stress-activated relaxation time, resulting in a sharp, stress dependent, transition from elastic to plastic deformation.

Nonlinear viscoelastic deformation

In the previous two subsections, the linear viscoelastic and plastic response was described using a mechanical analogon. The time dependence, characteristic for the linear viscoelastic range, including the ultimate flow behaviour was modelled using a spectrum of linear relaxation times, whereas the stress-dependent yield behaviour was modelled using a single stress-dependent relaxation time. The nonlinear viscoelastic range is positioned in-between the linear viscoelastic and plastic range. To cover its behaviour we use a model that contains the characteristics of both bounding regions, having a spectrum of nonlinear stress-dependent relaxation times. For simplicity, the stress dependence a_σ , governed by the activation volume V^* , is taken the same for each relaxation time. This leads to a situation that is comparable to a ther-

morheological simple material where all relaxation times are the same function of temperature. The resulting model is shown in terms of mechanical model analogies in Figure 2.6(a) and Figure 2.6(b).

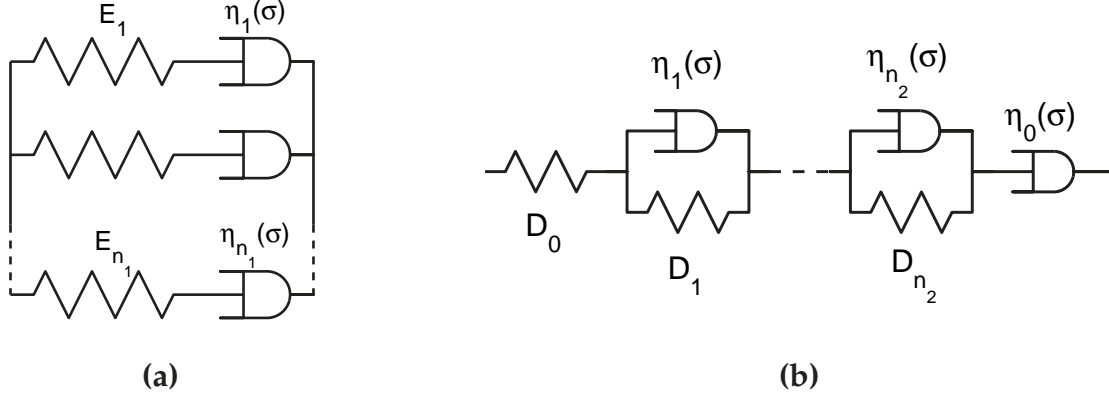


Figure 2.6: Schematic representation of the generalized nonlinear Maxwell (a), and Kelvin-Voigt model (b).

For the generalized nonlinear Maxwell model we have:

$$E(t) = \sum_{i=1}^{n_1} E_i \exp\left(-\frac{t}{\tau_i(\sigma)}\right) \quad (2.15)$$

where $\tau_i(\sigma)$ ($= \tau_i a_\sigma(\sigma)$) and E_i refer to the i -th Maxwell element and n_1 is the number of elements. For the generalized nonlinear Kelvin-Voigt model the creep function is:

$$D(t) = D_0 + \sum_{i=1}^{n_2} D_i \left[1 - \exp\left(-\frac{t}{\tau_i(\sigma)}\right)\right] + \frac{t}{\eta_0(\sigma)} \quad (2.16)$$

with D_0 the initial elastic response, $\tau_i(\sigma)$ ($= \tau_i a_\sigma(\sigma)$) and D_i referring to the i -th Kelvin-Voigt element, n_2 the number of elements, and $\eta(\sigma)$ is the stress-dependent viscosity (Eq. (2.8)).

Both models correctly describe the material behaviour in the linear viscoelastic and plastic range, since for stresses below σ_0 , the shift function a_σ equals one and all relaxation times become linear, whereas for high stresses all relaxation times decrease exponentially resulting in yield. At intermediate stresses the typical stress and time-dependence observed in the nonlinear viscoelastic region is obtained.

The important feature that all relaxation times have the same total stress dependent shift function a_σ , is rationalized since, according to the Eyring theory, the stress activation of a molecular process is governed by the total stress applied. As a con-

sequence, this approach implies that the material shows time-stress superposition, similar to time-temperature superposition, where all relaxation times are the same function of temperature. In accordance with this analogy, a stress-reduced time ψ can be defined:

$$\psi = \int_{-\infty}^t \frac{dt''}{a_{\sigma}[\sigma(t'')]}$$

where a_{σ} is the ratio of the relaxation time at a stress σ and the relaxation time for a stress well below σ_0 .

To verify whether or not the model is capable of accounting for the entire range of deformation up to and including yield, experiments are compared with model predictions. For the predictions we need a constitutive relation, that can be obtained by using the concept of stress-reduced time in combination with the Boltzmann single integral representation. This leads to two possible stress-strain relations, since the Boltzmann single integral can be used in both its stress and strain form:

$$\sigma(t) = \int_{-\infty}^t E(\psi - \psi') \dot{\varepsilon}(t') dt' \quad \text{and} \quad \varepsilon(t) = \int_{-\infty}^t D(\psi - \psi') \dot{\sigma}(t') dt' \quad (2.17)$$

where

$$\psi = \int_{-\infty}^t \frac{dt''}{a_{\sigma}[\sigma(t'')]}$$

$$\text{and} \quad \psi' = \int_{-\infty}^{t'} \frac{dt''}{a_{\sigma}[\sigma(t'')]}$$

and $E(t)$ and $D(t)$ are the linear relaxation modulus and creep compliance, given by Eqs. (2.2) and (2.3), respectively. The major advantage of a stress-strain relation of this form is the separation of the stress and time-dependence through which the relation can be treated according to the linear viscoelastic theory.

Before any calculations can be done, the necessary material parameters have to be determined, in this case the linear relaxation modulus $E(t)$, or creep compliance $D(t)$, and the shift function a_{σ} by means of the characteristic stress σ_0 . First of all, however, the applicability of time-stress superposition has to be experimentally verified. This can be done in a way similar to the verification of the time-temperature superposition [1]. Data obtained at constant stress levels must shift horizontally along the logarithmic time-axis to a smooth master-curve for a certain reference stress, and the resulting shift factors plotted as a function of stress must obey a *familiar* relationship, in this case the shift function derived from the Eyring theory. This will be dealt with first. Next, the material parameters are determined and finally numerical predictions are compared with experimental results.

2.4 Results

In section 2.3 it was argued that the deformation of a thermorheological simple polymer is determined by a linear relaxation, or retardation, time spectrum which is shifted to shorter times when stress is applied. First, the applicability of the time-stress superposition principle is experimentally verified. Accordingly, the parameters are determined and model predictions will be compared to experimental data for constant strain-rate experiments at different strain rates and stress relaxation experiments at different strains applied.

Applicability of time-stress superposition

To verify the applicability of time-stress superposition experimentally for polycarbonate, it is first attempted to construct a smooth master-curve from a number of creep tests at different stress levels. The results of these creep tests are shown in Figure 2.7(a).

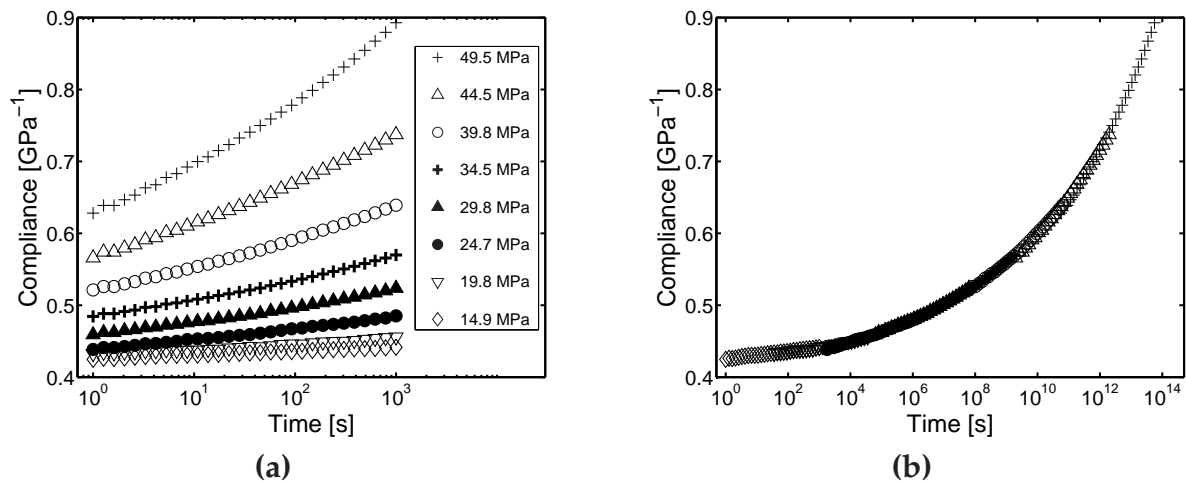


Figure 2.7: (a) Creep compliance of polycarbonate at 22 °C and various stress levels. (b) Master curve of the data in Figure 2.7(a), for a reference stress of 15 MPa.

The creep curves in Figure 2.7(a) are shifted horizontally along the logarithmic time axis with respect to the 15 MPa reference curve, see Figure 2.7(b) for the resulting master curve. A smooth compliance master curve can be constructed by horizontal shifting of the creep curves at different stresses. It must be emphasized that the compliance master curve at 15 MPa is a *virtual* curve that will strongly deviate from an experimental creep test on the same time scale due to ageing effects.

The logarithm of the shift factors $\log(a_{15})$, necessary to construct the master compliance curve at 15 MPa (Figure 2.7(b)), are tabulated in Table 2.3 as a function of the creep load applied.

σ [MPa]	$\log(a_{15})$
14.9	0.00
19.8	-1.55
24.7	-3.25
29.8	-4.80
34.5	-6.25
39.8	-7.80
44.5	-9.30
49.5	-10.75

Table 2.3: Values of $a_{15}(\sigma)$ obtained from the construction of the master curve in Figure 2.7(b).

The second part of the experimental verification of time-stress superposition consists of fitting the shift data from Table 2.3 with the Eyring shift equation, Eq. (2.11). Although the shift function at the reference stress was set equal to one, comparison with the previously obtained value for σ_0 learns that the reference stress is in the nonlinear range. To correct for this deviation from linearity, the shift data are fitted using a modified shift function:

$$a_{15}(\sigma) = c \cdot a_{\sigma}(\sigma) \quad (2.18)$$

where $c (= a_{\sigma}^{-1}(15))$ is a constant that accounts for the shift of the 15 MPa master curve with respect to the linear range. The constant c does not affect the shape of the shift function which is completely determined by the parameter σ_0 . A plot of the shift factors with respect to the 15 MPa reference curve is shown in Figure 2.8.

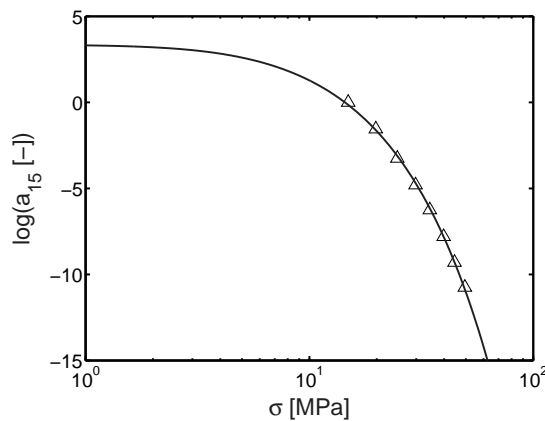


Figure 2.8: Symbols represent the shift factors tabulated in Table 2.3, and the solid line is a fit using Eq. (2.18).

From Figure 2.8 it is clear that the shift data obtained can be described using a single

Eyring function. Therefore, the second condition is also met, and it may be assumed that time-stress superposition is allowed. Furthermore, the fit yields $\sigma_0 = 1.334$ MPa, which agrees with the value for σ_l obtained in the previous yield experiments, and $\log(c) = -\log(a_\sigma(15)) = 3.496$.

Linear viscoelastic behaviour

In section 2.4 it was verified experimentally that time-stress superposition applies to polycarbonate. Since the characteristic stress is already known, only the viscoelastic behaviour has to be determined in terms of the linear relaxation/retardation time spectrum. The 15 MPa compliance master curve was obtained through application of the time-stress superposition principle. However, it was already pointed out that the 15 MPa compliance master curve does not constitute the true linear compliance curve. The value of the characteristic stress σ_0 indicates that above a stress of 1.334 MPa, polycarbonate already behaves in a nonlinear way. Therefore, the true linear compliance curve can only be obtained indirectly by shifting the 15 MPa master curve horizontally by a factor $a_\sigma^{-1}(\sigma = 15 \text{ MPa})$, see Figure 2.9.

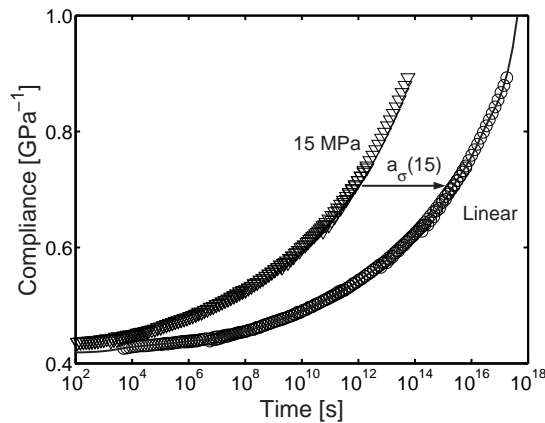


Figure 2.9: Construction of the linear compliance from the 15 MPa master curve, including the fit using a generalized linear Kelvin-Voigt model (solid line).

To obtain the discrete relaxation spectrum that can be used for further calculations a three-step process, similar to that described by Dooling *et al.* [8], is used. In the first step, a discrete linear Kelvin-Voigt model (Eq. (2.3)) is fitted to the experimentally obtained linear creep compliance (solid line in Figure 2.9). In addition to the initial compliance D_0 and flow viscosity η_0 , 14 modes ($n_2 = 14$ in Eq. (2.3)) were needed to get a good description of the data, which is approximately one mode per decade. To constrain the fit parameters to physically realistic positive values a nonnegative least-squares procedure was employed [9]. All values for the discrete retardation spectrum are listed in Appendix 2.A.

In the second step the retardation spectrum obtained in the preceding step is used in combination with the linear Boltzmann integral to numerically predict a linear stress relaxation experiment. The relaxation modulus resulting from this calculation is shown in Figure 2.10.

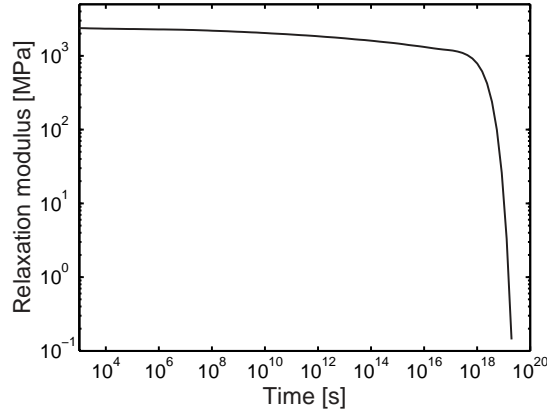


Figure 2.10: Linear relaxation modulus obtained from the conversion of the linear compliance in Figure 2.9.

In the final step a discrete relaxation spectrum (Maxwell model) is fitted to the calculated stress relaxation modulus. Using 17 modes ($n_1 = 17$ in Eq. (2.2)) a satisfactory description is obtained. This number is higher than that for the retardation spectrum since the initial modulus and flow viscosity are implicitly included in this representation. The same fit routine (nonnegative least-squares) was used to ensure that all parameters are again positive, thus preventing unrealistic negative values. All values for the discrete relaxation spectrum are tabulated in Appendix 2.B.

It must, however, be emphasized that the linear Maxwell and Kelvin-Voigt parameters bear no real physical meaning, only the relaxation modulus $E(t)$ and compliance $D(t)$ are material functions.

Model verification

In section 2.3 it was argued that the nonlinear viscoelastic behaviour of a polymer glass is determined by the linear relaxation/retardation time spectrum, which is shifted to shorter times when stress is applied. In section 2.4, the linear spectra were approximated using a discrete Maxwell and Kelvin-Voigt model, the relaxation/retardation times of which are all subdued to the same stress dependence. In this section, the stress-strain relations of Eq. (2.17) are verified by constant strain-rate experiments (uniaxial tensile tests) at different strain rates, and stress relaxation experiments at various strains.

The first verification experiment considered is a standard uniaxial tensile test at various linear strain rates (constant cross-head speeds). Figure 2.11(a) shows a comparison between the experimental data (open symbols) and the numerical predictions (solid lines). From this figure it is clear that the model gives a good description of the nonlinear viscoelastic behaviour and provides a quantitative description of the strain-rate-dependent yield of polycarbonate. However, after the yield point the predictions deviate from the experiments due to strain localization and strain softening, which are not yet incorporated in the model.

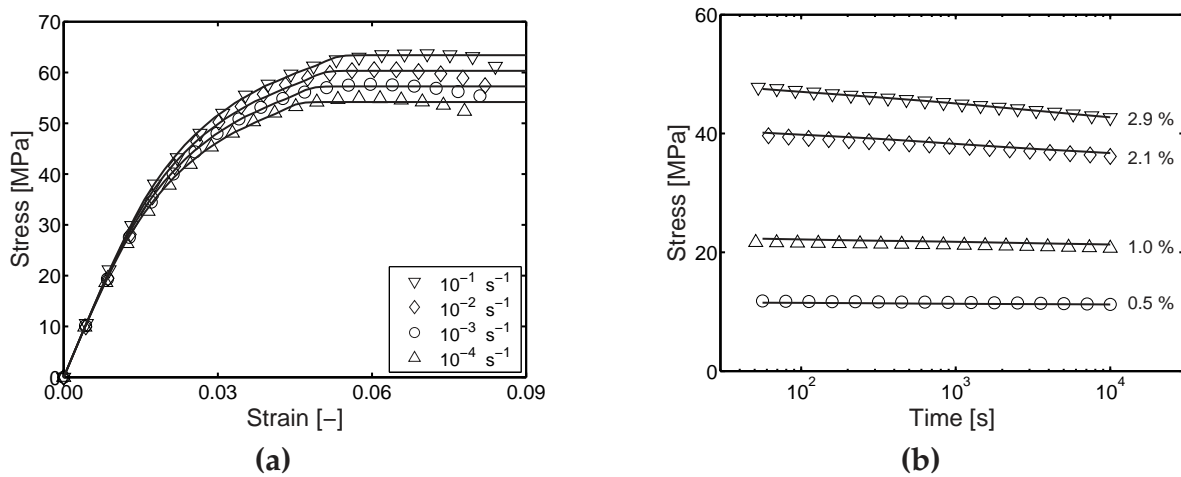


Figure 2.11: (a) Tensile tests at various strain-rates (symbols) compared to model predictions (solid lines). (b) Stress relaxation at different strains (symbols) compared to model predictions (solid lines).

In addition to the tensile experiments, nonlinear stress relaxation experiments were considered as well. The resulting experimental data and numerical calculations at various strain levels are depicted in Figure 2.11(b). It should be noted that all the stress relaxation experiments displayed in Figure 2.11(b) are essentially in the nonlinear regime, since all stresses exceed the characteristic stress $\sigma_0 = 1.334 \text{ MPa}$. In contrast, visually the response up to 1% strain appears to be quite linear, which illustrates that conclusions concerning true linear behaviour can only be drawn with great precaution. This becomes evident when describing these nonlinear stress-relaxation experiments. In an ideal stress relaxation experiment, loading is assumed to take place instantaneously. In practice, loading always occurs over a finite time. In case of true linear behaviour, the difference in response is negligible after ten times the loading time [10]. To obtain a good agreement between experimental data and calculations, as displayed in Figure 2.11(b), it proved necessary to take into account the exact experimental loading path. When using an instantaneous loading program in the calculations, differences with experiments persisted much longer than ten times the experimental loading time. This kind of 'hidden' nonlinearity could be of importance when considering the influence of a short stress pulse on creep behaviour [10], as was also mentioned by McKenna [11].

2.5 Conclusions

The present work is aimed at the development of a model, that can be employed to identify the separate contributions of the various molecular processes to macroscopic deformation. By considering a material with only a single (active) molecular process, that is a thermorheological simple material, a constitutive model describing all types of deformation up to yield is obtained. The model is based on the assumption that the material's response is determined by a spectrum of linear relaxation times, which shifts to shorter times under the influence of stress. Further, the influence of stress is equivalent for each relaxation time, which is comparable with the influence of temperature, since all relaxation times are the same function of temperature (thermorheological simple). Therefore, the material should show time-stress superposition in analogy with time-temperature superposition. By means of creep experiments at different stress levels it is shown that time-stress superposition is indeed applicable. Further, the characteristic stress which could be obtained from the resulting shift parameters, shows good agreement with that determined from yield experiments. From the constructed master curve the remaining model parameters can be determined. Concluding simulations of both tensile tests for various strain rates, and stress relaxation at different applied strains, show excellent agreement with experimental data.

References

- [1] Ferry, J.D. (1980). *Viscoelastic Properties of Polymers*. John Wiley & Sons Inc., New York.
- [2] Tschoegl, N.W. (1989). *The Phenomenological Theory of Linear Viscoelastic Behaviour: an Introduction*. Springer-Verlag, Berlin.
- [3] Tobolsky, A. and Eyring, H. (1943). Mechanical properties of polymeric materials. *J. Chem. Phys.*, **11**, 125-134.
- [4] Eyring, H. (1936). Viscosity, plasticity, and diffusion as examples of absolute reaction rates. *J. Chem. Phys.*, **4**, 283-295.
- [5] Ward, I.M. (1983). *Mechanical Properties of Solid Polymers*. John Wiley & Sons, Chichester.
- [6] Robertson, R.E. (1963). On the cold-drawing of plastics. *J. Appl. Pol. Sci.*, **7**, 443-450.
- [7] Bauwens-Crowet, C., Bauwens, J.-C. and Homès, G. (1969). Tensile yield-stress behavior of glassy polymers. *J. Pol. Sci. Part A-2*, **7**, 735-742.
- [8] Dooling, P.J., Buckley, C.P., Hinduja, S. (1997). An intermediate model method for obtaining a discrete relaxation spectrum from creep data. *Rheol. Acta*, **36**, 472-482.
- [9] Lawson, C.L., Hanson, R.J. (1974). *Solving Least Squares Problems*. Prentice-Hall, Englewood Cliffs.

-
- [10] Struik, L.C.E. (1978). *Physical Aging in Amorphous Polymers and Other Materials*. Elsevier, Amsterdam.
- [11] McKenna, G.B., Schultheisz, C.R., Leterrier, Y. (1994). Volume recovery and physical aging: Dilatometric evidence for different kinetics, in the *9th International Conference on Deformation, Yield and Fracture of Polymers* (The Institute of Materials, London, 1994), 31/1.

2.A Appendix: retardation time spectrum

The linear compliance curve (Figure 2.9) is fitted using a generalized Kelvin-Voigt model (Eq. (2.3)). By means of a nonnegative least squares method [9], the following values were obtained, $D_0 = 0.419 \text{ GPa}^{-1}$, $\eta_0 = 2.74 \cdot 10^{21} \text{ MPa s}$, whereas the values of the remaining parameters are tabulated in Table 2.4 below.

i	τ_i [s]	D_i [GPa^{-1}]
1	$3.14 \cdot 10^3$	0.00878
2	$3.59 \cdot 10^4$	0.00485
3	$4.10 \cdot 10^5$	0.00524
4	$4.68 \cdot 10^6$	0.00470
5	$5.34 \cdot 10^7$	0.01283
6	$6.10 \cdot 10^8$	0.01634
7	$6.97 \cdot 10^9$	0.02057
8	$7.96 \cdot 10^{10}$	0.02559
9	$9.09 \cdot 10^{11}$	0.03076
10	$1.04 \cdot 10^{13}$	0.04076
11	$1.19 \cdot 10^{14}$	0.04839
12	$1.35 \cdot 10^{15}$	0.06606
13	$1.55 \cdot 10^{16}$	0.09883
14	$1.77 \cdot 10^{17}$	0.04723

Table 2.4: Values for the linear Kelvin-Voigt parameters.

2.B Appendix: relaxation time spectrum

The linear relaxation modulus after conversion of the linear compliance (Figure 2.10) was approximated using a generalized linear Maxwell model (Eq. (2.2)). By means of a nonnegative least squares method [9] the parameter values tabulated in Table 2.5 were obtained.

i	τ_i [s]	E_i [MPa]
1	$1.08 \cdot 10^3$	25.2
2	$1.12 \cdot 10^4$	42.1
3	$1.17 \cdot 10^5$	22.3
4	$1.21 \cdot 10^6$	23.8
5	$1.26 \cdot 10^7$	36.7
6	$1.31 \cdot 10^8$	70.5
7	$1.36 \cdot 10^9$	76.1
8	$1.41 \cdot 10^{10}$	90.5
9	$1.47 \cdot 10^{11}$	98.5
10	$1.52 \cdot 10^{12}$	109.5
11	$1.58 \cdot 10^{13}$	123.0
12	$1.64 \cdot 10^{14}$	128.4
13	$1.71 \cdot 10^{15}$	141.5
14	$1.23 \cdot 10^{16}$	33.8
15	$1.57 \cdot 10^{16}$	124.7
16	$2.17 \cdot 10^{18}$	1173.0
17	$2.77 \cdot 10^{18}$	71.0

Table 2.5: Values for the linear Maxwell parameters.

Deformation of thermorheological complex materials¹

3.1 Introduction

In Chapter 2, a constitutive model was derived based on the assumption that a polymer material behaves thermorheological simple. For such a material the deformation is completely determined by the time-dependent linear relaxation modulus, or compliance, and a nonlinear stress-dependent shift function. For polycarbonate the model was shown to correctly describe the nonlinear response to different strain rates and constant strains applied.

Many polymers, however, behave thermorheological complex, that is, they have multiple relaxation mechanisms actively contributing to the deformation. Since the temperature dependencies of the underlying molecular processes are generally different, this leads to a break-down of the time-temperature superposition principle, which assumes that all relaxation times are equally influenced by temperature. Because a similar principle, time-stress superposition, forms the basis of the previously derived model, it can be anticipated that an extension of the model with an additional process has a similar effect. Therefore, in this chapter it is investigated what the consequences are for the stress-strain relation, and whether it is possible to isolate the contributions to the overall deformation caused by the different mechanisms.

For an experimental verification of the deformation, polymethylmethacrylate (PMMA) is selected as model material. From Figure 3.1(a) it can be seen that PMMA

¹Reproduced in part from: Klompen, E.T.J., Govaert, L.E. (1999). Nonlinear viscoelastic behaviour of thermorheologically complex materials - A modelling approach. *Mech. Time-Dep. Mat.*, **3**, 49–69.

displays both a secondary (denoted by β), and a primary transition (denoted by α) at, and above, room temperature. In addition, the loss angle of polycarbonate (PC) is also shown to demonstrate the difference in position of the secondary mechanisms with respect to the primary transition. Although the main part of the work will be concerned with PMMA, PC will be regarded as well to explore under which experimental conditions the secondary transition gives a substantial contribution to the deformation in this material. In addition, we included isotactic polypropylene (i-PP) to investigate separate relaxation mechanisms that are due to the crystalline phase (indicated by ζ in Figure 3.1(b)). First, the deformation in

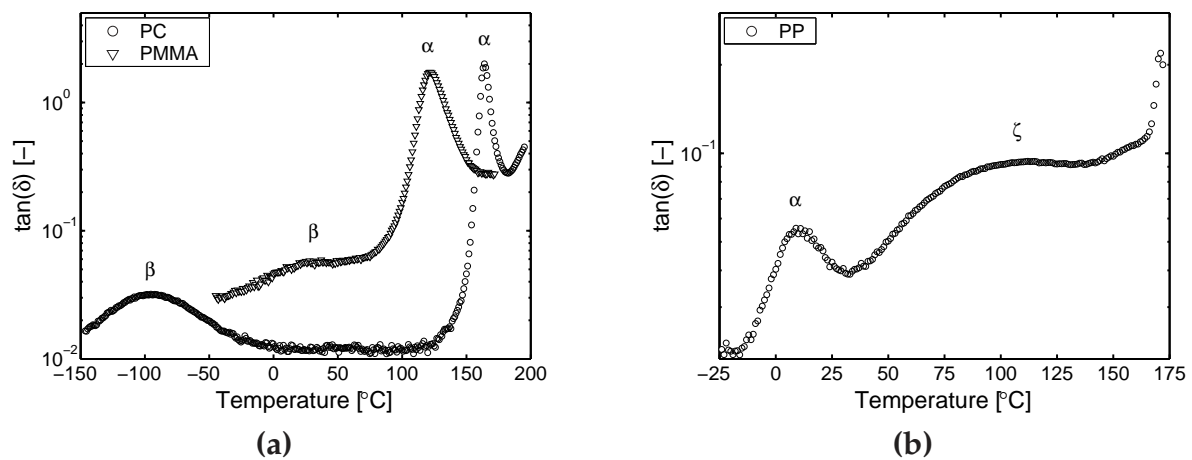


Figure 3.1: Loss angle $\tan(\delta)$ versus temperature for (a) polycarbonate and polymethylmethacrylate, and (b) isotactic polypropylene at a frequency of 1 Hz.

the linear viscoelastic and plastic range is regarded, and the previously employed mechanical model analogy is extended to account for an additional contribution. A comparison of the similarities between the two regions leads to an enhanced model including nonlinear viscoelastic deformation. In the remainder of this chapter this enhanced model is numerically explored to reveal the relevant processes underlying the deformation behaviour, including a comparison with experimental results from literature.

Similar to Chapter 2, this investigation is restricted to monotone loading paths and iso-age tests, thus neglecting the influence of both physical ageing and mechanical rejuvenation.

3.2 Experimental

Materials

Unless stated otherwise all experiments were performed on injection moulded tensile bars. Polycarbonate tensile bars were produced according to ISO R527, from

General Electric Lexan 161R, whereas polymethylmethacrylate and polypropylene tensile bars were produced according to ASTM D 638, from Rohm and Haas Orogas V052 and DSM Stanyl P46M10, respectively.

Mechanical testing

Dynamic experiments, using samples cut from 2 mm thick compression moulded sheets, were performed on a Rheometrics Scientific DMTA MK III in uniaxial extension at 1 Hz, and temperatures ranging from -150 to 200 °C for polycarbonate, from -50 to 175 °C for polymethylmethacrylate, and from -25 to 175 °C for polypropylene. Tensile experiments on polycarbonate were performed on a Zwick Rel servo-hydraulic tensile tester, while those on both polymethylmethacrylate and polypropylene were performed on a Frank 81565 tensile tester, both equipped with an extensometer and a thermostatically controlled oven. The relative accuracy in force and strain measurements was 1%. Tensile tests at various strain-rates were performed for polycarbonate from -20 to 40 °C, for polymethylmethacrylate and polypropylene from 30 to 70 °C.

Each experiment used a new sample. All test samples had the same age, which exceeded by far the longest time in the experiments.

3.3 Deformation behaviour

Linear viscoelastic deformation

Linear viscoelastic deformation is commonly described using a Boltzmann single integral representation (Eq. (2.1)), whereas the information concerning the time dependence is contained in the relaxation modulus $E(t)$ and creep compliance $D(t)$. For thermorheological complex materials the shape of these viscoelastic functions reveals the contribution of an additional molecular transition, see Figure 3.2.

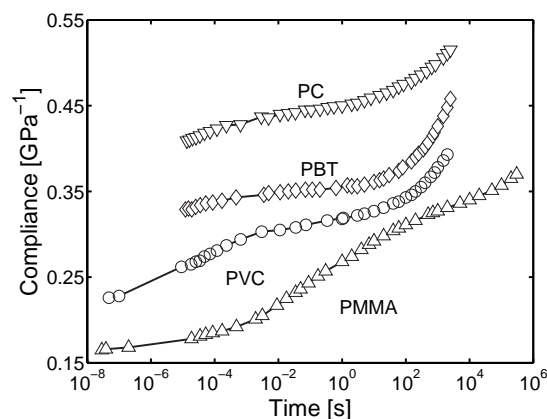


Figure 3.2: Creep curves at room temperature for various materials exhibiting secondary transitions, data from Read [1].

Despite this change in shape, the viscoelastic functions can still be represented by either a generalized Maxwell or Kelvin-Voigt model, where usually a distinction is made between the contributions caused by specific molecular transitions. In terms of the previously employed mechanical models this leads to the representations shown in Figures 3.3(a) and 3.3(b), where the rubber contribution is again neglected. For both models a distinction is made between relaxation/retardation times due to a particular transition, indicated by α and β respectively.

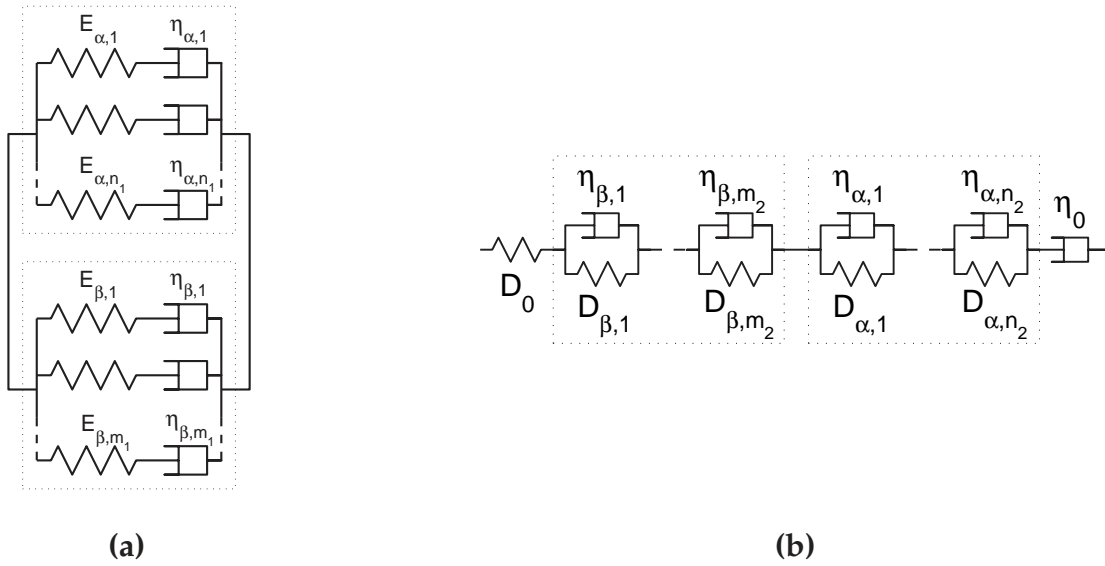


Figure 3.3: Schematic representation of the generalized linear Maxwell (a), and Kelvin-Voigt model (b) for two molecular processes α and β .

Besides graphically, the analogies can also be expressed in equations, giving for the generalized Maxwell model:

$$E(t) = \sum_{i=1}^{m_1} E_{\beta,i} \exp\left(-\frac{t}{\tau_{\beta,i}}\right) + \sum_{j=1}^{n_1} E_{\alpha,j} \exp\left(-\frac{t}{\tau_{\alpha,j}}\right) \quad (3.1)$$

where $\tau_{x,k} = \eta_{x,k}/E_{x,k}$, the index k referring to the k -th Maxwell element of process x ; and m_1, n_1 are the number of elements for the β and α -process, respectively. The generalized linear Kelvin-Voigt model results in:

$$D(t) = D_0 + \sum_{i=1}^{m_2} D_{\beta,i} \left[1 - \exp\left(-\frac{t}{\tau_{\beta,i}}\right)\right] + \sum_{j=1}^{n_2} D_{\alpha,j} \left[1 - \exp\left(-\frac{t}{\tau_{\alpha,j}}\right)\right] + \frac{t}{\eta_0} \quad (3.2)$$

where D_0 is the initial elastic response, η_0 represents the end flow viscosity, $\tau_{x,k} = \eta_{x,k} D_{x,k}$, the index k referring to the k -th element of process x ; and m_2, n_2 are the number of elements of the β and α process, respectively. Again it should

be noted that compared to $\tau_{\beta,i}$ the relaxation/retardation times $\tau_{\alpha,j}$ are influenced differently by temperature.

An alternative representation of the Kelvin-Voigt model frequently encountered in literature uses continuous creep functions rather than discrete elements [2–4]:

$$D(t) = D_U + (D_{R\beta} - D_U)\phi_{\beta}(t) + (D_{R\alpha} - D_{R\beta})\phi_{\alpha}(t) \quad (3.3)$$

where D_U is the unrelaxed compliance at short times, $D_{R\beta}$ and $D_{R\alpha}$ are the relaxed compliances for the β - and α -regions and $\phi_{\beta}(t)$ and $\phi_{\alpha}(t)$ are the normalized creep functions. The various relaxed and unrelaxed compliances are indicated schematically in Figure 3.4.

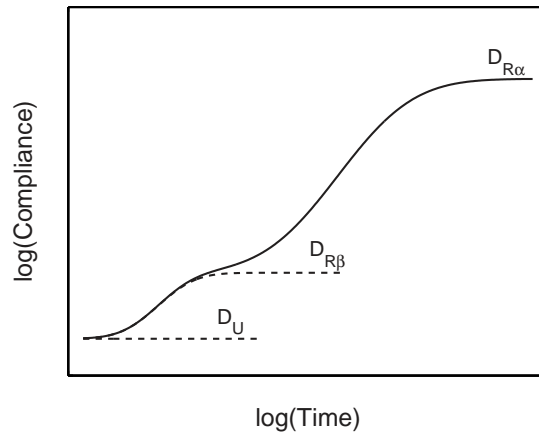


Figure 3.4: Schematic representation of the approach advocated by Read [2].

Although both a Kelvin-Voigt and a Maxwell model give a correct representation of the overall time-dependent deformation, there are two noteworthy differences originating from the distinction of two processes. First, the Maxwell model distinguishes between the initial elastic response due to a certain transition, whereas the Kelvin-Voigt model only shows a single initial deformation independent of a particular transition. The second difference lies in the description of the flow behaviour, where the Maxwell model shows two independent contributions, while the Kelvin-Voigt model only shows a single contribution.

Which of these approaches is more appropriate, and if the differences encountered are relevant, might be clarified by an investigation of the yield behaviour, since it was recognized in the previous chapter that yield is in fact stress-accelerated flow.

Plastic deformation

In Chapter 2, plastic deformation was described using a single, stress-dependent, Maxwell element. The stress dependence of the model was accounted for by the Eyring theory of nonlinear flow. Furthermore, a single Eyring process already gives a good description of the yield behaviour of a material that behaves thermorheological simple. Whether this observation is still valid for thermorheological complex materials can easily be verified by performing tensile tests at various strain-rates, alternatively at different temperatures. For the three selected model materials the results of these experiments are shown in Figure 3.5.

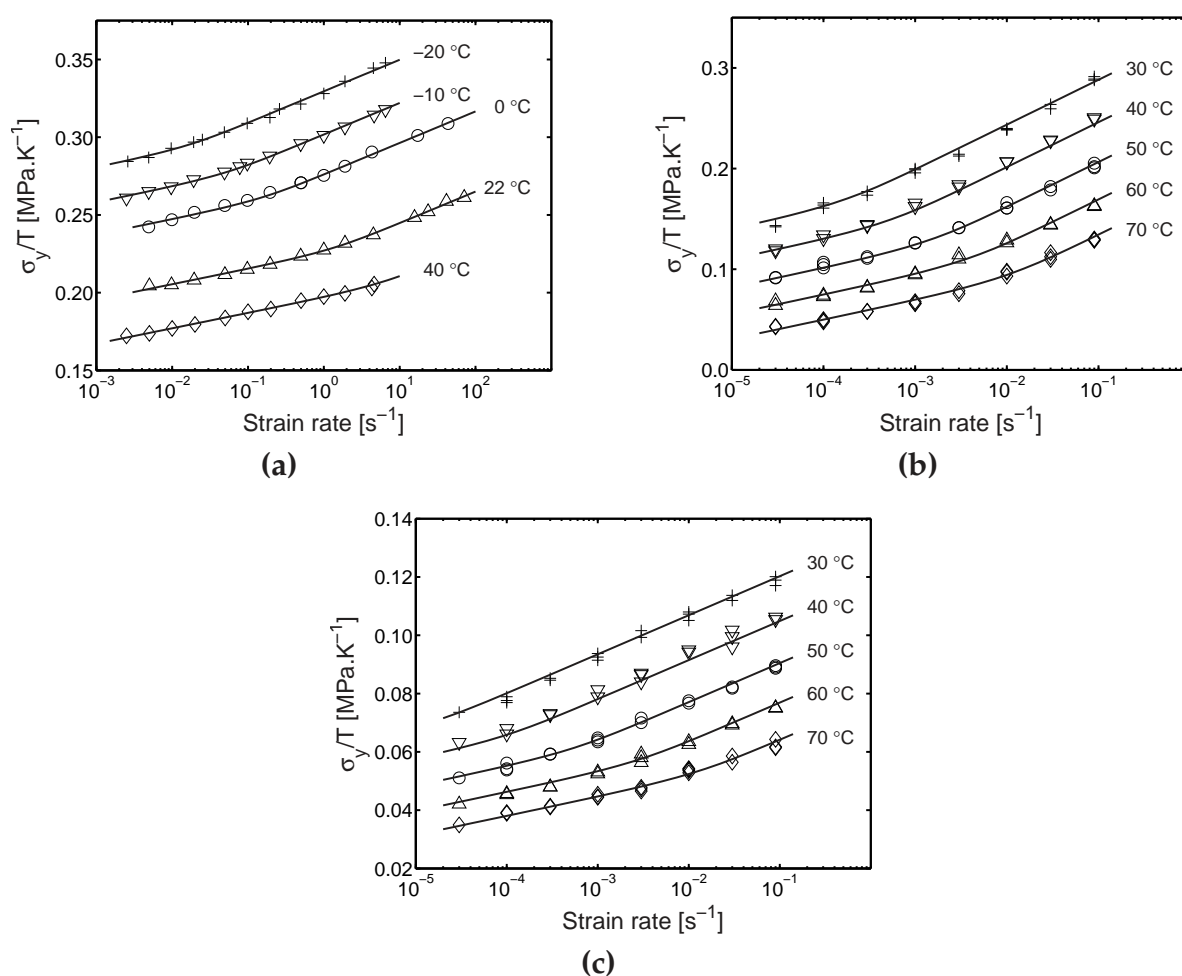


Figure 3.5: Ratio of yield stress to temperature as a function of strain rate for polycarbonate (a), polymethylmethacrylate (b), and polypropylene (c). Symbols represent experimental data and solid lines fits using Eq. (3.4).

Instead of a straight line, characteristic for a single transition, a change in slope is observed, and thus it is obvious that a single process is no longer sufficient to de-

scribe yield data from a material possessing a secondary transition. This was already reported by Roetling [5] and Bauwens-Crowet *et al.* [6], who used a Ree-Eyring modification [7] of Eyring's theory to describe these yield data. This modification assumes that all segments move at the same average rate, the stresses being additive. Following this procedure, one arrives at an equation of the form:

$$\frac{\sigma}{T} = \sum_{x=\alpha,\beta} \frac{k}{V_x^*} \sinh^{-1} \left(\frac{\dot{\epsilon}}{\dot{\epsilon}_{0,x}^*} \right) \quad (3.4)$$

where

$$\dot{\epsilon}_{0,x}^* = \dot{\epsilon}_{0,x} \exp \left(-\frac{\Delta U_x}{RT} \right) \quad x = \alpha, \beta. \quad (3.5)$$

with V_x^* the activation volume, ΔU_x the activation energy, and $\dot{\epsilon}_{0,x}$ the rate constant of process x . R is the universal gas constant, T the absolute temperature and k Boltzmann's constant.

Using this theory, a good description of the yield data is again obtained as is shown by the solid lines in Figures 3.5(a–c). Apparently, each molecular process contributes to the yield behaviour and the proper way of describing this is by a parallel configuration of nonlinear flow elements. The parameters resulting from the fit of the yield data for the three model materials are listed in Table 3.1.

Material	x	V_x^* [nm ³]	ΔU_x [kJ mol ⁻¹]	$\dot{\epsilon}_{0,x}$ [s ⁻¹]
PC	α	3.11	289.9	$5.76 \cdot 10^{28}$
	β	2.96	64.7	$6.42 \cdot 10^{11}$
PMMA	α	1.60	281.6	$3.99 \cdot 10^{36}$
	β	1.21	87.9	$4.30 \cdot 10^{11}$
i-PP	α	4.70	273.4	$1.33 \cdot 10^{32}$
	β	4.49	146.3	$4.39 \cdot 10^{20}$

Table 3.1: Eyring parameters for polycarbonate, polymethylmethacrylate, and polypropylene obtained from the yield data in Figure 3.5.

For polycarbonate Bauwens-Crowet *et al.* [8] found the values: $V_\alpha^* = 3.13 \text{ nm}^3$ and $V_\beta^* = 1.02 \text{ nm}^3$, while Roetling found for polymethylmethacrylate [5]: $V_\alpha^* = 2.00 \text{ nm}^3$ and $V_\beta^* = 0.96 \text{ nm}^3$, and for polypropylene [9]: $V_\alpha^* = 8.28 \text{ nm}^3$ and $V_\beta^* = 2.53 \text{ nm}^3$ (all values were recalculated in accordance with Eq. (3.4)). Compared to the values tabulated in Table 3.1, these values show some deviations in particular for the activation volumes of the β -processes. It is difficult to determine the exact cause of the deviations, but it might be attributed to differences in the materials employed, e.g. with regard to additives. A second possibility is a difference in the fitting

procedure, Roetling [5] uses a visual verification for the quality of the fit, whereas the values in Table 3.1 are obtained from a least-squares fit.

Instead of a single viscosity there are now viscosities due to the α - and β -processes, defined as:

$$\eta_x(\sigma_x) = \frac{\sigma_x}{\dot{\epsilon}(\sigma_x)}; \quad x = \alpha, \beta \quad (3.6)$$

where $\dot{\epsilon}$ is the strain rate applied and σ_x the stress response due to process x . Since both processes move at the same average rate, the stresses due to both transitions are related to the strain rate $\dot{\epsilon}$ by:

$$\dot{\epsilon} = \dot{\epsilon}_{0,x}^* \sinh\left(\frac{\sigma_x V_x^*}{kT}\right); \quad x = \alpha, \beta \quad (3.7)$$

Substitution of Eq. (3.6) in Eq. (3.7) yields:

$$\eta_x(\sigma_x) = \eta_{0,x} \frac{(\sigma_x/\sigma_{0,x})}{\sinh(\sigma_x/\sigma_{0,x})}; \quad x = \alpha, \beta \quad (3.8)$$

where $\sigma_{0,x}$ is the characteristic stress σ_0 for process x :

$$\sigma_{0,x} = \frac{kT}{V_x^*} \quad (3.9)$$

and $\eta_{0,x}$ the zero-viscosity η_0 for process x :

$$\eta_{0,x} = \frac{\sigma_{0,x}}{\dot{\epsilon}_{0,x}^*} \exp\left(\frac{\Delta U_x}{RT}\right) \quad (3.10)$$

Introduction of the stress shift functions a_{σ_x} for process x , defined as:

$$a_{\sigma_x}(\sigma_x) = \frac{(\sigma_x/\sigma_{0,x})}{\sinh(\sigma_x/\sigma_{0,x})} \quad (3.11)$$

for $x = \alpha, \beta$, in Eq. (3.8), finally yields:

$$\eta_x(\sigma_x) = \eta_{0,x} a_{\sigma_x}(\sigma_x); \quad x = \alpha, \beta \quad (3.12)$$

The difference with Chapter 2 is that the viscosity function of a process x no longer depends on the total stress, but only on the part of the total stress contributed by that particular process.

Using these viscosity functions, the nonlinear Maxwell model of Figure 2.4(a) can be adapted to give a representation of the plastic behaviour of a thermorheological complex material. A one-dimensional, two mode mechanical analogy is given in Figure 3.6.

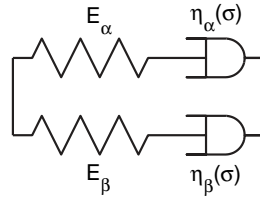


Figure 3.6: Two parallel nonlinear Maxwell elements used to describe the plastic deformation behaviour of a thermorheological complex material.

Or analytically:

$$E(t) = E_{\beta} \exp\left(-\frac{t}{\tau_{\beta}(\sigma_{\beta})}\right) + E_{\alpha} \exp\left(-\frac{t}{\tau_{\alpha}(\sigma_{\alpha})}\right)$$

where $\tau_x(\sigma_x) = (\eta_x(\sigma_x))/E_x$, with $x = \alpha, \beta$. No expression can be obtained for the creep compliance, since the retardation form is based on strain instead of stress additivity.

Using the values for the Eyring parameters tabulated in Table 3.1, the characteristic stresses and zero-viscosities of the model materials are calculated for a temperature of 20 °C, see Table 3.2.

Material	x	$\sigma_{c,x}$ [MPa]	$\eta_{0,x}$ [MPa s]
PC	α	1.259	$1.00 \cdot 10^{22}$
	β	1.325	$6.996 \cdot 10^{-1}$
PMMA	α	2.453	$9.899 \cdot 10^{13}$
	β	3.223	$3.469 \cdot 10^4$
i-PP	α	0.833	$3.403 \cdot 10^{16}$
	β	0.872	$2.419 \cdot 10^5$

Table 3.2: Parameters of the nonlinear viscosity function, Eq. (3.12), for polycarbonate Lexan 161R, polymethylmethacrylate Oroglas V052 and polypropylene Stanyl P46M10 for a reference temperature of 20 °C.

Nonlinear viscoelastic deformation

As for thermorheological simple materials there are a number of similarities between the material's response in the linear viscoelastic and plastic range. The time-dependent deformation is again described using a spectrum of relaxation times, thereby distinguishing between relaxation times caused by a specific transition. Yield is described using two, stress-dependent, Maxwell elements in parallel, indicating stress additivity. Analogous to the thermorheological simple approach, a model for

the complete range is derived by combining the characteristics from both bounding regions. However, unlike in Chapter 2, here there only results a single model since the Kelvin-Voigt model is based on strain additivity, and is therefore not capable of describing the typical yield behaviour. The resulting model is shown in terms of a mechanical model analogy in Figure 3.7.

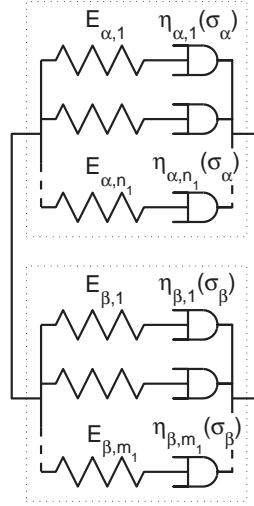


Figure 3.7: Generalized nonlinear Maxwell model, accounting for the presence of two processes.

The matching analytical expression reads:

$$E(t) = \sum_{i=1}^m E_{\beta,i} \exp\left(-\frac{t}{\tau_{\beta,i}(\sigma_{\beta})}\right) + \sum_{j=1}^n E_{\alpha,j} \exp\left(-\frac{t}{\tau_{\alpha,j}(\sigma_{\alpha})}\right)$$

where $\tau_{x,k}(\sigma_x)$ ($= \tau_{x,k} a_{\sigma_x}(\sigma_x)$), index k referring to the k -th Maxwell element of process x , and m and n are the number of elements.

In this representation, the linear viscoelastic and plastic response are again preserved. For low stress levels, the stress shift functions a_{σ_x} equal one, and the linear form follows, whereas for high stresses both shift functions decrease exponentially resulting in two flow contributions as observed in the yield experiments.

In this formulation, each distribution of relaxation times is governed by its own characteristic stress dependence, and for each process separate reduced times can be defined:

$$\psi_x = \int_{-\infty}^t \frac{dt''}{a_{\sigma_x}[\sigma_x(t'')]}; \quad x = \alpha, \beta$$

where a_{σ_x} is the ratio of the relaxation time at a stress σ , and the linear relaxation

time (that is the relaxation time for a stress well below $\sigma_{0,x}$) for process x .

Using the reduced times ψ_x , a stress-strain relation can be formulated separating the stress and time-dependencies of the spectra:

$$\sigma(t) = \int_{-\infty}^t [E_\alpha(\psi_\alpha - \psi'_\alpha) + E_\beta(\psi_\beta - \psi'_\beta)] \dot{\epsilon}(t') dt' \quad (3.13)$$

where

$$\psi_x = \int_{-\infty}^t \frac{dt''}{a_{\sigma_x}[\sigma_x(t'')]} \quad \text{and} \quad \psi'_x = \int_{-\infty}^{t'} \frac{dt''}{a_{\sigma_x}[\sigma_x(t'')]}$$

and, $E_x(t)$ is the linear relaxation time spectrum for process x ($= \alpha, \beta$).

Before performing any calculations, the material parameters have to be determined; in this case it concerns the linear relaxation spectra $E_x(t)$, and the characteristic stresses $\sigma_{0,x}$. In the previous chapter the relevant parameters were determined using time-stress superposition, the applicability of which is questionable in this case since both spectra have different stress dependencies. Analogous to time-temperature superposition this can lead to a potential breakdown of the superposition principle. The comparison to temperature is, however, not entirely valid since the stress shift functions are not governed by the total applied stress, but only a part of the total stress. To understand the possible consequences of this difference for the characterization of a polymer material, a numerical investigation was undertaken, using the previously obtained stress-strain relation, Eq. (3.13).

3.4 Numerical investigation

To investigate the consequences of the enhanced model for the characterization strategy followed in the previous chapter, creep experiments are numerically simulated. For this purpose, we first generate suitable relaxation spectra; second numerical calculations of creep experiments at various loads are performed leading, third, to conclusions regarding the characterization strategy employed previously.

Model parameters

For numerical simulations, two characteristic stresses and two linear Maxwell spectra are required. In contrast to the linear spectra, the characteristic stresses can also be obtained from yield experiments. Here, the values for PMMA determined in section 3.3 are used for further calculations. Since the spectra can not be determined experimentally using time-stress superposition, they will be generated numerically.

To ensure that the simulations are as realistic as possible these spectra have to satisfy the following three conditions:

1. the zero-viscosity values for both the α - and β -spectrum should match the values for polymethylmethacrylate obtained from the yield experiments in section 3.3;
2. from DMTA experiments it follows that the initial modulus of the α -contribution should be approximately twice as large as the initial modulus due to the β -process;
3. the spectra should produce plastic flow within 5 to 6 % strain.

To obtain suitable spectra for the numerical simulations, the spectrum for polycarbonate determined in Chapter 2 was used as a starting point. This spectrum was then shifted both horizontally and vertically, until correct values for the viscosities and moduli were obtained. The resulting discrete spectra for the α and β -process are shown in Figure 3.8, whereas the numerical values are listed in Appendix 3.A. It should, however, be kept in mind that both are actually *virtual* spectra.

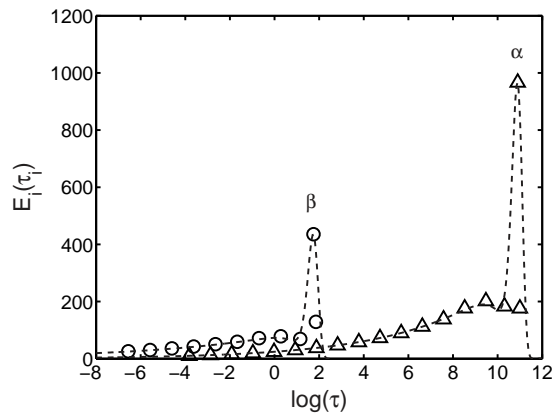


Figure 3.8: Numerically generated α and β spectrum, symbols indicate the actual discrete spectra, dashed lines are continuous approximations used for illustration purposes.

The first two conditions are satisfied by the spectra shown in Figure 3.8, while the third is verified by simulating tensile tests at strain rates varying from 10^{-10} till 10^{-1} s^{-1} . For this purpose Eq. (3.13) is solved using an iterative procedure. The resulting stress-strain curves, Figure 3.9(a), show that for all strain-rates plastic flow is established well within the required 6% strain. Furthermore, at a strain rate of approximately 10^{-5} s^{-1} there is an acceleration in the increase of the yield stress with strain rate due to the β -contribution. This can be visualized more clearly by plotting the resulting yield stresses against the strain-rate applied (Figure 3.9(b)). Comparison to the analytically calculated yield stress using Eq. (3.4) shows an excellent agreement.

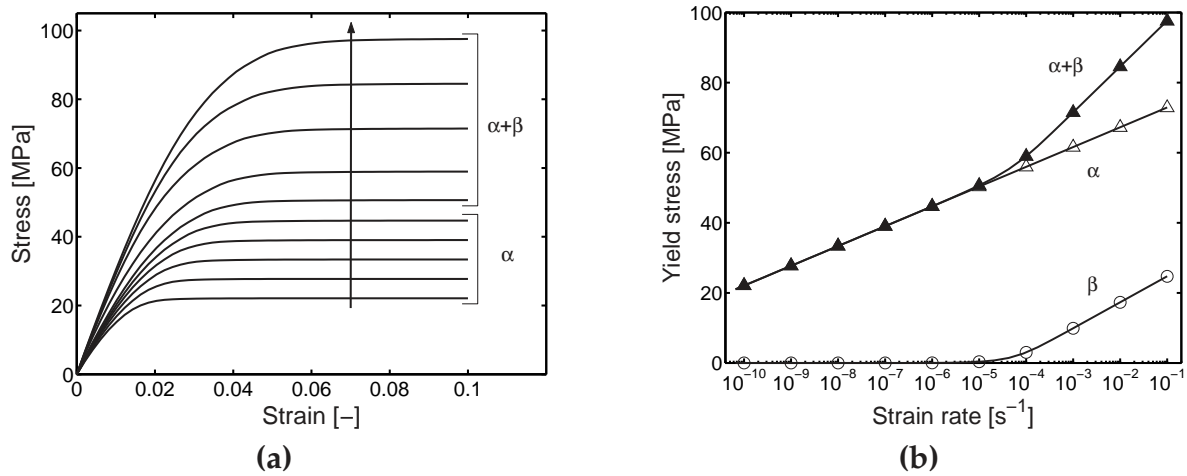


Figure 3.9: (a) Calculated tensile stresses for log-equidistant strain rates from 10^{-10} to 10^{-1} s^{-1} (the arrow indicates an increasing strain rate). (b) Yield stress versus applied strain rate, symbols indicate the values from the numerical tensile tests in (a), the solid line is the analytical solution (Eq. (3.4)).

The results show that the spectra lead to the desired response, and will therefore be used for further calculations.

Numerical creep simulations

Using the discrete spectra shown in Figure 3.8, together with the values for the characteristic stress from section 3.3, Eq. (3.13) was solved numerically for constant load levels from 5 to 75 MPa and room temperature. Each load was applied in 10^{-2} s , and the length of the time scale used for the calculations was chosen such that a constant creep-rate was reached for each load. The resulting calculated creep compliance curves are shown in Figure 3.10.

Compared to the observations from section 3.3, the lower stress levels show the expected behaviour, initially elastic, followed by time-dependent creep ending with a marked transition where the β -process starts to flow. A constant plateau creep-rate is not established however, since at this stage the plastic flow is rapidly stabilized due to the comparatively small drop in modulus. The subsequent time-dependent creep is exclusively due to the α -process, finally resulting in flow of the α -process, which in this numerical exercise is not stabilized as the rubber contribution was neglected. For the higher stress levels an increased merger of both processes can be observed, which ultimately results in the complete disappearance of the transition. This type of behaviour is reported for polypropylene at a temperature of 60°C by Cessna [10], and for polyethylene at room temperature by Beijer and Spoormaker [11]. No references were found for PMMA, most probably due to the location of the transition at fairly short times.

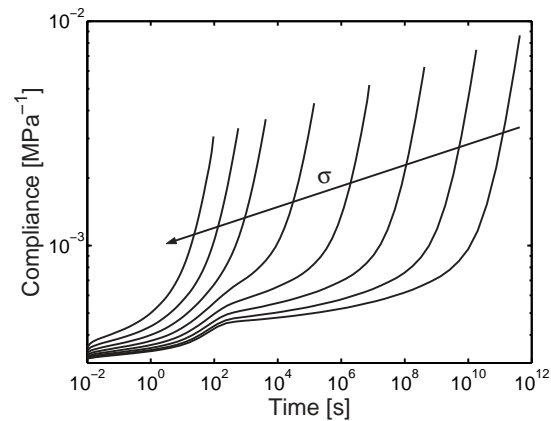


Figure 3.10: Calculated creep compliance versus time for equidistantly distributed stress levels from 5 to 75 MPa (the arrow indicates the direction of increasing stress) and room temperature (20 °C).

A remarkable result of the numerical simulations is that the position of the β -transition on the time axis appears to be independent of the applied stress, where it might be expected to shift to shorter times with increasing stress. This apparent contradiction can, however, be explained when looking more closely to the development of stress for both processes (Figure 3.11).

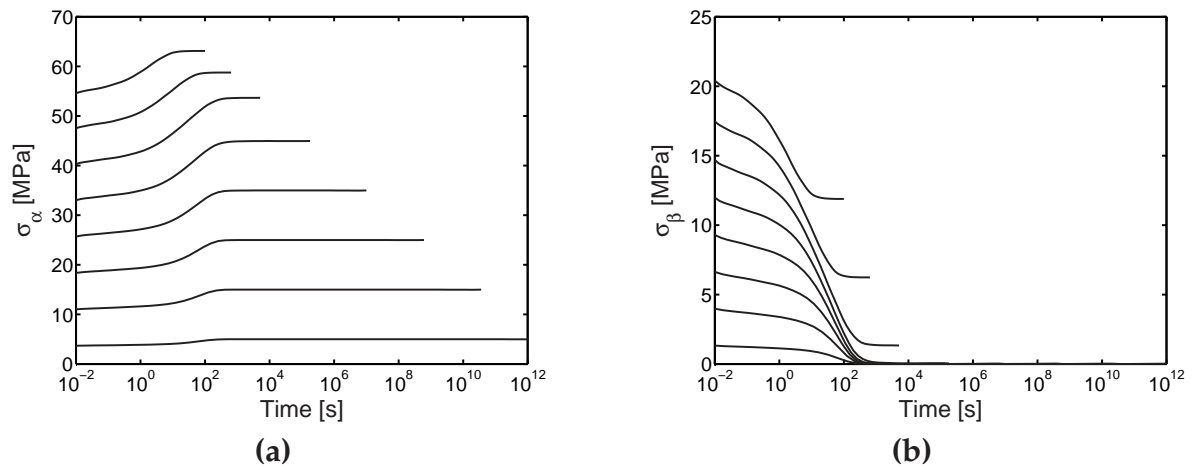


Figure 3.11: Development of stress in the α -spectrum (a), and the β -spectrum (b), for creep tests at loads from 5 to 75 MPa.

After an initial increase in both stresses upon loading, the β -contribution to the total stress starts to decrease due to relaxation, thus automatically increasing the α -contribution since the total stress applied is constant. For the lower stress levels this process ends when the stress in the β -contribution reaches zero implying that the β -spectrum has returned to its linear representation ($a_{\sigma_\beta}(0)=1$). As a consequence, the position of the transition will be independent of stress and, therefore, will always

be observed at the same time. This process is illustrated in Figure 3.12 for a stress of 15 MPa, by means of the shape of the overall spectrum at two different times during a creep experiment.

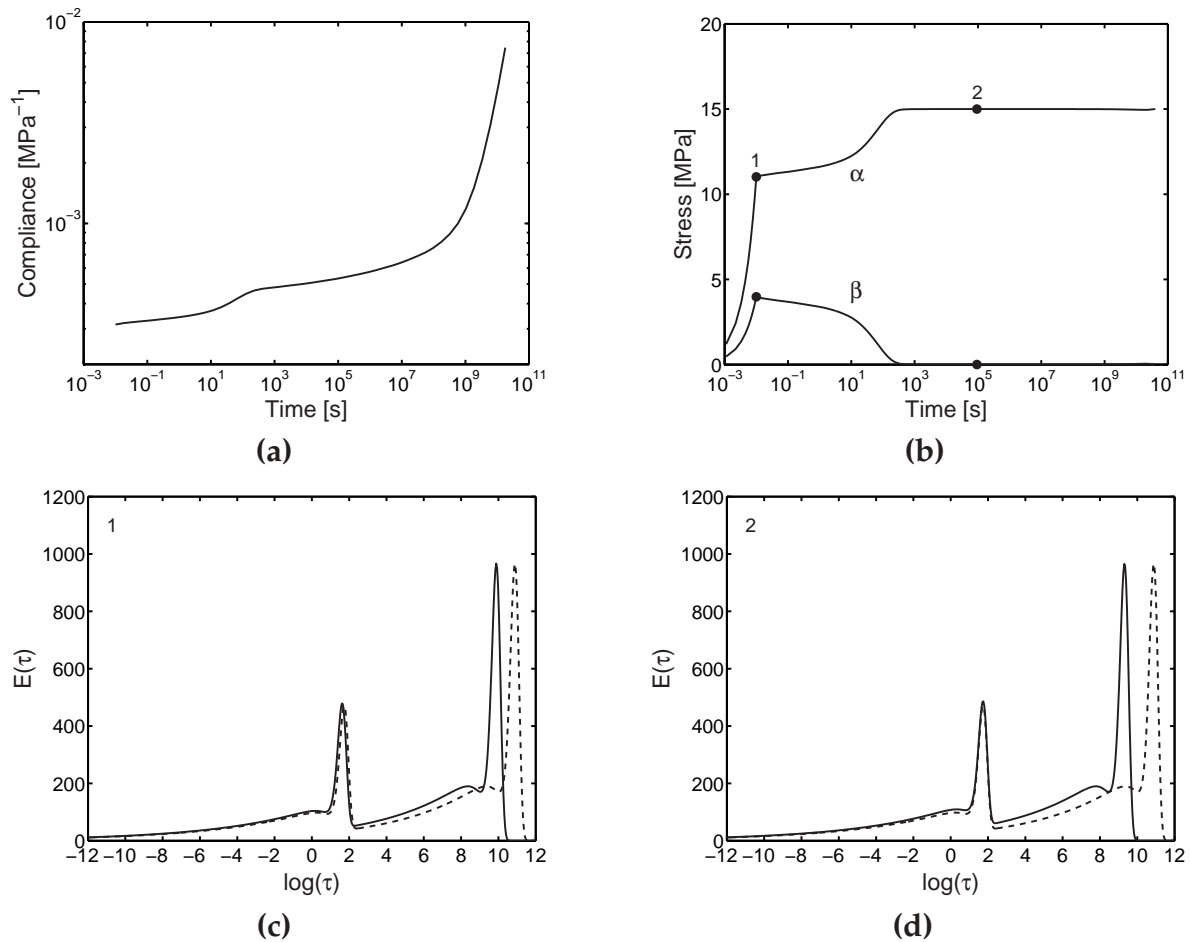


Figure 3.12: Creep compliance versus time for a stress level of 15 MPa (a). Development of the stress in both α and β -process (b). Shape of the total spectrum on the times indicated in (b), where the dotted line indicates the initial spectrum before load is applied, and the solid lines the momentary spectra ((c) and (d)).

As the applied stress is increased, it reaches a level at which the β -process can no longer completely relax to zero stress, since at that level the time scale of the α -process approaches that of the β -process. This level is the stress at which the transition in Figure 3.10 is no longer visible since both spectra have merged. This process is shown in Figure 3.13, again in terms of the shape of the spectrum at two different stages of a creep experiment at a stress of 75 MPa.

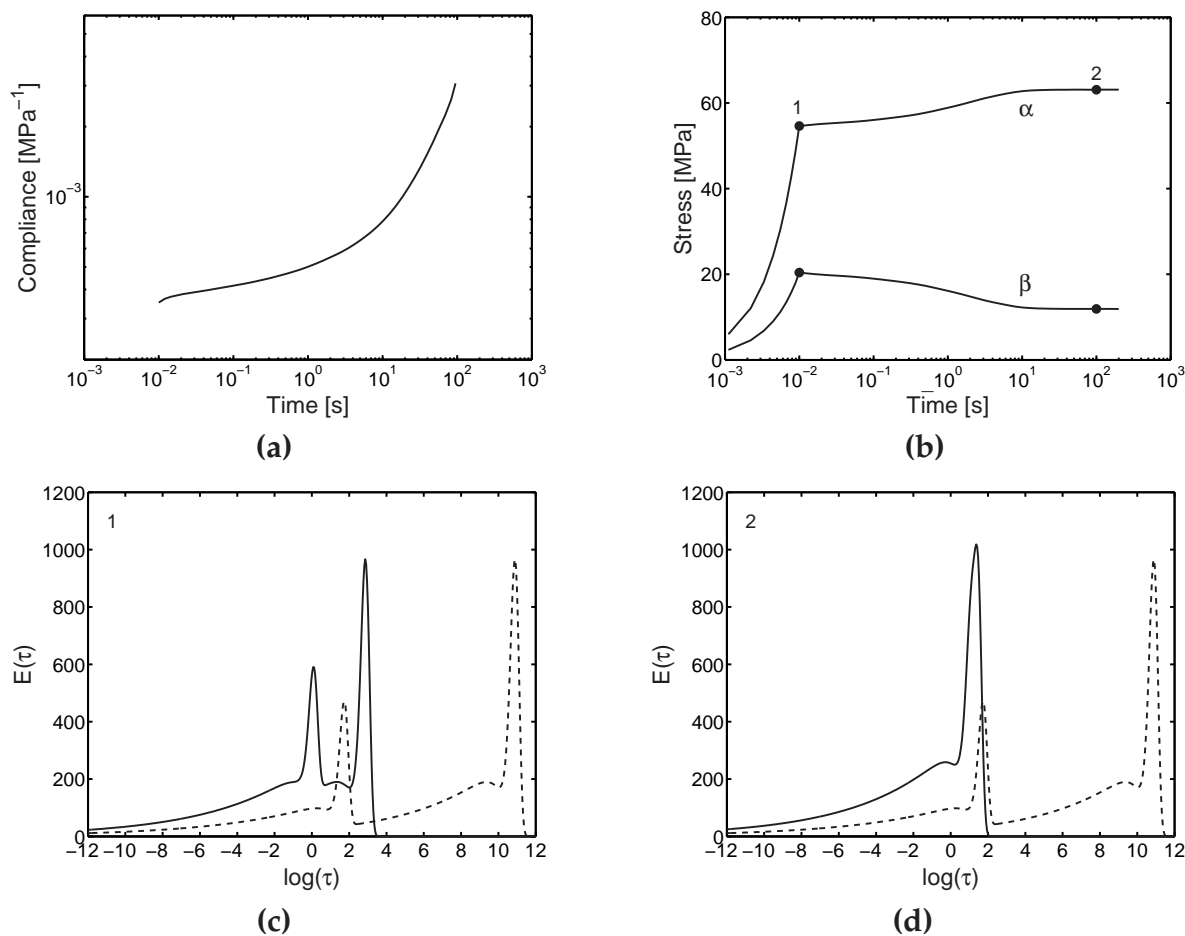


Figure 3.13: Creep compliance versus time for a stress level of 75 MPa (a). Development of the stress in both α and β -process (b). Shape of the spectrum on the times indicated in (b), where the dotted line indicates the initial spectrum before load is applied, and the solid lines the momentary spectra ((c) and (d)).

The fact that the β -process does not completely relax at higher loads indicates that it also has a contribution to the final flow behaviour. This can be demonstrated by plotting the applied creep stress against the established plateau creep-rates, which can be determined using Sherby-Dorn plots [12]. Figure 3.14 shows that this is indeed the case, and that the final flow matches the yield behaviour calculated analytically using Eq. (3.4).

The conclusion that the absence of a β -contribution to the flow behaviour at the lower stress levels implies an absence of the β -process at these stresses, is certainly not true, since both Figures 3.10 and 3.11 show the presence of the β -process, but only at short times.

To demonstrate the difference between the behaviour of a thermorheological com-

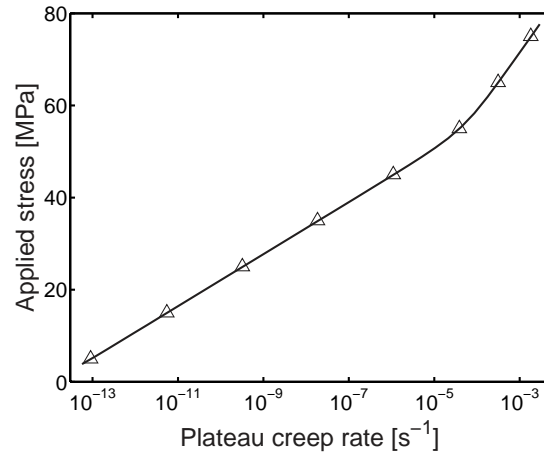


Figure 3.14: Applied stress versus the plateau creep-rate determined from Figure 3.10 (symbols), compared to the analytically calculated yield behaviour according to Eq. (3.4) (solid line).

plex material under constant stress and that under constant temperature, numerical simulations of creep tests at various temperatures are performed, using the temperature dependencies determined for PMMA (Table 3.1). The results are shown in Figure 3.15.

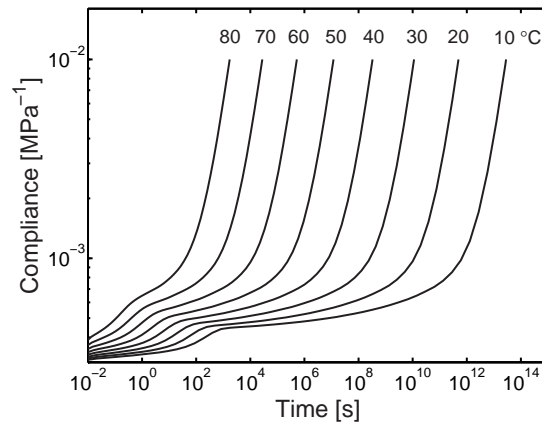


Figure 3.15: Calculated creep compliance versus time at temperatures from 10 to 80 °C and a load of 5 MPa.

The difference with the constant stress experiments at a constant temperature, Figure 3.10, is clear, since now both contributions shift to shorter times as temperature increases. In contrast, for increasing stress the spectra moved in opposite directions due to relaxation of the β -process. Furthermore, the simulations show that as temperature increases the so-called relaxed β -compliance, $D_{R\beta}$ (see Figure 3.4), increases, which is in agreement with observations by Tomlins *et al.* [13] and Read *et al.* [14]. However, they attribute this increase to the β -process, whereas in our approach it

finds its origin in the α -mechanism. More precisely, it is due to the stronger temperature dependence of the α -process, which therefore moves faster to shorter times than the β -process.

Consequences for characterization

Even though the linear spectra used for the calculations in the previous section should be regarded as virtual, and are likely to have an influence on the course of creep deformation, a good qualitative agreement with experimental observations in literature is obtained. From the creep data numerically predicted at different loads (Figure 3.10), it is evident that a superposition of complete curves, as was used in Chapter 2, is no longer possible. In this particular case, however, there is a limited applicability of time-stress superposition for times larger than the fixed transition time, since that range is exclusively controlled by the primary process. Crissman and McKenna successfully applied time-stress superposition to experimental creep data of PMMA at intermediate loads (30-60 MPa) [15, 16]. The characteristic stress that can be calculated from their shift data, 2.2 MPa, agrees well with the value found from yield data for the α -process, and that was used for the numerical creep simulations (2.45 MPa). From our results it is also evident that only an extrapolation towards longer times is valid, since an extrapolation to shorter times, as reported by Crissman and McKenna [15], would lead to a severe over-prediction of creep, due to the presence of the β -process at short times. This was also pointed out by Cessna for extrapolation towards longer times, when applying time-stress superposition to the range below the transition (combined α and β) in his case for i-PP at room temperature and, subsequently, at 60 °C [10].

From this it can be concluded that, depending on the material, temperature and loads applied, a limited time-stress superposition may still be applicable and will result in either a single or combined spectrum, which should be used with great care (particularly when extrapolating towards another range). To allow for a more general use, the separate spectra have to be determined by isolating their contributions to the deformation. From the numerical simulations it is clear that this is best done in the linear viscoelastic range where there will be no acceleration of the time scale due to stress. Consequently, it is essential that the experiments cover a time interval that is as large as possible, thereby including the transition zone [1]. This can be achieved by combining different experimental techniques [17, 18], or using temperature to accelerate, or even decelerate, the time scale. Due to the thermorheological complexity of the material changing the temperature is, however, likely to introduce additional problems such as, for example, the necessity for vertical shifts.

If it is not possible to completely eliminate the overlap between contributions of different molecular processes, it will be necessary to make assumptions regarding

the shape of at least one of the contributions in the overlapping range, for instance, Nakayasu *et al.* assume that the β -contribution is symmetrical [4]. The same assumption is made by Read [1], whose model also assumes that there is no α -contribution in the β -range, while the β -contribution in the α -range is constant.

Since either route will also comprise long term measurements, the effects of physical aging can no longer be avoided and should be accounted for. This aspect is subject of our investigation in Chapter 5.

3.5 Conclusions

Since most polymers exhibit multiple transitions, the approach of Chapter 2 is extended to account for an additional molecular process. The contribution of this additional process to the linear viscoelastic deformation can be modelled by either two processes in parallel or in series. Plastic flow can only be modelled by assuming stress additivity, that is, by means of two parallel processes (two groups of Maxwell elements). This results in an extension of the model derived in Chapter 2 to incorporate two linear relaxation time spectra in parallel, each governed by its own characteristic stress and temperature dependence. While the influence of temperature and stress is comparable in a thermorheological simple material, in a thermorheological complex material it is not, because the spectra depend on a part of the total stress rather than the total stress. Numerical calculations of a tensile test at various strain rates show that the plastic deformation predicted by the model agrees well with that observed in practice. Further, numerical simulations of creep experiments at various stress levels and temperatures show a good qualitative agreement with experimental results concerning the linear viscoelastic and temperature dependent deformation reported in literature.

References

- [1] Read, B.E. (1991). Analysis of creep and physical aging in glassy polymers. *J. Non-Cryst. Solids*, **131-133**, 408-419.
- [2] Read, B.E. (1987). Dynamic mechanical and creep studies of PMMA in the α - and β -relaxation regions. Physical ageing effects and non-linear behaviour. In Dorfmueller and Williams, editors, *Molecular dynamics and relaxation phenomena in glasses*, page 61-74. Springer, Berlin.
- [3] Chai, C.K., McCrum, N.G. (1984). The freezing-in of non-equilibrium values of the limiting compliances as a mechanism of physical aging. *Polymer*, **25**, 291-298.
- [4] Nakayasu, H., Markovitz, H., Plazek, D.J. (1961). The frequency and temperature dependence of the dynamic mechanical properties of a high density polyethylene. *Trans. Soc. Rheol.*, **5**, 261-283.

- [5] Roetling, J.A. (1965). Yield stress behaviour of poly(methyl methacrylate). *Polymer*, **6**, 311-317.
- [6] Bauwens-Crowet, C., Bauwens, J.-C., Homès, G. (1969). Tensile yield-stress behavior of glassy polymers. *J. Pol. Sci. Part A-2*, **7**, 735-742.
- [7] Ree, T. and Eyring, H. (1955). Theory of non-Newtonian flow. I. Solid plastic system. *J. Appl. Phys.*, **26**, 793-800.
- [8] Bauwens-Crowet, C., Bauwens, J.-C., Homès, G. (1972). The temperature dependence of yield of polycarbonate in uniaxial compression and tensile tests. *J. Mat. Sci.*, **7**, 176-183.
- [9] Roetling, J.A. (1966). Yield stress behaviour of isotactic polypropylene. *Polymer*, **7**, 303-307.
- [10] Cessna, L.C. (1971). Stress-time superposition of creep data for polypropylene and coupled glass-reinforced polypropylene. *Pol. Eng. Sci.*, **11**, 211-219.
- [11] Beijer, J.G.J., Spoormaker, J.L. (2000). Modelling of creep behaviour in injection-moulded HDPE. *Polymer*, **41**, 5443-5449.
- [12] Sherby, O.D., Dorn, J.E. (1958). Anelastic creep of polymethyl methacrylate. *J. Mech. Phys. Solids*, **6**, 145-162.
- [13] Tomlins, P.E., Read, B.E., Dean, G.D. (1994). The effect of temperature on creep and physical aging of poly(vinyl chloride). *Polymer*, **35**, 4376-4381.
- [14] Read, B.E., Dean, G.D., Tomlins, P.E. (1994). Creep and physical aging of PVC: dependence on stress and temperature. *J. Non-Cryst. Solids*, **172-174**, 562-568.
- [15] Crissman, J.M., McKenna, G.B. (1987). Relating creep and creep rupture in PMMA using a reduced variable approach. *J. Pol. Sci.: Part B: Pol. Phys.*, **25**, 1667-1677.
- [16] Crissman, J.M., McKenna, G.B. (1990). Physical and chemical aging in PMMA and their effects on creep and creep rupture behavior. *J. Pol. Sci.: Part B: Pol. Phys.*, **28**, 1463-1473.
- [17] Read, B.E. (1981). Influence of stress state and temperature on secondary relaxations in polymer glasses. *Polymer*, **22**, 1580-1586.
- [18] Read, B.E., Duncan, J.C. (1981). Measurement of dynamic properties of polymeric glasses for different modes of deformation. *Polymer Testing*, **2**, 135-150.

3.A Appendix: numerical spectra

For the numerical calculations two discrete spectra have been constructed, using the shape of the previously obtained Maxwell spectrum for polycarbonate as a starting point. This is then shifted horizontally and vertically until it satisfies the requirements imposed by viscosity and modulus. The resulting parameter values of the discrete linear α - and β -Maxwell spectrum are listed in Table 3.3.

i	$\tau_{\beta,i}$ [s]	$E_{\beta,i}$ [MPa]	j	$\tau_{\alpha,j}$ [s]	$E_{\alpha,j}$ [MPa]
1	$2.78 \cdot 10^{-7}$	25.7	1	$1.52 \cdot 10^{-4}$	10.1
2	$2.63 \cdot 10^{-6}$	30.5	2	$1.35 \cdot 10^{-3}$	12.6
3	$2.50 \cdot 10^{-5}$	36.0	3	$1.20 \cdot 10^{-2}$	15.6
4	$2.37 \cdot 10^{-4}$	42.5	4	$1.10 \cdot 10^{-1}$	19.5
5	$2.24 \cdot 10^{-3}$	50.6	5	$9.53 \cdot 10^{-1}$	24.2
6	$2.13 \cdot 10^{-2}$	59.2	6	$8.49 \cdot 10^0$	30.1
7	$2.02 \cdot 10^{-1}$	71.8	7	$7.56 \cdot 10^1$	37.5
8	$1.91 \cdot 10^0$	78.2	8	$6.74 \cdot 10^2$	46.7
9	$1.42 \cdot 10^1$	69.0	9	$6.00 \cdot 10^3$	58.0
10	$5.58 \cdot 10^1$	435.7	10	$5.35 \cdot 10^4$	72.3
11	$7.16 \cdot 10^1$	128.9	11	$4.76 \cdot 10^5$	89.7
			12	$4.24 \cdot 10^6$	11.2
			13	$3.78 \cdot 10^7$	138.0
			14	$3.37 \cdot 10^8$	176.2
			15	$3.00 \cdot 10^9$	201.6
			16	$2.04 \cdot 10^{10}$	183.0
			17	$7.97 \cdot 10^{10}$	966.4
			18	$9.99 \cdot 10^{10}$	176.0

Table 3.3: Parameter values for the generated discrete α - and β -spectrum.

Verification of the boundary conditions imposed on the spectra:

- $\eta_{0,\alpha} = \sum_{j=1}^{18} \tau_{\alpha,j} \cdot E_{\alpha,j} = 9.899 \cdot 10^{13}$ MPa s, and
- $\eta_{0,\beta} = \sum_{i=1}^{11} \tau_{\beta,i} \cdot E_{\beta,i} = 3.4695 \cdot 10^4$ MPa s,

whereas the ratio of the moduli yields

$$\frac{E_{0,\alpha}}{E_{0,\beta}} = \frac{\sum_{j=1}^{18} E_{\alpha,j}}{\sum_{i=1}^{11} E_{\beta,i}} = 2.3$$

The viscosity values match the values obtained in Chapter 3 for PMMA (Table 3.2), and the ratio of the moduli is approximately 2.

Post-yield response of glassy polymers: influence of thermorheological complexity

4.1 Introduction

In Chapter 2 the deformation of a thermorheological simple material, i.e. a material with a single relaxation mechanism actively contributing to the deformation, was investigated. It was shown that up to the yield point the deformation can be described using a single, stress- and temperature activated, spectrum of relaxation times. For strains larger than the strain-at-yield, this approach predicts a constant (true) flow stress. In reality, the stress beyond the yield point decreases due to strain softening, and with further deformation molecular orientation causes the stress to rise again (strain hardening).

While the influences of strain softening and hardening may be neglected at small strains, they play a key-role in the initiation, growth and stabilization of strain localization involving large (local) strains. Localization depends on the balance between the amounts of softening and hardening, and determines whether the material behaves macroscopically ductile or brittle. The amount of softening can be expressed as the yield drop, i.e. the decrease in stress following the yield point, and is influenced by the thermomechanical history. Increasing the softening induces embrittlement, while a reduction promotes ductile deformation [1].

Accurate numerical predictions of strain localizations in solid polymers required the development of a separate class of large strain constitutive models. Most present models are based on the original approach by Haward and Thackray of 1968 [2],

who distinguished two main contributions to the large strain deformation; a stress induced plastic flow, and deformation induced molecular orientation, whereas the initial deformation was assumed linear elastic. Later, this approach was extended to full 3D representations including pressure dependent flow and softening by Boyce *et al.* [3], Govaert *et al.* [4], and Buckley *et al.* [5, 6]. A common feature of all these models is that they use a single, stress activated, relaxation time to describe the plastic deformation process, similar to the approach presented for plastic flow in Chapter 2. As such, these models can be classified as representing the large strain deformation of thermorheological simple materials.

In Chapter 1 it was pointed out that many polymer materials behave thermorheological complex, in which case there are additional contributions to the deformation due to e.g. secondary relaxation mechanisms. It may thus be concluded that the constitutive models mentioned above can not adequately describe the (strain rate dependence of the) yield stress of these materials. It was demonstrated in Chapter 3 that the description of small strain responses could be improved by adding an extra flow element, generally with a different stress dependence, in parallel (stress additivity). Although an extension towards large strain models seems straightforward following this same approach, the introduction of an additional flow element may have unforeseen implications for the post-yield behaviour.

To verify potential implications for the post-yield deformation, the intrinsic stress-strain response of both thermorheological simple and complex materials is investigated. First, the response of a large strain model for a thermorheological simple material is discussed, and applied to experimental data of a suitable model material, polycarbonate (PC). Subsequently, this model is enhanced with a second process along the lines derived in Chapter 3. Since no prior knowledge exists about the presence of softening in this additional contribution, two cases are considered; one with and one without softening. Both these cases are compared to experimentally obtained data for a thermorheological complex material, polymethylmethacrylate (PMMA).

4.2 Experimental

Materials

Two different materials were used: polycarbonate (General Electric, Lexan 121R), supplied as granules, and polymethylmethacrylate (Röhm GmbH, Plexiglas, type unknown) supplied as 6 mm diameter extruded rod. Molecular weight distributions were determined using gel permeation chromatography (GPC) and the resulting number-averaged and weight-averaged molecular weights are tabulated in Table 4.1.

Material	M_n [kg/mol]	M_w [kg/mol]
Lexan 121R	9.8	23.4
Plexiglas	35.9	123.8

Table 4.1: *Number-averaged and weight-averaged molecular weights of the polycarbonate and polymethylmethacrylate used in this study measured with respect to a PC and PMMA-standard, respectively.*

For uniaxial compression tests, cylindrical samples ($\varnothing 6 \text{ mm} \times 6 \text{ mm}$) were machined from either the extruded rod, or plates ($200 \times 200 \times 10 \text{ mm}^3$) that were compression moulded from granular material at a temperature of $250 \text{ }^\circ\text{C}$. First the dried granulate was heated for 15 minutes and next compressed up to 300 kN in five subsequent intervals of 5 minutes. After each step the force was released to allow for degassing. Finally, the mould was placed in a cold press and cooled to room temperature ($20 \text{ }^\circ\text{C}$) under a moderate force (100 kN). Prior to machining the extruded rod was heated to $120 \text{ }^\circ\text{C}$ for half an hour, and then cooled rapidly to room temperature to remove any orientation caused by the extrusion process.

Mechanical testing

Uniaxial compression tests were performed on a servo-hydraulic MTS Elastomer Testing System 810. The cylindrical shaped specimens were compressed under true strain control, at constant true strain rates of 10^{-5} to 10^{-1} s^{-1} between two parallel, flat steel plates. Friction between samples and plates was reduced by an empirically optimized method. Onto the sample a thin film of PTFE tape (3M 5480, PTFE skived film tape) was applied and the contact area between steel and tape was lubricated using a 1:1 mixture of liquid soap and water. During the test no bulging of the sample was observed, indicating that the friction was sufficiently reduced. True stresses were calculated under the assumption that the sample volume remains constant during deformation.

4.3 Thermorheological simple materials

Constitutive modelling

In Chapter 2, it was demonstrated that the deformation up to yield of a thermorheological simple material can be described using a spectrum of stress-activated relaxation times. At the yield point all the modes of the spectrum flow simultaneously and can be replaced by a single stress-activated viscosity, which for large strains displays the same response as the initial spectrum. For the description of large deformations, where the pre-yield range is considered less important, the spectrum is, therefore, generally replaced by a single mode representation.

A 3D version of such a stress-dependent, compressible, single mode model suitable for large deformations was derived by Tervoort *et al.* [7], separating the volume and deviatoric responses. The volume response is assumed to be linear elastic, while the deviatoric response is elasto-viscoplastic. The plastic deformation is controlled by a non-Newtonian flow rule with a 3D stress-dependent Eyring viscosity [7].

Although this model accurately describes the characteristic strain rate dependence of plastic flow in polymers, it lacks several important features in the post-yield description such as strain softening and strain hardening. These features, as well as pressure dependence, were included by Govaert *et al.* [4]. In this extended model the total Cauchy stress is the sum of the driving stress σ_s and the hardening stress σ_r :

$$\boldsymbol{\sigma} = \boldsymbol{\sigma}_s + \boldsymbol{\sigma}_r \quad (4.1)$$

The hardening stress is described by a simple neo-Hookean relation [8]:

$$\boldsymbol{\sigma}_r = G_r \tilde{\mathbf{B}}^d \quad (4.2)$$

where G_r is the strain hardening modulus and $\tilde{\mathbf{B}}^d$ the deviatoric part of the isochoric left Cauchy-Green deformation tensor.

The driving stress is decomposed into a deviatoric stress $\boldsymbol{\sigma}_s^d$, and a hydrostatic stress $\boldsymbol{\sigma}_s^h$:

$$\boldsymbol{\sigma}_s^d = G \tilde{\mathbf{B}}_e^d \quad \text{and} \quad \boldsymbol{\sigma}_s^h = \kappa(J - 1)\mathbf{I} \quad (4.3)$$

where G is the shear modulus, $\tilde{\mathbf{B}}_e^d$ the deviatoric part of the isochoric elastic left Cauchy-Green strain tensor, κ the bulk modulus, J the volume change factor, and \mathbf{I} the unity tensor. Superscripts d and h denote, respectively, the *deviatoric* and *hydrostatic* part. J and $\tilde{\mathbf{B}}_e$ are given by the following evolution equations:

$$\dot{J} = J \text{tr}(\mathbf{D}) \quad (4.4)$$

$$\overset{\circ}{\tilde{\mathbf{B}}}_e = (\mathbf{D}^d - \mathbf{D}_p) \cdot \tilde{\mathbf{B}}_e + \tilde{\mathbf{B}}_e \cdot (\mathbf{D}^d - \mathbf{D}_p) \quad (4.5)$$

where $\overset{\circ}{\tilde{\mathbf{B}}}_e$ is the Jaumann rate of $\tilde{\mathbf{B}}_e$, \mathbf{D}^d the deviatoric part of the rate of deformation tensor, and \mathbf{D}_p the plastic part of the rate of deformation tensor. Subscripts e , and p indicate, respectively, the use of an *elastic*, and *plastic* quantity.

A non-Newtonian flow rule with a stress-dependent Eyring viscosity is used to relate

the plastic deformation rate tensor, \mathbf{D}_p , to the deviatoric driving stress, $\boldsymbol{\sigma}_s^d$ [7]:

$$\mathbf{D}_p = \frac{\boldsymbol{\sigma}_s^d}{2\eta(T, p, \bar{\tau}, D)} \quad (4.6)$$

The viscosity η strongly depends on the equivalent stress $\bar{\tau}$ and was originally described by an Eyring relationship [7]. Subsequently, pressure dependence (μ) and intrinsic strain softening (D) were incorporated in the viscosity function [4]:

$$\eta(T, p, \bar{\tau}, D) = A_0(T)\tau_0 \exp\left(\frac{\mu p}{\tau_0}\right) \frac{\bar{\tau}/\tau_0}{\sinh(\bar{\tau}/\tau_0)} \exp(-D) \quad (4.7)$$

where the temperature dependent pre-exponential factor $A_0(T)$ equals:

$$A_0(T) = A_0 \exp\left(\frac{\Delta U}{RT}\right) \quad (4.8)$$

with A_0 a constant, ΔU the activation energy, R the gas constant, and T the absolute temperature. The characteristic stress τ_0 , pressure p , and equivalent stress $\bar{\tau}$ are defined as:

$$\tau_0 = \frac{kT}{V^*} \quad (4.9)$$

$$p = -\frac{1}{3}\text{tr}(\boldsymbol{\sigma}) \quad (4.10)$$

$$\bar{\tau} = \sqrt{\frac{1}{2}\text{tr}(\boldsymbol{\sigma}_s^d \cdot \boldsymbol{\sigma}_s^d)} \quad (4.11)$$

with V^* the activation volume and k Boltzmann's constant.

The intrinsic strain softening is represented by the (structural) parameter D , that evolves from an initial value D_0 to an equilibrium value $D_\infty > D_0$ with increasing equivalent plastic strain $\bar{\gamma}_p$ thereby strongly reducing the material's viscosity η . Hasan *et al.* [9] suggested a first order evolution equation for the change in D :

$$\dot{D} = h \left(1 - \frac{D}{D_\infty}\right) \dot{\bar{\gamma}}_p \quad (4.12)$$

where h determines the initial softening rate, and the equivalent plastic strain rate, $\dot{\bar{\gamma}}_p$, is provided by the following equation:

$$\dot{\bar{\gamma}}_p = \sqrt{2 \text{tr}(\mathbf{D}_p \cdot \mathbf{D}_p)} \quad (4.13)$$

In the original equation proposed by Hasan *et al.* [9] the parameter D represents the *density of shear transformation sites*, which is derived from Positron Annihilation

Lifetime Spectroscopy (PALS) measurements. Since the initial value D_0 depends on the thermal history a new value has to be determined for each sample with a different thermal history using either PALS measurements or a numerical fit. To circumvent this Govaert *et al.* [4] approached the parameter D as a fitting parameter, using for zero plastic strain a value of 0, which leaves only D_∞ to be determined from a fit.

Application to polycarbonate

The constitutive model describes the true stress-strain behaviour of a polymer material. Experimentally, this intrinsic deformation can only be determined in special loading geometries that allow for homogeneous deformation, suppressing strain localization phenomena, such as crazes, shear bands, and necks. An example of such a loading geometry is uniaxial compression. The results of uniaxial compression tests at different true strain-rates on the thermorheological simple model material, polycarbonate, are shown in Figure 4.1(a). Initially, the deformation is nonlinear viscoelastic until a maximum stress, the yield stress, is reached, after which the stress decreases due to softening and eventually increases again due to entropic hardening. Over the range of strain rates studied, the yield stress increases linearly with strain rate, see Figure 4.1(b). The lowest stress after yield, denoted as “lower yield”, has the same strain rate dependence as the yield stress. Consequently, the yield drop, here defined as the difference between the yield stress and the lower yield stress, is independent of strain rate.

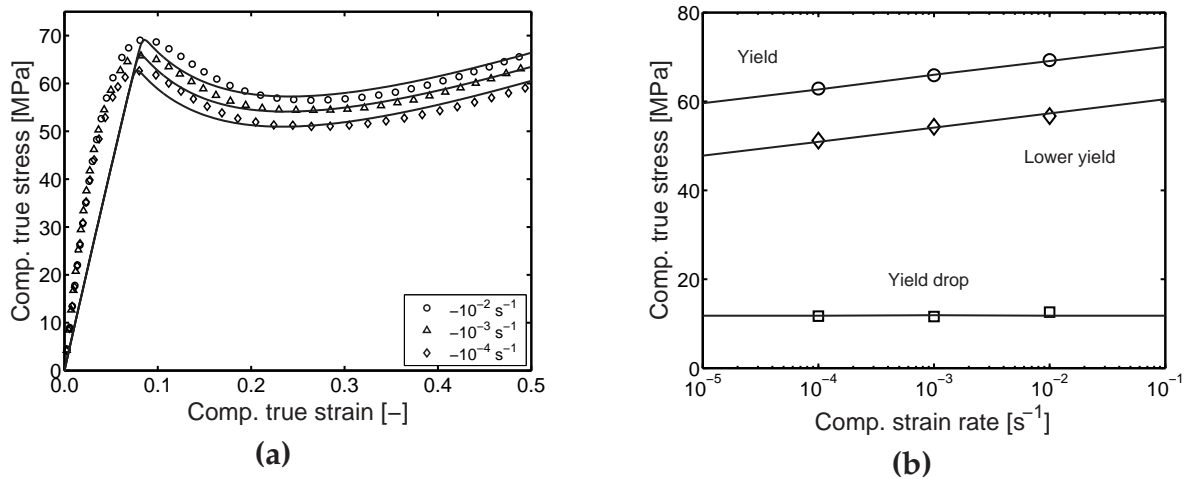


Figure 4.1: (a) Compression tests on polycarbonate at different true strain rates and room temperature (23 °C). (b) Yield stress, lower yield stress, and yield drop versus strain rate determined from Figure 4.1(a). Symbols: experiments; lines: model prediction.

To verify how well the model captures the experimentally determined post-yield deformation and its strain rate dependence, the model response is fitted to the

experimental data. From these experimental data the pressure dependence μ and Poisson ratio ν can not be determined directly, and they are therefore adopted from literature. A value of 0.07 is taken for the pressure dependence [4], and 0.4 for the Poisson ratio [7]. In addition, the strain hardening modulus is set to 26 MPa, a value determined by Tervoort and Govaert from three different loading geometries [8].

To determine the remaining parameters the constitutive relation is solved numerically for uniaxial compression at different true strain-rates under the assumption of a homogeneous stress distribution and constant temperature. With the parameters tabulated in Table 4.2 the calculated results (lines in Figure 4.1(a)) are obtained.

E [MPa]	ν	A_0 [s]	τ_0 [MPa]	μ	D_∞	h	G_r [MPa]
800	0.4	$2.0 \cdot 10^{23}$	0.7	0.07	26.1	145	26

Table 4.2: Material parameters obtained from fitting the constant strain-rate compression data at room temperature (23 °C) in Figure 4.1(a).

Since the emphasis was on the description of the post-yield deformation, in the single mode model used here the value for the modulus was chosen too low such that the strain-at-yield is accurately predicted, consequently resulting in a under-prediction of the stress in the pre-yield region. This can be improved significantly by employing a spectrum of relaxation times instead of the single mode representation used here [10]. Figure 4.1(a) also shows that the yield stress as well as its strain rate dependence is captured well, which is illustrated even more clearly in Figure 4.1(b). The latter figure also shows that the predicted lower yield stress has the same strain rate dependence as the yield point, and that, therefore, the predicted yield drop is constant. Although the amount of softening is captured well, the sudden sharp onset of strain softening, see Figure 4.1(a), that results from the first order evolution equation, Eq. (4.12), used to describe the softening kinetics could use some improvement. This issue will be addressed in Chapter 5.

In Chapter 3 it was shown that at high strain rates, or low temperatures, polycarbonate no longer behaves thermorheological simple. Under these conditions an extra contribution to the yield stress is observed, which could be described by adding a nonlinear Maxwell element in parallel. How to incorporate this in the 3D constitutive relation presented here, and the possible consequences of such an extension for the post-yield deformation, is the main issue of this chapter and is dealt with in the next section.

4.4 Thermorheological complex materials

Constitutive modelling

In Chapter 3 it was shown that, given the proper conditions (strain rate, temperature), the presence of a secondary relaxation process leads to an additional contribution to the response. For large deformations, this contribution can be represented by a stress-activated nonlinear Maxwell element. In terms of the model discussed in the preceding section this implies an additional driving stress $\sigma_{s,\beta}$, such that the total Cauchy stress σ now reads:

$$\sigma = \sigma_{s,\alpha} + \sigma_{s,\beta} + \sigma_r \quad (4.14)$$

where $\sigma_{s,\alpha}$ is the driving stress due to the primary process (σ_s in Eq. (4.1)), and σ_r the hardening stress. The hardening stress can be regarded as an independent contribution and is, therefore, given by the same neo-Hookean relation of Eq. (4.2).

For each process x ($x = \alpha, \beta$), the driving stress $\sigma_{s,x}$ is decomposed into a deviatoric part $\sigma_{s,x}^d$ and a hydrostatic part $\sigma_{s,x}^h$:

$$\sigma_{s,x} = \sigma_{s,x}^h + \sigma_{s,x}^d = \kappa_x(J-1)\mathbf{I} + G_x \tilde{\mathbf{B}}_{e,x}^d \quad x = \alpha, \beta \quad (4.15)$$

where G_x is the shear modulus, $\tilde{\mathbf{B}}_{e,x}^d$ the deviatoric part of the isochoric elastic left Cauchy-Green strain tensor, κ_x the bulk modulus for process x , J the volume change factor, and \mathbf{I} the unity tensor. The superscripts d and h denote, respectively, the *deviatoric* and *hydrostatic* part. J and $\tilde{\mathbf{B}}_{e,x}$ are given by the following evolution equations:

$$\dot{J} = J \text{tr}(\mathbf{D}) \quad (4.16)$$

$$\overset{\circ}{\tilde{\mathbf{B}}}_{e,x} = (\mathbf{D}^d - \mathbf{D}_{p,x}) \cdot \tilde{\mathbf{B}}_{e,x} + \tilde{\mathbf{B}}_{e,x} \cdot (\mathbf{D}^d - \mathbf{D}_{p,x}), \quad x = \alpha, \beta \quad (4.17)$$

where $\overset{\circ}{\tilde{\mathbf{B}}}_{e,x}$ is the Jaumann rate of $\tilde{\mathbf{B}}_{e,x}$ of process x , \mathbf{D}^d the deviatoric part of the rate of deformation tensor, and $\mathbf{D}_{p,x}$ the plastic part of the rate of deformation tensor. Subscripts e , and p indicate, respectively, the use of an *elastic*, and *plastic* quantity.

Again the non-Newtonian flow rule with a stress-dependent Eyring viscosity is used to relate the plastic deformation rate tensor, $\mathbf{D}_{p,x}$, to the deviatoric driving stress, $\sigma_{s,x}^d$ for each process x :

$$\mathbf{D}_{p,x} = \frac{\sigma_{s,x}^d}{2\eta_x(T, p_x, \bar{\tau}_x, D_x)} \quad (4.18)$$

The viscosity, η_x , is governed by the equivalent stress, $\bar{\tau}_x$, pressure p_x through the

pressure dependence (μ_x) and intrinsic strain softening (D_x), associated the element x only:

$$\eta_x(T, p_x, \bar{\tau}_x, D_x) = A_{0,x}(T) \tau_{0,x} \exp\left(\frac{\mu_x p_x}{\tau_{0,x}}\right) \frac{\bar{\tau}_x / \tau_{0,x}}{\sinh(\bar{\tau}_x / \tau_{0,x})} \exp(-D_x) \quad (4.19)$$

where the temperature dependent pre-exponential factor $A_{0,x}(T)$ equals:

$$A_{0,x}(T) = A_{0,x} \exp\left(\frac{\Delta U_x}{RT}\right) \quad (4.20)$$

with $A_{0,x}$ a constant, ΔU_x the activation energy for process x , R the universal gas constant, and T the absolute temperature. The characteristic stress $\tau_{0,x}$, pressure p_x , and equivalent stress $\bar{\tau}_x$ of process x are defined as:

$$\tau_{0,x} = \frac{kT}{V_x^*} \quad (4.21)$$

$$p_x = -\frac{1}{3} \text{tr}(\boldsymbol{\sigma}_{s,x}) \quad (4.22)$$

$$\bar{\tau}_x = \sqrt{\frac{1}{2} \text{tr}(\boldsymbol{\sigma}_{s,x}^d \cdot \boldsymbol{\sigma}_{s,x}^d)} \quad (4.23)$$

with V_x^* the activation volume for process x and k Boltzmann's constant.

For the thermorheological simple model the intrinsic strain softening was represented by the (structural) parameter D , which evolves to an equilibrium value D_∞ with plastic strain. Although the presence of softening in the additional process has not yet been established, it is assumed that, when present, it can be described by a similar first order evolution equation:

$$\dot{D}_x = h_x \left(1 - \frac{D_x}{D_{\infty,x}}\right) \dot{\gamma}_{p,x} \quad (4.24)$$

where h_x determines the initial softening rate, and the equivalent plastic strain rate, $\dot{\gamma}_{p,x}$ of process x , is provided by the following equation:

$$\dot{\gamma}_{p,x} = \sqrt{2 \text{tr}(\mathbf{D}_{p,x} \cdot \mathbf{D}_{p,x})} \quad (4.25)$$

To investigate whether the post-yield deformation of a thermorheological complex material contains an additional softening contribution or not, the response of the model with and without softening will be compared to the experimentally determined intrinsic response of a suitable model material.

Application to polymethylmethacrylate

Although polycarbonate displays a secondary relaxation mechanism, this only shows up at high strain rates, or at low temperatures (see Chapter 3). Polymethylmethacrylate (PMMA) on the other hand has a secondary transition that gives a contribution within the experimentally available range of strain rates at room temperature, and is therefore used instead of PC. The results of uniaxial compression tests on PMMA at different constant true strain rates are shown in Figure 4.2(a).

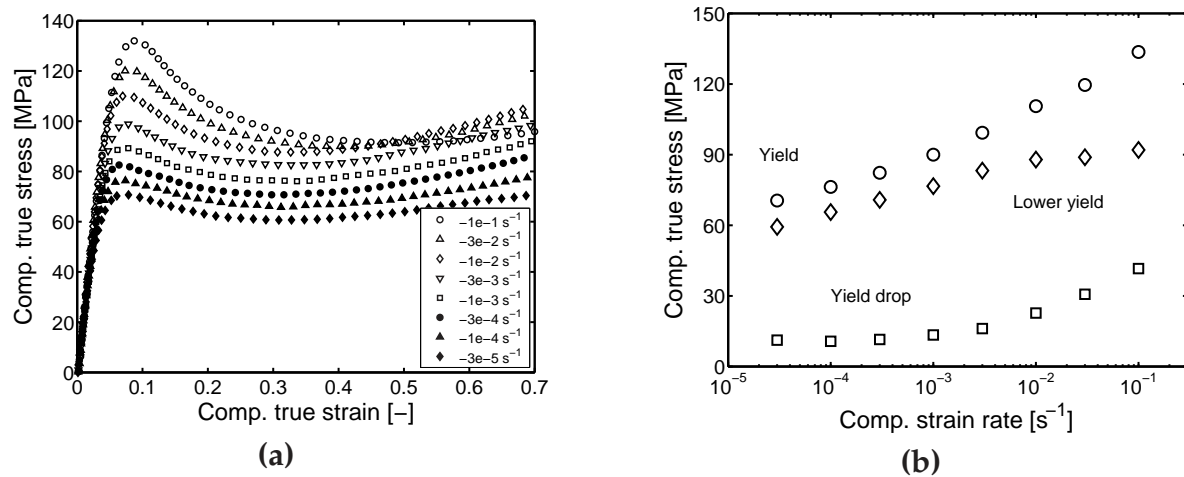


Figure 4.2: (a) True stress versus true strain at different compressive true strain-rates for PMMA at room temperature (23 °C). (b) Yield stress, lower yield stress, and yield drop as a function of strain rate determined from Figure 4.2(a).

At the lowest strain rates the material response strongly resembles that of polycarbonate (compare Figure 4.1), both the yield stress and lower yield stress increasing at the same rate, leading to a constant yield drop, Figure 4.2(b). With increasing strain rates, however, the contribution of the secondary process to the yield stress becomes more pronounced. Since the slope of the lower yield stress appears not to be affected, the yield drop increases with strain rate.

To compare the response of the two-process model to the experimentally obtained results, the appropriate parameters have to be determined. Therefore, the model response for uniaxial compression is fitted to the experimental data. Since it is not possible to determine all the required parameter values from a single loading geometry, the fitted parameters were supplemented by some values from literature. The fitting procedure comprises two stages, first the model response is determined for the strain rates where only the primary process contributes to the deformation (this is comparable to the polycarbonate case), and in the second step the contribution of the secondary process is included.

To determine the parameters for the α -process, the values for the Poisson ratio ν_α and pressure dependence μ_α were taken from literature to be 0.33 and 0.20, respectively [11]. The remaining parameters were determined from a fit to the data at the four lowest strain rates used experimentally.

Process	E [MPa]	ν	A_0 [s]	τ_0 [MPa]	μ	D_∞	h	G_r [MPa]
α	1500	0.33	$1.0 \cdot 10^{10}$	2.55	0.2	10.5	29	-
Rubber	-	-	-	-	-	-	-	26

Table 4.3: Material parameters obtained from fitting the constant strain-rate compression data at room temperature (23 °C) in Figure 4.3(a).

With the parameters tabulated in Table 4.3, the response shown in Figure 4.3(a) is obtained (solid lines). From this figure it is clear that in this range the post-yield deformation is captured well with a single driving stress contribution only. Based on the results of Chapter 3 it can, however, be anticipated that for increasing strain rates the description of, in particular, the yield stress will no longer be accurate. This is confirmed by Figure 4.3(b), which shows a comparison of the experimental yield stress (symbols) and the calculated yield stress (solid lines). More surprising is that the lower yield stress is described well at rates where the yield stress already shows considerable deviation. Further, the predicted yield drop shows no strain rate dependence, as could have been expected on the basis of the results for polycarbonate.

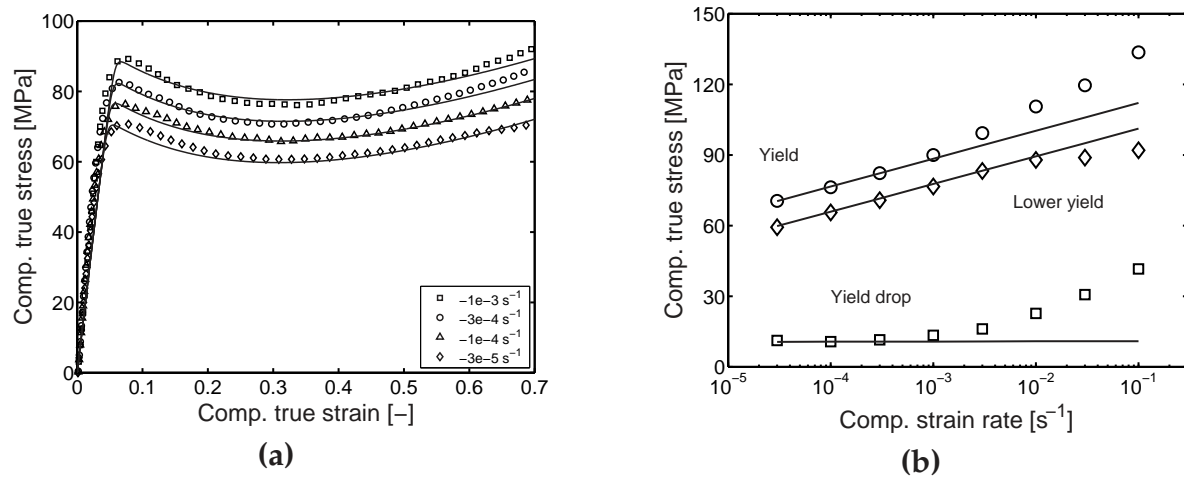


Figure 4.3: (a) Compression tests on PMMA at different true strain-rates and room temperature (23 °C). (b) Yield stress, lower yield stress, and yield drop versus strain rate determined from Figure 4.3(a). Symbols: experiments; lines: model prediction.

Where the poor performance at high strain rates of the model with only a single driving stress contribution could have been expected, it can also be anticipated that by

adding a contribution, the description of the yield stress will improve significantly. For the additional process again some parameter values are obtained from literature, in particular the Poisson ratio and the pressure dependence of the secondary process. The Poisson ratio ν_β is assumed to be equal to that of the primary process, 0.33, whereas no pressure dependence for the second process is assumed, i.e. $\mu_\beta = 0$ [12]. The remaining parameters were obtained by fitting the response to the data, where it was assumed that, to a first approximation, the additional contribution shows no softening, i.e. $\dot{D}_\beta = D_\beta = 0$. This will be referred to as case one. With the parameter values tabulated in Table 4.4, the yield stresses at the highest strain rates are captured well, whereas the calculated post-yield deformation shows no signs of the strain rate dependence observed in the experiments, see Figure 4.4(a) and (b). This indicates that to improve the description under the current isothermal conditions, the secondary contribution should also include softening.

Process	E [MPa]	ν	A_0 [s]	τ_0 [MPa]	μ	D_∞	h	G_r [MPa]
α	1500	0.33	$1.0 \cdot 10^{10}$	2.55	0.2	10.5	29	-
β	300	0.33	$2.0 \cdot 10^2$	2.75	0.0	-	-	-
Rubber	-	-	-	-	-	-	-	26

Table 4.4: Material parameters obtained from fitting the constant strain-rate compression data at room temperature (23 °C) in Figure 4.4(a).

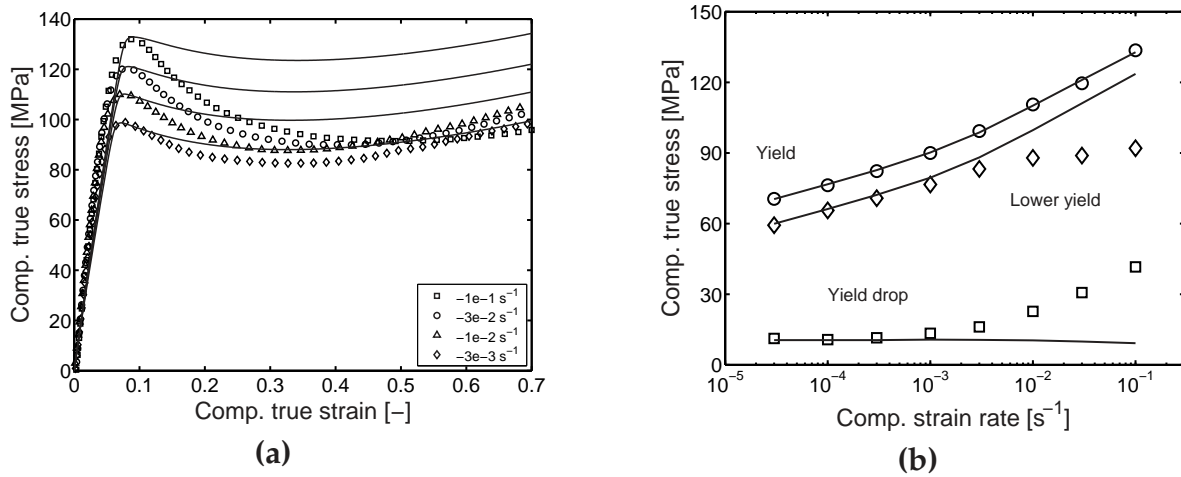


Figure 4.4: (a) Compression tests on PMMA at different true strain-rates and room temperature (23 °C). (b) Yield stress, lower yield stress, and yield drop versus strain rate determined from Figure 4.4(a). Symbols: experiments; lines: model prediction.

In what will be referred to as case two, it is assumed that both the expression for softening and the relevant parameter values for the second process are identical to those obtained for the primary process. With the values listed in Table 4.5, the model responses shown in Figure 4.5(a) are obtained. While the yield stress is still captured

fairly accurately, the additional softening leads to a significant improvement in the description of the yield drop, see Figure 4.5(b). Only at the highest rate there is some deviation from the experimentally obtained values.

Process	E [MPa]	ν	A_0 [s]	τ_0 [MPa]	μ	D_∞	h	G_r [MPa]
α	1500	0.33	$1.0 \cdot 10^{10}$	2.55	0.2	10.5	29	-
β	300	0.33	$4.0 \cdot 10^2$	2.75	0.0	10.5	29	-
Rubber	-	-	-	-	-	-	-	26

Table 4.5: Material parameters obtained from fitting the constant strain-rate compression data at room temperature (23 °C) in Figure 4.5(a).

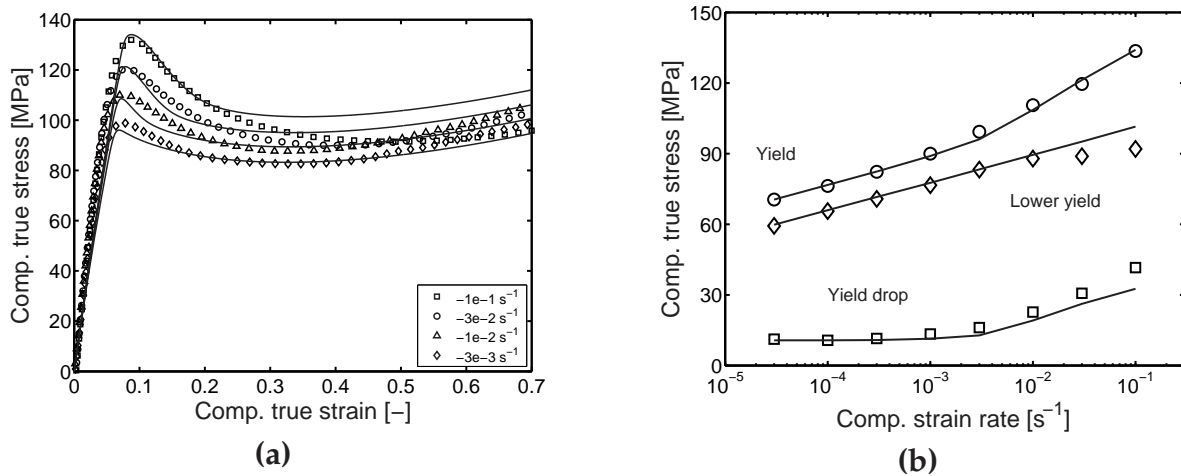


Figure 4.5: (a) Compression tests on PMMA at different true strain-rates and room temperature (23 °C). (b) Yield stress, lower yield stress, and yield drop versus strain rate determined from Figure 4.5(a). Symbols: experiments; lines: model prediction.

In this second case the strain rate dependent yield drop originates from the additional softening of the secondary process, and can, therefore, be regarded as an intrinsic feature. The origin of this strain rate dependence can be understood from the fact that softening shifts the viscosity function to higher strain rates. In the case of a single process this shift, which is determined by both D_∞ and G_r , is the same for all strain rates, and thus gives a constant yield drop. This behaviour corresponds with region I in Figure 4.6, where this mechanism is illustrated schematically. Region I represents the behaviour observed for PC (see Figure 4.1(b)) and that of PMMA at low strain rates only. When an additional flow contribution is present, there is a transition in the slope of the yield stress versus strain rate. If both contributions show softening this transition also shifts to higher strain rates, creating a region where the yield drop increases with strain rate. This region II in Figure 4.6, corresponds with the behaviour observed for PMMA at the highest strain rates. Extrapolation to even larger strain rates, finally results in a plateau at a higher constant value for the yield

drop (region III in Figure 4.6). The strain rate at which this plateau would be reached depends on the parameter values of both softening characteristics.

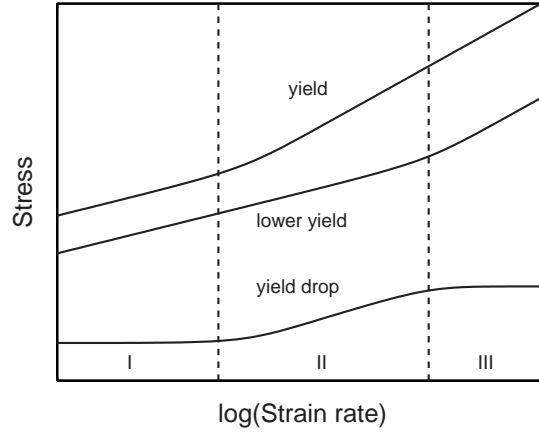


Figure 4.6: Schematic explanation of the strain rate dependence in yield drop caused by the use of two contributions with strain softening.

In practice, an experimental verification of this plateau will be difficult since it involves high strain rates, at which heating effects become apparent. This deformation induced heating may also be responsible for the deviations observed at the highest strain rates. At these strain rates the stress response at large deformations crosses that of the lower strain rates, see Figure 4.5(a), an effect also reported in literature [13], and which can not be explained by the model response under plain isothermal conditions. Next, the deformation induced heating will be considered more closely, to investigate to what extent this influences the calculated results presented above.

Deformation induced heating

The origin of deformation induced heating lies in the dissipation of mechanical work. While for metals the amount of dissipated energy can be as much as 90 to 95%, Adams and Farris [14] showed that during cold drawing of polycarbonate only 50 to 80% of the mechanical work is converted to heat. Using a model study employing the BPA-model, Boyce *et al.* [11] showed that this corresponds to the work done by the driving stress portion of the total stress $\sigma_s^d : D_p$, whereas the remaining part of the total work is stored as a change in configurational entropy and elastic energy. For the extended model presented above this implies that the amount of dissipative work \dot{Q}_d equals:

$$\dot{Q}_d = V (\sigma_{s,\alpha}^d : D_{p,\alpha} + \sigma_{s,\beta}^d : D_{p,\beta}) \quad (4.26)$$

where V is the volume of the cylindrical sample used in the experiments.

Due to the deformation induced heating the temperature in the sample increases. To a first approximation it is assumed that the temperature is homogenous throughout the sample. Considering the magnitude of the deformations involved, the influence of thermal expansion is ignored. Although some parameters are known to depend on temperature, all model parameters, with the exception of both stress dependencies ($\tau_{0,\alpha}$ and $\tau_{0,\beta}$) and pre-exponential factors ($A_{0,\alpha}$ and $A_{0,\beta}$), are assumed to be independent of temperature. The temperature dependence of the pre-exponential factors is determined by the activation energies ΔU_α and ΔU_β , for these the values obtained in Chapter 3 (Table 3.1) are adopted.

Two boundary conditions are used, one representing the natural convection of heat from the sample to the surrounding air, and the other conduction of heat from the sample to the steel compression plates. Due to their large volume compared to that of the sample, and high conductivity the steel compression plates are regarded as heat sinks. The heat flux \dot{Q}_s due to conduction through the Teflon film to the steel compression plates, with a constant temperature T_∞ ($= 296$ K), equals:

$$\dot{Q}_s = 2A_s \left(\frac{k_f}{t_f} \right) (T - T_\infty) \quad (4.27)$$

where A_s is the contact area between the sample and the steel compression plate, T is the absolute temperature, t_f is the thickness of the Teflon film ($t_f = 0.1$ mm) and k_f the conductivity of the Teflon film ($k_f = 0.25$ W/m² K, [15]). The heat flux \dot{Q}_a due to natural convection to the surrounding air with temperature T_∞ equals:

$$\dot{Q}_a = A_a h_c (T - T_\infty) \quad (4.28)$$

where A_a is the contact area between the sample and the air, h_c is the heat transfer coefficient of the boundary layer. This coefficient can be calculated from the Nusselt-number which, for the given geometry (finite cylinder), is estimated at 3.22 [16], yielding a heat transfer coefficient of approximately 14.4 W/m² K. Since this is close to the value of 13.6 W/m² K determined experimentally by Koenen [17] for polycarbonate, the latter value will be adopted here for further calculations.

Combining the expressions for heat generation and heat flux with the energy balance gives the following evolution equation for the absolute temperature T :

$$\dot{T} = \frac{1}{\rho c_p} \left[(\boldsymbol{\sigma}_{s,\alpha}^d : \mathbf{D}_{p,\alpha} + \boldsymbol{\sigma}_{s,\beta}^d : \mathbf{D}_{p,\beta}) - \left(\frac{2k_f}{l t_f} + \frac{2h_c}{r} \right) (T - T_\infty) \right] \quad (4.29)$$

where ρ is the density, c_p the specific heat capacity, r the momentary radius, and l the momentary length of the cylindrical sample (initial values for the radius and length are 3 mm and 6 mm, respectively).

The relevant thermal properties of PMMA used for the calculations are listed in Table 4.6.

ρ [kg/m ³]	c_p [J/kg K]	ΔU_α [kJ/mol K]	ΔU_β [kJ/mol K]
1200	1460	280	90

Table 4.6: Values for the thermal properties of PMMA.

First, the influence of deformation induced heating on the model response without additional softening is calculated, and subsequently that for the model with additional softening.

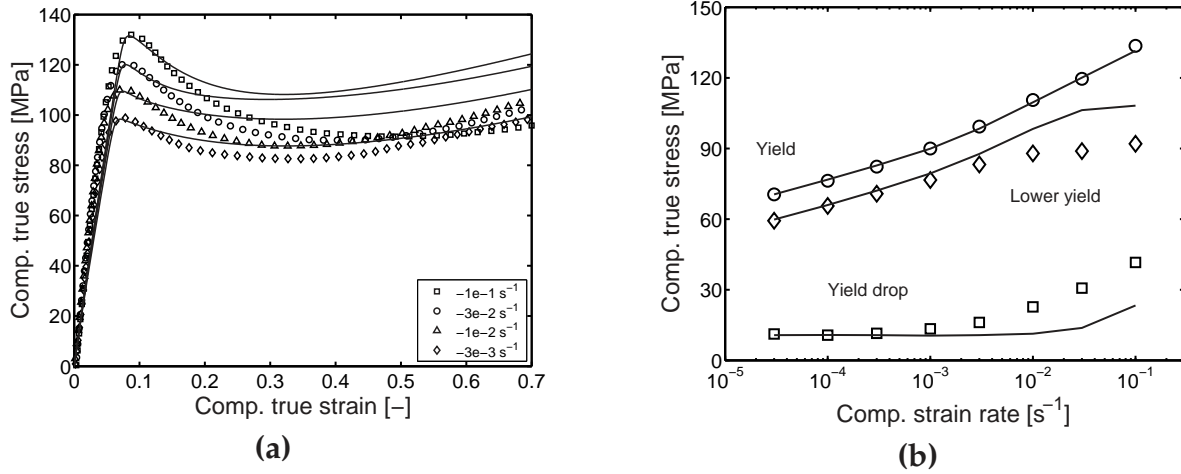


Figure 4.7: (a) Compression tests on PMMA at different true strain-rates and room temperature (23 °C). (b) Yield stress, lower yield stress, and yield drop versus strain rate determined from Figure 4.7(a). Symbols: experiments; lines: model predictions from a thermomechanically coupled analysis using a model without additional softening.

Figure 4.7(a) shows the results of the coupled analysis for the model without additional softening (compare Figure 4.4). Although there is some increase in the amount of softening with increasing strain rate, this is less than the amount observed experimentally. This is illustrated more clearly in Figure 4.7(b). The onset of the predicted strain rate dependence is caused by an enhanced heat generation due to the dissipative work by the secondary process at increased strain rates. Keeping in mind that the thermal model used is only a very basic one, and in particular the assumption of a homogeneous temperature distribution is a very crude one, especially in axial direction, a more detailed analysis, using e.g. the finite element method, is required to get a more quantitative result.

The results of the coupled analysis for the model with softening (compare Figure 4.5) in the secondary contribution is shown in Figure 4.8(a). In this case, the additional thermal softening enhances the intrinsically present strain rate dependent softening, see Figure 4.8(b).

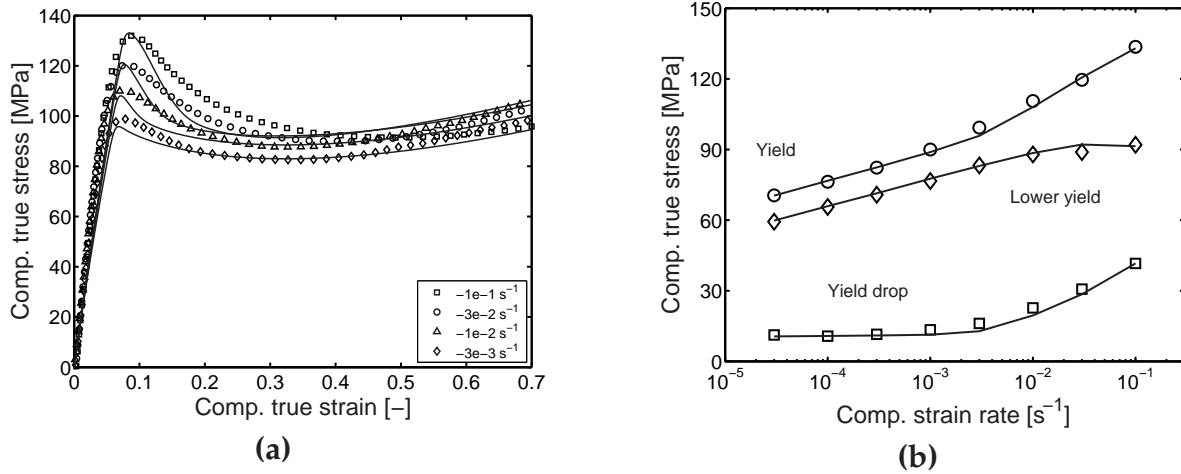


Figure 4.8: (a) Compression tests on PMMA at different true strain-rates and room temperature (23 °C). (b) Yield stress, lower yield stress, and yield drop versus strain rate determined from Figure 4.8(a). Symbols: experiments; lines: model predictions from a thermomechanically coupled analysis using a model with additional softening.

From the experimental results it is evident that there indeed is deformation induced heating at the highest strain rates. The resulting thermal softening enhances the intrinsic softening, whether this includes softening due to the secondary contribution or not. Both cases lead to a strain rate dependent yield drop. If no softening is present, the secondary flow contribution enhances the heat generation with increasing strain rate, while with softening present the intrinsic strain rate dependence is enhanced. At current, the results are not conclusive with respect to the presence of softening in the secondary contribution or not. A more detailed study using the finite element method might shed some more light on this matter.

4.5 Conclusions

The aim of this chapter was to investigate the influence of molecular relaxation mechanisms on the post-yield response, and to verify suitable modelling techniques for describing the behaviour observed. Emphasis was put on an accurate description of the yield drop, i.e. the amount the stress falls beyond the yield point, since this has been identified as a measure for the stability of the macroscopic deformation process. Increasing the yield drop leads to more brittle deformation, while decreasing the

yield drop promotes ductile deformation.

For polycarbonate, a thermorheological simple material, no strain rate dependence is observed for the yield drop within the experimental window, and the intrinsic deformation as well as the yield drop could be described accurately using a large strain model with a single relaxation time.

For polymethylmethacrylate, a thermorheological complex material, a change in both the yield and post-yield response was observed, leading to a strain rate dependent yield drop. The additional contribution to the yield stress with increasing strain rate is related to the secondary relaxation mechanism, and since the moment this sets in coincides with the change in yield drop, this secondary mechanism is also likely to be responsible for the change in the post-yield response.

Using an extended model, two mechanisms were identified that could be responsible for the observed strain rate dependence of the yield drop. For one mechanism, the observed strain rate dependence is an intrinsic property, while for the other it is due to thermal softening, which is enhanced by the secondary relaxation mechanism.

The strain rate at which the secondary relaxation mechanism becomes active depends on the position of the β -transition temperature T_β relative to the operating temperature. For PMMA ($T_\beta = 30\text{ }^\circ\text{C}$) or PS ($T_\beta = 80\text{ }^\circ\text{C}$) at room temperature, the secondary transition already has a contribution at relatively low strain rates. PC ($T_\beta = -100\text{ }^\circ\text{C}$) on the other hand requires much higher strain rates for the secondary mechanism to become active (see Figure 3.5(a) in Chapter 3).

Since the presence of a secondary relaxation mechanism leads to an increase in yield drop with strain rate, the macroscopic deformation will become increasingly unstable. For very high strain rates, e.g. under impact conditions, this instability can ultimately result in brittle failure. This finding appears to fit the classic picture which states that the presence of a low temperature secondary transition promotes ductile deformation under impact conditions (high strain-rates), and consequently the opposite, a high T_β , leads to a more brittle type of failure.

It should, however, be emphasized that other factors such as thermal history and strain hardening also have a pronounced influence on the post-yield response and, consequently on the macroscopic deformation. Annealing for example is known to cause embrittlement of polycarbonate, even in the absence of a secondary relaxation mechanism [1].

References

- [1] van Melick, H.G.H., Govaert, L.E., Meijer, H.E.H. (2003). Localisation phenomena in glassy polymers: influence of thermal and mechanical history. *Polymer*, **44**, 3579–3591.
- [2] Haward, R. and Thackray, G. (1968). The use of a mathematical model to describe isothermal stress-strain curves in glassy thermoplastics, *Proc. Roy. Soc. A*, **302**, 453–472.
- [3] Boyce, M.C., Parks, D.M., Argon, A.S. (1988). Large inelastic deformation of glassy polymers. Part I: Rate dependent constitutive model, *Mech. Mat.*, **7**, 15–33.
- [4] Govaert, L.E., Timmermans, P.H.M., Brekelmans, W.A.M. (2000). The influence of intrinsic strain softening on strain localization in polycarbonate: modeling and experimental validation, *J. Eng. Mat. Techn.*, **122**, 177–185.
- [5] Buckley, C.P. and Jones, D.C. (1995). Glass-rubber constitutive model for amorphous polymers near the glass transition. *Polymer*, **36**, 3301–3312.
- [6] Buckley, C.P., Dooling, P.J., Harding, J., Ruiz, C. (2004). Deformation of thermosetting resins at impact rates of strain. Part 2: constitutive model with rejuvenation. *J. Mech. Phys. Solids*, **52**, 2355–2377.
- [7] Tervoort, T.A., Smit, R.J.M., Brekelmans, W.A.M., Govaert, L.E. (1998). A constitutive equation for the elasto-viscoplastic deformation of glassy polymers. *Mech. Time-Dep. Mat.*, **1**, 269–291.
- [8] Tervoort, T.A. and Govaert, L.E. (2000). Strain hardening behavior of polycarbonate in the glassy state, *J. Rheol.*, **44**, 1263–1277.
- [9] Hasan, O.A., Boyce, M.C., Li, X.S., Berko, S. (1993). An investigation of the yield and postyield behavior and corresponding structure of poly(methyl methacrylate). *J. Pol. Sci.: Part B: Pol. Phys.*, **31**, 185–197.
- [10] Tervoort, T.A., Klompen, E.T.J., Govaert, L.E. (1996). A multi-mode approach to finite, three-dimensional, nonlinear viscoelastic behavior of polymer glasses. *J. Rheol.*, **40**, 779–797.
- [11] Boyce, M.C., Montagut, E.L., Argon, A.S. (1992). The effects of thermomechanical coupling on the cold drawing process of glassy polymers. *Pol. Eng. Sci.*, **32**, 1073–1085.
- [12] Bauwens-Crowet, C. (1973). The compression yield behaviour of polymethylmethacrylate over a wide range of temperatures and strain rates. *J. Mat. Sci.*, **8**, 968–979.
- [13] Arruda, E.M., Boyce, M.C., Jayachandran, R. (1995). Effects of strain rate, temperature and thermomechanical coupling on the finite strain deformation of glassy polymers. *Mech. Mat.*, **19**, 193–212.
- [14] Adams, G.W., Farris, R.J. (1988). Latent energy of deformation of bisphenol A polycarbonate. *J. Pol. Sci.: Part B: Pol. Phys.*, **26**, 433–445.
- [15] van Krevelen, D.W. (1990). *Properties of Polymers: their correlation with chemical structure, their numerical estimation and prediction from additive group contributions*. Elsevier, Amsterdam.

- [16] Hagen, K.D. (1999). *Heat Transfer with Applications*. Prentice Hall, New Jersey.
- [17] Koenen, J.A. (1992). Observation of the heat exchange during deformation using an infra-red camera. *Polymer*, **33**, 4732–4736.

Post-yield response of glassy polymers: influence of thermomechanical history¹

In the introductory chapter the influence of physical ageing on the macroscopic deformation was briefly discussed. Both in Chapter 2 and 3 this influence was, however, ignored on the assumption that the experimental time is less than the initial age of the sample. Although ageing was also ignored in Chapter 4, it is known that the structural state has a profound influence on the post-yield deformation, and hence on the macroscopic failure behaviour. Therefore, in this chapter it is attempted to account for the structural evolution of the material, and the changes in yield stress that result from it.

5.1 Introduction

In the last decades considerable attention has been awarded to the development of constitutive relations for the large strain deformation of solid polymeric materials [1–5]. These efforts were motivated by the desire to predict mechanical properties and performance and to develop (numerical) tools for better understanding and, finally, improving properties of homogeneous, as well as heterogeneous, polymer systems [6].

A landmark in this area of research is the original paper of Haward and Thackray

¹Reproduced from: Klompen, E.T.J., Engels, T.A.P., Govaert, L.E., Meijer, H.E.H., Elastoviscoplastic modelling of large strain deformation of glassy polymers: influence of thermomechanical history. *J. Rheol.*, submitted.

from 1968 [1], where they proposed to govern the large strain deformation of polymers below their glass transition temperature by two separate processes. The first process reflects the rate-dependent plastic flow related to temperature and stress-activated motion of chain segments, which is represented by an Eyring-viscosity [7]. The second process is related to the molecular alignment resulting from the plastic flow process, and is modelled using a finite extendable spring (a so-called Langevin spring) following the conventional theory of rubber elasticity [8].

The Haward and Thackray model was extended to a fully 3-D description by Boyce, Parks and Argon [2], in what is now known as the *BPA-model*. In this model the plastic flow contribution is described by a 3-D representation of the Argon flow theory [9], including pressure dependence and a phenomenological description of intrinsic strain softening. The entropic hardening is modelled by using the three-chain model of Wang and Guth [10], later improved by the more realistic eight chain model, Arruda and Boyce [11]. A modification of the BPA-model was proposed by Wu and van der Giessen [3], replacing the 3-chain model with a full network model (the *full-chain model*).

An alternative approach was presented by Tervoort *et al.* [12], who formulated a 3-D model for nonlinear viscoelastic behaviour based on a compressible version of Leonov's fluid model [13] as originally proposed by Baaijens [14]. The resulting elasto-viscoplastic model, with two basic elements: a linear elastic spring and a 3-D Eyring dashpot, was further refined by Govaert *et al.* [5] by adding pressure dependence and (phenomenological) softening based on the concept of Hasan *et al.* [15], and a neo-Hookean rubber spring representing strain hardening, as suggested by Tervoort and Govaert [16].

These models were amongst others used in the investigation of strain localization phenomena in polymers such as shear banding, necking, and crazing [5, 17, 18]. From these numerical investigations it became evident that the occurrence of these phenomena is completely captured by the polymers' intrinsic behaviour. Initiation of localization is caused by the intrinsic strain softening, whereas the way this localized zone evolves depends on the stabilizing effect of strain hardening [17–19]. Ultimately the balance between strain softening and hardening determines whether a polymer deforms macroscopically ductile (stable), or brittle (unstable) [20].

These numerical findings were supported by experimental observations, which showed that a change in softening can have dramatic effects on the macroscopic behaviour. Such a change can be realized by application of thermal or mechanical treatments. The resulting thermo-mechanical history, however, only influences the yield stress, since the final rejuvenated state is known to be independent of any prior history [15, 20, 21]. Quenching a sample for instance, results in a lower yield stress leading to less softening in a compression test and less localized deformation

in a tensile test. A prime example of this is reported by Cross and Haward [22] who observed uniform deformation for quenched polyvinylchloride samples, whereas slowly cooled samples developed a neck. Various authors showed that by mechanical pre-conditioning, or pre-deformation, the amount of strain softening can be reduced or even eliminated [5, 23–25]. This pre-treatment results in uniform deformation of polycarbonate (no neck) [5], and even induces complete ductile deformation in polystyrene (no crazing) [25]. Increasing the amount of softening by increasing the yield stress, on the other hand, e.g. by annealing, leads to severe localization of strain and can even induce brittle fracture in (relatively low molecular weight) polycarbonate [20, 26–28].

In modelling practice and in experiments it is usually assumed that the initial age exceeds the experimental time which implies that material properties do not change and are time invariant during the test. In case of long term loading conditions, or conditions where accelerated ageing can be expected, e.g. at high temperatures, this assumption might no longer hold and, consequently, the parameters will change during the experiment: *progressive ageing* [29]. At room temperature such a spontaneous increase of the yield stress is indeed observed experimentally, in particular with samples where the softening is reduced through a thermal, or mechanical, treatment. For quenched PVC samples at room temperature the yield stress was seen to increase with time by Cross and Haward [22], and Struik [29]. Van Melick *et al.* [30] reported an increasing yield stress at room temperature after mechanical pre-deformation of polystyrene, leading to re-embrittlement within a time scale of hours. In addition it was shown that the kinetics involved depend on the material and are accelerated at elevated temperatures. For both as-received samples [26, 31–33], as well as rejuvenated samples [34, 35], the yield stress is seen to increase with time and annealing temperature.

To account for such changes in yield stress, and thus changes in softening, the model should include a time-dependent yield stress. To describe such behaviour, an extension of the current elasto-viscoplastic models is proposed and the relevant characteristics and parameters are experimentally determined using polycarbonate as model material. Application of the model to long term loading will be dealt with in Chapter 6.

5.2 Experimental

Materials

Different grades of polycarbonate were used, including Bayer Makrolon CD2000 and General Electric Lexan OQ1050, 101R, 121R, 141R, and 161R. Apart from these materials, that were supplied as granules, also an extrusion grade of Lexan (type un-

known) supplied as 6 mm diameter extruded rod was studied. Molecular weight distributions were determined using gel permeation chromatography (GPC), the resulting number-averaged and weight-averaged molecular weights are tabulated in Table 5.1.

Grade	M_n [kg/mol]	M_w [kg/mol]
Lexan OQ1050	8.1	16.8
Makrolon CD2000	8.2	18.7
Lexan 141R	9.2	25.8
Lexan 121R	9.8	23.4
Lexan 161R	11.6	27.9
Lexan 101R	12.7	28.9
Extruded rod	14.0	35.9

Table 5.1: Number-averaged and weight-averaged molecular weights of the polycarbonate grades used in this study measured with respect to a PC-standard.

For uniaxial compression tests, cylindrical samples ($\varnothing 6 \text{ mm} \times 6 \text{ mm}$) were machined from either the extruded rod or from plates ($200 \times 200 \times 10 \text{ mm}^3$) that were compression moulded from granular material at a temperature of $250 \text{ }^\circ\text{C}$. First the dried granulate was heated for 15 minutes and next compressed up to 300 kN in five subsequent intervals of 5 minutes. After each step the force was released to allow for degassing. Finally, the mould was placed in a cold press and cooled to room temperature ($20 \text{ }^\circ\text{C}$) under a moderate force (100 kN). Tensile samples were prepared either through injection moulding, or milled from compression moulded plates ($160 \times 160 \times 3 \text{ mm}^3$) (moulded also according to the procedure outlined above). Geometry of all tensile specimens was according to ISO 527.

Thermo-mechanical treatments

Annealing of samples was performed for different periods of time in an air circulated oven at various temperatures ($80\text{-}130 \text{ }^\circ\text{C}$). Initial equilibration of the sample temperature was measured to be approximately 15 minutes. After a predefined time, the samples were removed from the oven and allowed to cool to room temperature in air before being tested.

Mechanical pre-conditioning was performed both in the pre-yield and post-yield range. The latter involved mechanical rejuvenation of specimens by either torsion or rolling. With torsion, cylindrical samples were twisted to-and-fro over a twist angle of 1150° , whereas with rolling, samples were run through a two-roll mill ($\varnothing 45 \text{ mm}$), yielding a thickness reduction of about 10%. In the pre-yield range samples were pre-conditioned under constant force on either a Zwick Rel servo-hydraulic tensile tester equipped with a temperature chamber or a long-term dead-weight setup at room temperature for different amounts of time. Samples were tested after a short equilibration time.

A number of samples was subjected to a combined thermal and mechanical history, consisting of a constant applied load at different temperatures for various amounts of time. After this time the samples were unloaded and allowed to cool to room-temperature in air prior to testing.

Mechanical testing

Uni-axial compression tests were performed on a servo-hydraulic MTS Elastomer Testing System 810. The specimens were cylindrical shaped and compressed under true strain control, at constant true strain rates of 10^{-4} to 10^{-2} s^{-1} between two parallel, flat steel plates. Friction between samples and plates was reduced by an empirically optimized method. Onto the sample ends a thin film of PTFE tape (3M 5480, PTFE skived film tape) was applied and the contact area between steel and tape was lubricated using a 1:1 mixture of liquid soap and water. During the test no bulging of the sample was observed, indicating that the friction was sufficiently reduced.

Tensile tests were performed on a Zwick Z010 tensile tester, at constant linear strain rate of 10^{-4} to 10^{-2} s^{-1} , at distinct ageing times after pre-deformation. Besides the stress-strain curve, the yield stress was recorded. True stresses were calculated assuming a constant sample volume.

5.3 Numerical modelling

Constitutive model

In the constitutive model used, a distinction is made concerning the contribution of secondary interactions between polymer chains, that determine the (visco-) elastic properties at small deformations and plastic flow, and the entangled polymer network that governs strain hardening [5].

Accordingly, the total Cauchy stress σ is decomposed in a driving stress σ_s , and a hardening stress σ_r :

$$\sigma = \sigma_s + \sigma_r \quad (5.1)$$

Hardening is modelled with a neo-Hookean relation [16]:

$$\sigma_r = G_r \tilde{\mathbf{B}}^d \quad (5.2)$$

where G_r is the strain hardening modulus and $\tilde{\mathbf{B}}^d$ the deviatoric part of the isochoric left Cauchy-Green deformation tensor.

The driving stress is decomposed into a deviatoric stress σ_s^d , and a hydrostatic stress σ_s^h :

$$\sigma_s^d = G\tilde{\mathbf{B}}_e^d \quad \text{and} \quad \sigma_s^h = \kappa(J - 1)\mathbf{I} \quad (5.3)$$

where G is the shear modulus, $\tilde{\mathbf{B}}_e^d$ the deviatoric part of the isochoric elastic left Cauchy-Green strain tensor, κ the bulk modulus, J the volume change factor, and \mathbf{I} the unity tensor. The evolution of J and $\tilde{\mathbf{B}}_e^d$ is given by the following equations:

$$\dot{J} = J\text{tr}(\mathbf{D}) \quad (5.4)$$

$$\overset{\circ}{\tilde{\mathbf{B}}}_e = (\mathbf{D}^d - \mathbf{D}_p) \cdot \tilde{\mathbf{B}}_e + \tilde{\mathbf{B}}_e \cdot (\mathbf{D}^d - \mathbf{D}_p) \quad (5.5)$$

where $\overset{\circ}{\tilde{\mathbf{B}}}_e$ is the Jaumann rate of $\tilde{\mathbf{B}}_e$, \mathbf{D}^d the deviatoric part of the rate of deformation tensor, and \mathbf{D}_p the plastic part of the rate of deformation tensor.

A non-Newtonian flow rule with a stress-dependent Eyring viscosity is used to relate the plastic deformation rate tensor, \mathbf{D}_p , to the deviatoric driving stress, σ_s^d [12]:

$$\mathbf{D}_p = \frac{\sigma_s^d}{2\eta(T, p, \bar{\tau}, D)} \quad (5.6)$$

The viscosity, η , strongly depends on the equivalent stress, $\bar{\tau}$, and was originally described by an Eyring relationship [12]. Govaert *et al.* [5] extended the model by incorporating pressure dependence (μ) and intrinsic strain softening (D) in the viscosity function:

$$\eta(T, p, \bar{\tau}, D) = A_0(T)\tau_0 \exp\left(\frac{\mu p}{\tau_0}\right) \frac{\bar{\tau}/\tau_0}{\sinh(\bar{\tau}/\tau_0)} \exp(-D) \quad (5.7)$$

where the temperature dependent pre-exponential factor $A_0(T)$ equals:

$$A_0(T) = A_0 \exp\left(\frac{\Delta U}{RT}\right) \quad (5.8)$$

with A_0 a constant, ΔU the activation energy, R the gas constant, and T the absolute temperature. The characteristic stress τ_0 , pressure p , and equivalent stress $\bar{\tau}$ are defined as:

$$\tau_0 = \frac{kT}{V^*} \quad (5.9)$$

$$p = -\frac{1}{3}\text{tr}(\boldsymbol{\sigma}) \quad (5.10)$$

$$\bar{\tau} = \sqrt{\frac{1}{2}\text{tr}(\boldsymbol{\sigma}_s^d \cdot \boldsymbol{\sigma}_s^d)} \quad (5.11)$$

with V^* the activation volume, and k Boltzmann's constant.

The intrinsic strain softening is represented by the (structural) parameter D , that evolves from an initial value D_0 to an equilibrium value $D_\infty > D_0$ with increasing equivalent plastic strain $\bar{\gamma}_p$ thereby strongly reducing the material's viscosity η . In general form this can be represented by:

$$D(\bar{\gamma}_p) = D_\infty \cdot R_\gamma(\bar{\gamma}_p) \quad (5.12)$$

where R_γ increases monotonically from an initial value $R_\gamma(0) \leq 1$ to 1 with equivalent plastic strain, provided by the following equation:

$$\dot{\bar{\gamma}}_p = \sqrt{2 \operatorname{tr}(\mathbf{D}_p \cdot \mathbf{D}_p)} \quad (5.13)$$

In a precise form of Eq. (5.12) as originally proposed by Hasan *et al.* [15] (a phenomenological first order evolution) the parameter D represents the *density of shear transformation sites*, which is derived from Positron Annihilation Lifetime Spectroscopy (PALS) measurements. Since the initial value $D_0 = D_\infty \cdot R_\gamma(0)$ depends on thermal history a new value has to be determined for each sample with a different thermal history using either PALS measurements or a numerical fit.

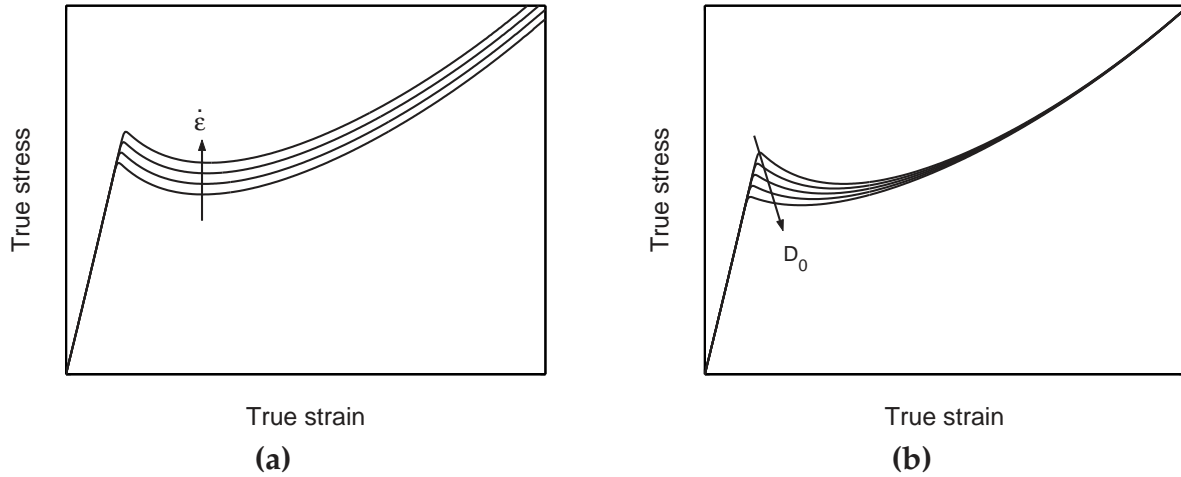


Figure 5.1: Schematic representation of the response of the elasto-viscoplastic model to uniaxial extension at different strain rates (a), and for different initial states D_0 (b).

To illustrate some of the characteristic features of the model, using a first order evolution equation for D , Figure 5.1(a) shows its response to different strain rates. The initial linear elastic deformation is followed by a strain rate dependent yield point, while post yield behaviour (both softening and hardening) is strain rate independent. This behaviour is found e.g. in experimental observations on polycarbonate [36]. Figure 5.1(b) shows the effect of different initial states. Yield stress, and the amount of

softening can be seen to decrease with an increasing value of D_0 . The response at large deformations is independent of the initial state which corresponds to the experimentally observed deformation induced erasure of thermo-mechanical history (mechanical rejuvenation) [15,20,21].

Incorporation of ageing kinetics

From Figure 5.1(b) it is clear that the initial condition D_0 can be used to describe the yield stress induced by different thermo-mechanical histories. Using a first order evolution an increasing yield stress with time can, however, not be obtained, e.g. by letting D_0 evolve with time, since the initial condition only has an effect on $t = 0$. This was also recognized by Hasan *et al.* [15], who therefore schematically proposed an extension by adding an additional term representing the ageing behaviour. Dependence of temperature, pressure and structural state was suggested, but no explicit expression was given. Under the assumption that the initial age exceeds the experimental time under consideration the term was neglected anyway. As pointed out in the introduction there are however circumstances, e.g. a small initial age or elevated temperatures, where this assumption does not hold.

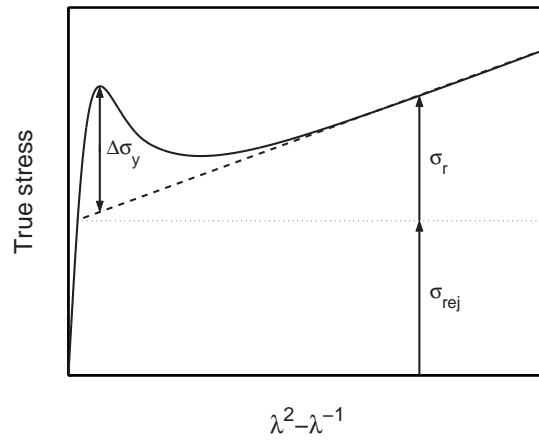


Figure 5.2: Schematic representation of the decomposition of the true stress in three separate contributions.

In a first attempt to enable a combined description of relevant ageing and softening kinetics, a simplified approach is proposed here. Essence is the decomposition of the intrinsic flow stress σ in three components, see Figure 5.2, similar to an approach proposed by G'Sell [23]:

$$\sigma(\dot{\varepsilon}, S, \varepsilon) = \sigma_{rej}(\dot{\varepsilon}) + \Delta\sigma_y(S) + \sigma_r(\varepsilon) \quad (5.14)$$

Together with the history independent flow stress σ_{rej} of the fully rejuvenated state, the strain hardening stress σ_r represents the steady state, or homogeneous

deformation behaviour of the material [23]. The remaining transient component, the yield drop² $\Delta\sigma_y$, depends on the thermo-mechanical history of the material, represented by the state parameter S . With regard to the yield drop it is assumed that it is independent of both strain rate, and test temperature, which for polycarbonate at moderate temperatures is a fair assumption [36].

In terms of the previously described elasto-viscoplastic model, this decomposition can be easily realized by modifying the viscosity definition (Eq. (5.7)) to that of the rejuvenated state:

$$\eta(T, p, \bar{\tau}) = \eta_{0,r}(T) \exp\left(\frac{\mu p}{\tau_0}\right) \frac{\bar{\tau}/\tau_0}{\sinh(\bar{\tau}/\tau_0)} \quad (5.15)$$

where $\eta_{0,r}(T) = A_{rej}(T) \cdot \tau_0$, with $A_{rej}(T)$ the $A_0(T)$ -value for rejuvenated material, and τ_0 , p , $\bar{\tau}$ are defined by Eqs. (5.9)–(5.11). As can be seen, the resulting flow stress depends on temperature, pressure, and rate, but not on history. When this definition is applied, homogeneous deformation is predicted. The desired history dependence is added by introducing the state parameter S into Eq. (5.15):

$$\eta(T, p, \bar{\tau}, S) = \eta_{0,r}(T) \exp\left(\frac{\mu p}{\tau_0}\right) \frac{\bar{\tau}/\tau_0}{\sinh(\bar{\tau}/\tau_0)} \exp(S) \quad (5.16)$$

where, to a first approximation, the evolution of parameter S is assumed to be:

$$S(t, T, \bar{\gamma}_p) = S_a(t, T) \cdot R_\gamma(\bar{\gamma}_p) \quad (5.17)$$

Here $S_a(t, T)$ represents the ageing kinetics depending on time and temperature, whereas the softening kinetics $R_\gamma(\bar{\gamma}_p)$ are determined by the equivalent plastic strain. Furthermore, it is assumed that the initial value of parameter S is entirely determined by S_a , while the magnitude of $R_\gamma(\bar{\gamma}_p)$, normalized to 1, decreases monotonically to 0 with increasing (equivalent) plastic strain. Similar to Govaert *et al.* [5], S is used as a fitting parameter rather than a true physical parameter.

In contrast to the work of Govaert *et al.* [5], where D reduces an arbitrary history-dependent viscosity, in this approach S increases the fixed rejuvenated viscosity. This is demonstrated schematically in Figure 5.3, which shows the strain-rate dependent yield stress resulting from Eqs. (5.16) and (5.17). The yield stress can be seen to evolve from the rejuvenated reference level to its momentary value through the function S_a , whereas applying plastic deformation reduces the momentary yield stress to the rejuvenated reference level.

With regard to the definition of the state parameter S it should be noted that the

²Note that here the definition of the yield drop is different from that in Chapter 4, where it was defined as the difference between the yield stress and the lower yield stress, which is not the fully rejuvenated yield stress.

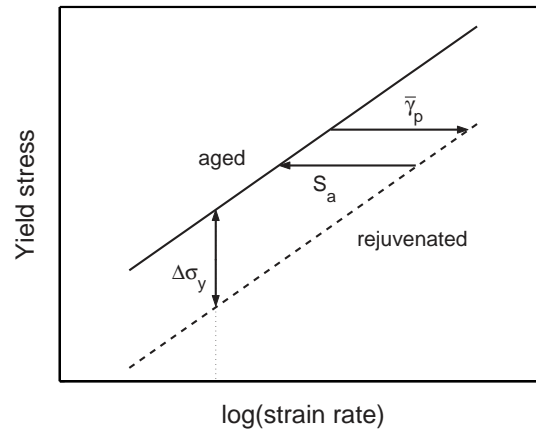


Figure 5.3: Schematic representation of the evolution of yield stress with time, and plastic strain for different strain rates.

effects of aging and rejuvenation are decoupled. This has the advantage that the relevant kinetics can be determined more easily. In reality, however, both kinetics depend on the momentary state of the material.

In the following section the relevant characteristics, kinetics, and material parameters are experimentally determined and validated.

5.4 Results

Two main parts are distinguished: the first concerns the derivation and validation of the intrinsic behaviour, more particularly the softening kinetics $R_\gamma(\bar{\gamma}_p)$, whereas the second concerns the ageing kinetics $S_a(t, T)$ and its validation.

Characterization of intrinsic behaviour

To determine the intrinsic deformation behaviour, a loading geometry that inhibits the occurrence of strain localization during the experiment has to be utilized. The most convenient solution is using a uniaxial compression test. Figure 5.4 shows the intrinsic behaviour of polycarbonate Lexan 121R determined in compression at a true strain rate of 10^{-3} s^{-1} . Following the yield point at a relatively small strain, the material shows true strain softening, and at deformations strains strain hardening sets in.

Assuming that the initial age of the sample is considerably larger than the experimental time scale, no ageing occurs during this experiment, i.e. S_a in Eq. (5.17) is constant. From Eq. (5.14) it follows that the total stress is made up of three main contributions: the rejuvenated stress, the yield drop, and the hardening stress. Assuming incompressible behaviour during plastic deformation, the driving stress σ_s

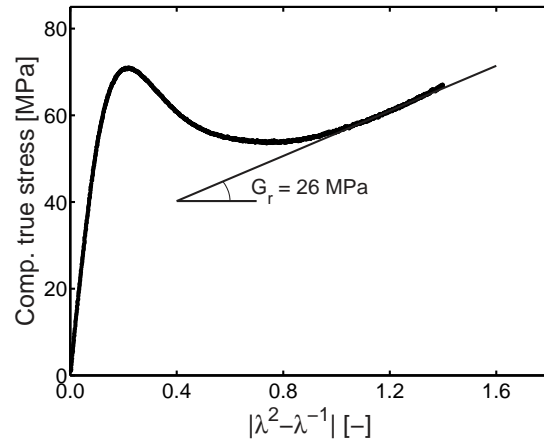


Figure 5.4: Intrinsic deformation behaviour of PC Lexan 121R measured in compression at a true compressive strain-rate of 10^{-3} s^{-1} .

(= $\sigma_{rej} + \Delta\sigma_y$) is given by:

$$\sigma_s = \sigma - \sigma_r = \sigma - G_r (\lambda^2 - \lambda^{-1}) \quad (5.18)$$

where σ is the experimentally determined true stress, σ_r the hardening stress, which is determined by the rubber modulus G_r , and draw ratio λ . The value of the strain hardening modulus is taken from Tervoort and Govaert [16], who obtained a strain hardening modulus for polycarbonate of 26 MPa from three different loading geometries. As seen in Figure 5.4 this value gives a good description of the experimentally determined large strain behaviour.

The resulting driving stress σ_s , shown in Figure 5.5(a), can be split into the contributions of the history independent rejuvenated stress σ_{rej} , and the history dependent transient yield drop $\Delta\sigma_y$:

$$\sigma_s(\dot{\epsilon}, S) = \sigma_{rej}(\dot{\epsilon}) + \Delta\sigma_y(S) \quad (5.19)$$

Equation (5.19) shows that this leads to a separation of strain rate and history dependence.

In Eq. (5.17) S_a determines the magnitude of S and thus the height of the yield drop $|\Delta\sigma_y|$, since at the yield point R_γ is taken to be equal 1. Therefore we can obtain the softening characteristic simply from:

$$R_\gamma(\bar{\gamma}_p) = \frac{\sigma_s - \sigma_{rej}}{|\Delta\sigma_y|} \quad (5.20)$$

where the equivalent plastic strain for uniaxial compression follows from integration of Eq. (5.13): $\bar{\gamma}_p = \sqrt{3}|\dot{\epsilon}|(t - t_y)$, assuming that plastic deformation starts at the yield point. The resulting experimentally determined softening characteristic is shown in Figure 5.5(b) (symbols).

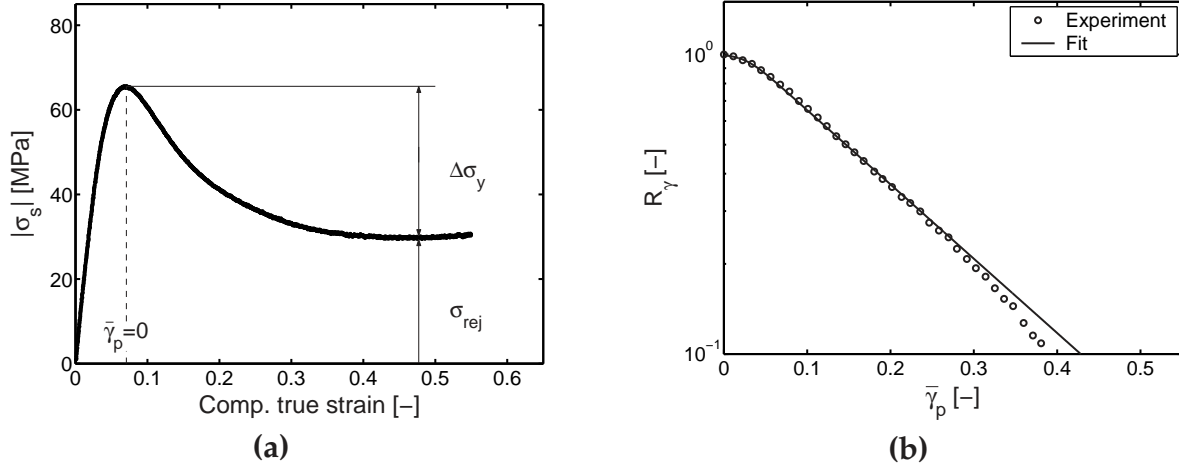


Figure 5.5: (a) Resulting driving stress component after removal of strain hardening. Also indicated are the steady-state rejuvenated, and transient part. (b) Softening characteristic R_γ versus equivalent plastic strain determined from a uniaxial compression experiment. Symbols (\circ) are experimental data, and the solid line is a fit using Eq. (5.21).

Having isolated the experimental softening characteristic, a suitable expression to describe the data can be selected. We propose a modified version of the Carreau-Yassuda function [37]:

$$R_\gamma(\bar{\gamma}_p) = \left(1 + (r_0 \cdot \exp(\bar{\gamma}_p))^{r_1}\right)^{\frac{r_2-1}{r_1}} \quad (5.21)$$

Here $\bar{\gamma}_p$ is the equivalent plastic strain, and r_0 , r_1 , and r_2 are fit parameters. Figure 5.5(b) shows that this expression provides a good description over the whole range of strains, and will therefore be adopted for further use.

Besides the parameters for softening, the model requires the determination of several other parameters. Most of them can be determined from fitting the results of uniaxial compression tests at different strain rates. This is specifically the case for the parameters τ_0 and $\eta_{0,r}$ which determine the rate-dependence of the plastic flow response of the rejuvenated material, and for the strain hardening modulus G_r . Also the parameters governing the softening kinetics (r_0 , r_1 , r_2), and the initial value of S_a can be determined directly in such a fitting procedure. A proven strategy is to start by fitting the response of a rejuvenated material ($S_a = 0$) on the strain hardening regime of the experimental curves giving values for τ_0 , $\eta_{0,r}$ and G_r . Next the softening can be added.

Finally, the three last parameters have to be found: the elastic modulus E , the Poisson ratio ν , and the pressure dependence μ . In the present, single mode, approach, the elastic modulus is chosen slightly too low such that the yield strain of the model ap-

proximately equals the experimentally observed strain-at-yield. In the case of polycarbonate this yielded a value of 900 MPa. The Poisson ratio ν can be determined by monitoring the transverse strain in a uniaxial tension or compression test, for polycarbonate a value of 0.4 was found [12]. The most commonly encountered method to obtain the pressure dependence μ is by measuring the strain rate dependence of the yield stress in different loading geometries (e.g. uniaxial, or planar, tension and compression, shear, etc.) [28, 38, 39]. Disadvantage of this method is that each geometry requires its own, optimized, sample shape and dimensions. In particular the latter can have a strong influence on the thermal history during processing, making it difficult to prepare samples with identical S_a -values for different loading geometries, which is essential to obtain a correct value for μ . This can be avoided by performing experiments directly under superimposed hydrostatic pressure [40–42]. Therefore, we determined μ by numerically predicting the yield data obtained from compression tests at different true strain rates and, finally, from the tensile tests under superimposed hydrostatic pressure as reported by Christiansen *et al.* [41]. Figures 5.6(a) and (b) show that an excellent description was obtained for the material parameters tabulated in Table 5.2 with an initial S_a -value of 27.0 for the compression, and 34.0 for the yield experiments, representing the difference in thermal history between the two material sets used.

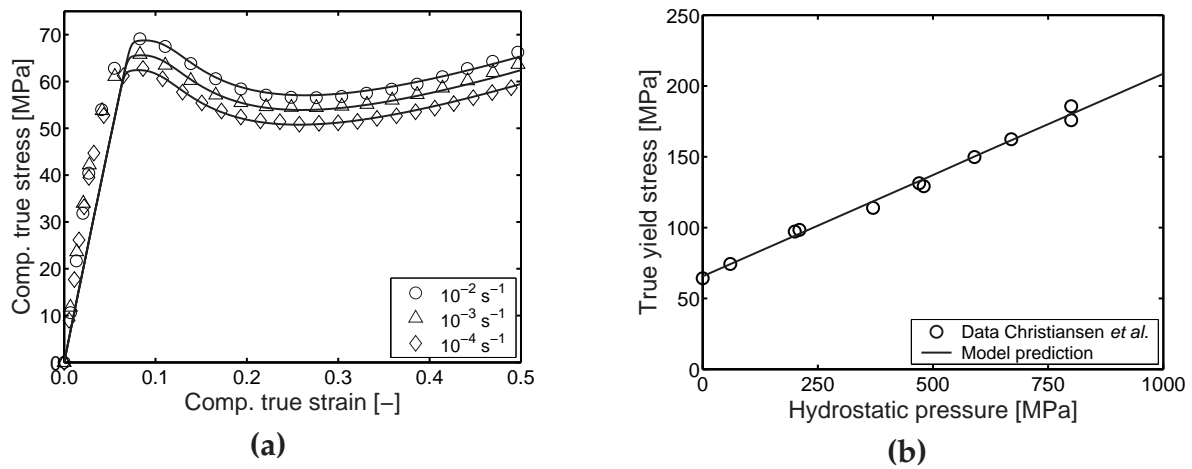


Figure 5.6: (a) True stress versus true strain in uniaxial compression, model prediction (solid lines) compared to experimental results (symbols), for different strain rates. (b) True yield stress versus applied hydrostatic pressure, model prediction (solid line) compared to experimental results (symbols) by Christiansen *et al.* [41] at a strain rate of $1.7 \cdot 10^{-4} \text{ s}^{-1}$.

To investigate whether the model is also quantitative for a different history in the post-yield range, a compression sample was annealed to change its initial state. Figure 5.7 shows that by only slightly increasing the value of S_a from 27.0 to 29.6 it is possible to describe the intrinsic behaviour of the annealed material accurately. It

E [MPa]	ν	$\eta_{0,r}$ [MPa s]	τ_0 [MPa]	μ	S_a	r_0	r_1	r_2	G_r [MPa]
900	0.4	$2.1 \cdot 10^{11}$	0.7	0.08	-	0.965	50	-5	26

Table 5.2: Material parameters obtained from fitting constant strain-rate compression data, Figure 5.6(a), and yield data under hydrostatic pressure, Figure 5.6(b), using the model.

also should be noted that in spite of the difference in initial state both samples show the same rejuvenated state as was already pointed out several times before.

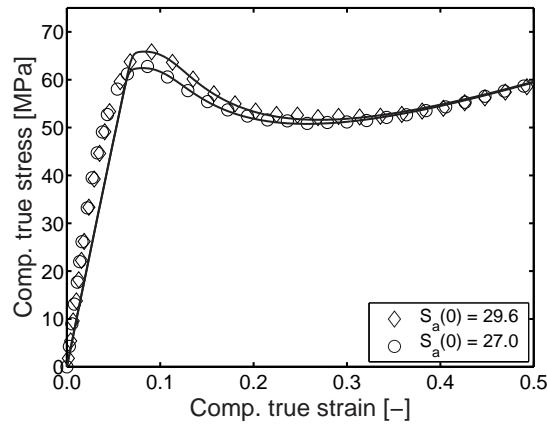


Figure 5.7: True stress versus true strain in uniaxial compression. Model prediction (solid lines) compared to experimental results (symbols), for different initial states at a strain rate of 10^{-4} s^{-1} .

Until now all experimental work was based on one single polycarbonate grade, Lexan 121R. To verify whether the approach is applicable to other grades with different molecular weights and molecular weight distributions, the influence thereof on the deformation behaviour was investigated. Compression, as well as tensile samples of different polycarbonate grades were prepared and tested. To enable a proper comparison, special care was taken to ensure that all samples had the same thermal history.

From Figure 5.8(a) it can be seen that molecular weight has no significant influence on the intrinsic deformation behaviour as obtained from compression tests. This result is in agreement with the observations of van Melick *et al.* [30], who performed similar experiments on polystyrene. Since compression tests can not provide information regarding the influence of molecular weight on the strength of a material, this property was verified using tensile tests. The results of these tests, Figure 5.8(b), show that the tensile strength increases considerably with increasing molecular weight.

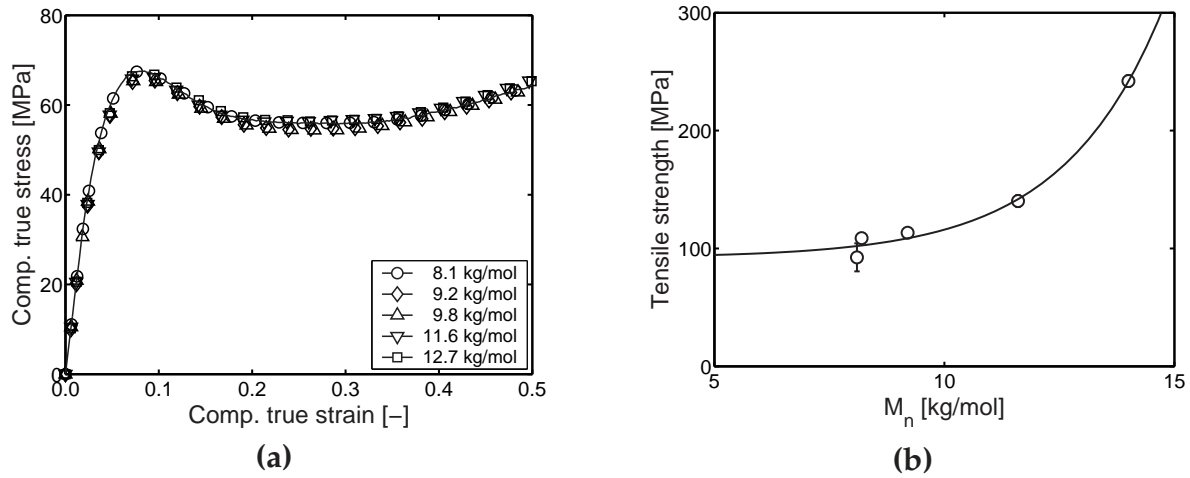


Figure 5.8: Influence of molecular weight M_n on the intrinsic deformation behaviour (a), and tensile strength (b) of polycarbonate. Symbols indicate experimental data, solid lines are guides to the eye.

Validation of intrinsic behaviour

To validate the model it is applied to predict the tensile behaviour of samples with an arbitrary thermal history at different strain rates. Variables that depend on the post-yield behaviour include the draw stress after neck formation, i.e. the constant stress at which the neck propagates, and the draw ratio in the neck. Together with the yield stress these quantities should therefore be predicted sufficiently accurate by the model. For the finite element simulations an axisymmetric model of a tensile bar with a small imperfection in the middle was used. This cylindrical tensile bar has a parallel length of 1 and a radius of 0.2. The circular imperfection has a radius of 0.02 and a maximum depth of 0.003, which is 1.5% of the bar's radius [20]. Govaert *et al.* [5] showed that size and shape of the imperfection have a minor influence on the deformation of the tensile bar. Only the draw ratio during stable neck growth is slightly affected. The finite element mesh consisted of 537 8-node second-order elements [20]. During the tensile test the bar is deformed at constant linear strain rates from 10^{-4} to 10^{-2} s^{-1} , similar to the actual tensile experiments.

From all the parameters in Table 5.2 only S_a needs to be evaluated, since it depends on the history of the material. Fitting the model prediction to the experimentally obtained yield stress at a reference strain rate of 10^{-3} s^{-1} , an initial S_a -value of 33.0 is found.

Figure 5.9(a) shows that the predicted values of both yield stresses and draw stresses, as function of applied strain rate, compare well to the experimentally determined values. The strain rate dependence of the draw ratio in the neck is also predicted well, although the absolute value is slightly too high, see Figure 5.9(b).

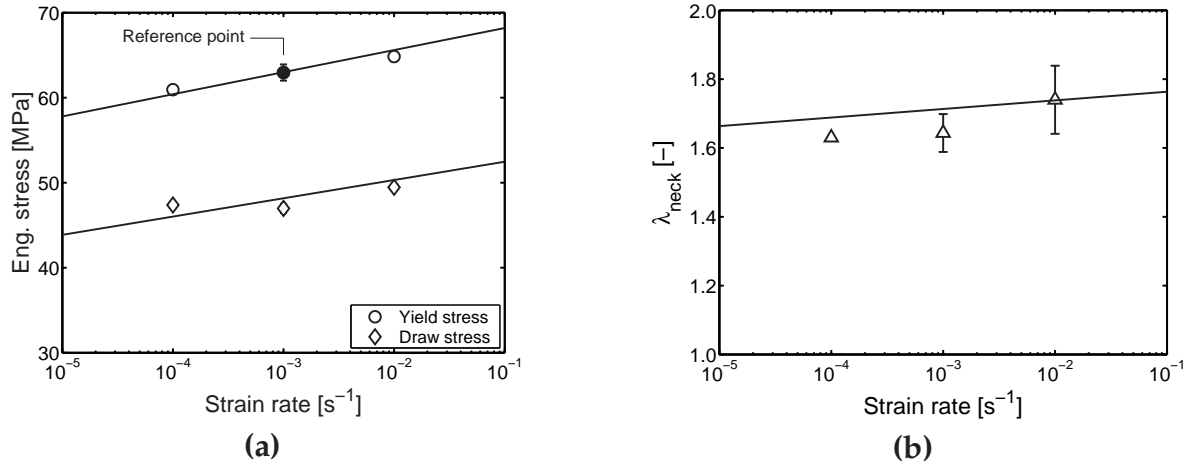


Figure 5.9: Validation of constitutive model, and parameter set. (a) Engineering yield and drawing stress versus strain rate, model prediction (solid lines) compared to experimental results (\circ , \diamond). (b) Draw ratio in the neck versus strain rate, model prediction (solid line) compared to experimental data (\triangle).

Characterization of ageing kinetics

It was shown that the initial state of the material, S_a , can be obtained from a point-fit on the yield stress obtained from a single tensile test. Similarly the ageing kinetics can be determined by monitoring the evolution of yield stress σ_y for a single strain rate, $\dot{\epsilon}_0$, with time. Since the model uses the rejuvenated state as a reference level, it seems straightforward to study the evolution of the yield stress for a rejuvenated material as a function of time. For this purpose cylindrical samples were rejuvenated in torsion and allowed to age at room temperature for different periods of time. Subsequently, the yield stress is determined in tensile at a strain rate $\dot{\epsilon}_0$ of 10^{-2} s^{-1} . In Figure 5.10 the resulting yield stress can be seen to increase linearly with the logarithm of time after an initial plateau.

To describe the kinetics experimentally obtained at 23 °C, we use the following simple expression:

$$\sigma_y(t) = \sigma_{y,0} + c \cdot \log(t + t_a) \quad (5.22)$$

where $\sigma_{y,0}$, c and t_a are fit parameters. For the fit shown in Figure 5.10, $\sigma_{y,0} = 26.1 \text{ MPa}$, the slope $c = 3.82 \text{ MPa/decade}$, and the initial age $t_a = 10715 \text{ seconds}$.

Although the yield stress of a rejuvenated material is expected to increase from the start of ageing, no change is observed during a certain (in this case relatively short) time period. This is due to the fact that the core of the cylindrical sample is not completely rejuvenated [5]. Furthermore, some heat is generated during the rejuvenation procedure, which has an accelerating effect on ageing. As a result the material already has a small initial age, t_a , and as long as the experimental time

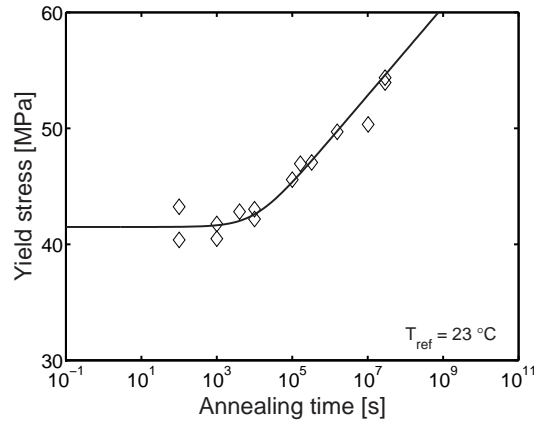


Figure 5.10: Evolution of yield stress at 10^{-2} s^{-1} as a function of time for mechanically rejuvenated samples at $23 \text{ }^\circ\text{C}$, experimental results (\diamond), and fit using Eq. (5.22) (solid line).

is smaller than this initial age no ageing effects are observed. This phenomenon is referred to as *progressive ageing*. Something comparable was also observed by Struik [29] in the long-term creep behaviour of polymers. Only for creep times longer than the age of the samples the mechanical behaviour is influenced during the test.

Compared to mechanically rejuvenated samples, in practice the thermo-mechanical history is either less well defined, or even completely unknown, and therefore most polymers will have a more or less arbitrary initial state, e.g. after injection moulding. Bauwens already showed that for an as-received polycarbonate at room temperature the yield stress did not change during a period of at least 3 years [43]. At elevated temperatures this, however, changes and, particularly for the range near the glass transition temperature, the yield stress again increases with time [31, 32]. Therefore, annealing experiments on injection moulded tensile bars of polycarbonate Lexan 161R were performed at different temperatures from 80 to $130 \text{ }^\circ\text{C}$. Figure 5.11(a) shows the increase in yield stress with annealing time for four annealing temperatures. The increase becomes more pronounced for the higher temperatures, as was also observed by Golden *et al.* [31], and Bauwens-Crowet and Bauwens [32].

The results obtained at various temperatures can be combined into a single master curve using annealing time-temperature superposition. In Figure 5.11(b) the resulting master curve is shown with respect to a reference temperature of $80 \text{ }^\circ\text{C}$. The shift factors used to construct the master curve are accurately described by an Arrhenius relation:

$$a_T(T) = \exp\left(\frac{\Delta U_a}{R} \left(\frac{1}{T} - \frac{1}{T_{ref}}\right)\right) \quad (5.23)$$

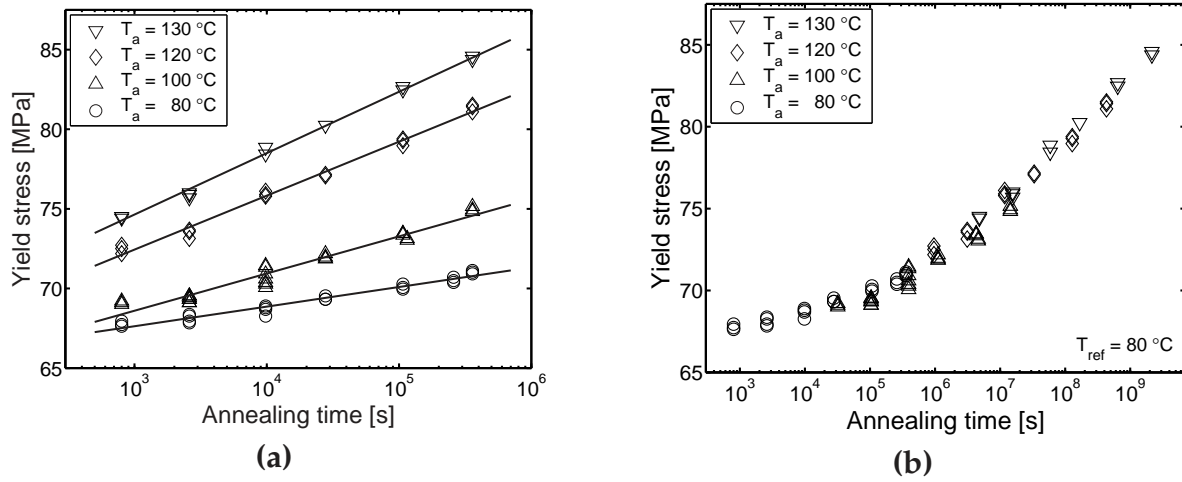


Figure 5.11: (a) Evolution of yield stress as a function of annealing time for different annealing temperatures. Solid lines are to guide the eye, symbols indicate experimental data. (b) Master curve for a reference temperature of 80 °C constructed from the data in Figure 5.11(a).

where ΔU_a denotes the activation energy, R the universal gas constant, T the annealing temperature, and T_{ref} the reference temperature (80 °C). A good description of the shift data was obtained for an activation energy ΔU_a of 205 kJ/mol . This value is only slightly smaller than the 220 kJ/mol that can be derived from data by Bauwens-Crowet and Bauwens [32].

Special caution has to be taken when extrapolating these results to temperatures above 130 °C , since in the temperature range from 130 °C upto T_g several authors observed that an equilibrium value for the yield stress is reached [31, 32]. Similar observations are reported for a DGEBA-epoxy in the range of $T_g - 10$ to T_g by Lee [44]. The equilibrium values are reported to decrease with increasing annealing temperature, as this reduces the time required to attain equilibrium. For decreasing temperatures such a plateau value may also be expected for increasing times. An onset to such a plateau value was, however, not observed in our experiments.

To enable a comparison of the master curve shown in Figure 5.11(b) with the data on the yield stress evolution of the rejuvenated samples, the master curve is shifted to a temperature of 23 °C . This comparison is shown in Figure 5.12(a). In this figure additional data of the same injection moulded samples aged at room temperature for different times are included.

Figure 5.12(a) also shows that the data for the quenched material are described well using Eq. (5.22) with the same values for $\sigma_{y,0}$, and slope c , but with a higher initial age, $t_{a,r}$ of $7.3 \cdot 10^{10}$ seconds. The value 3.82 MPa/decade of the slope is close to that found by Hutchinson *et al.* [33] and LeGrand [26], respectively 4.07 , and

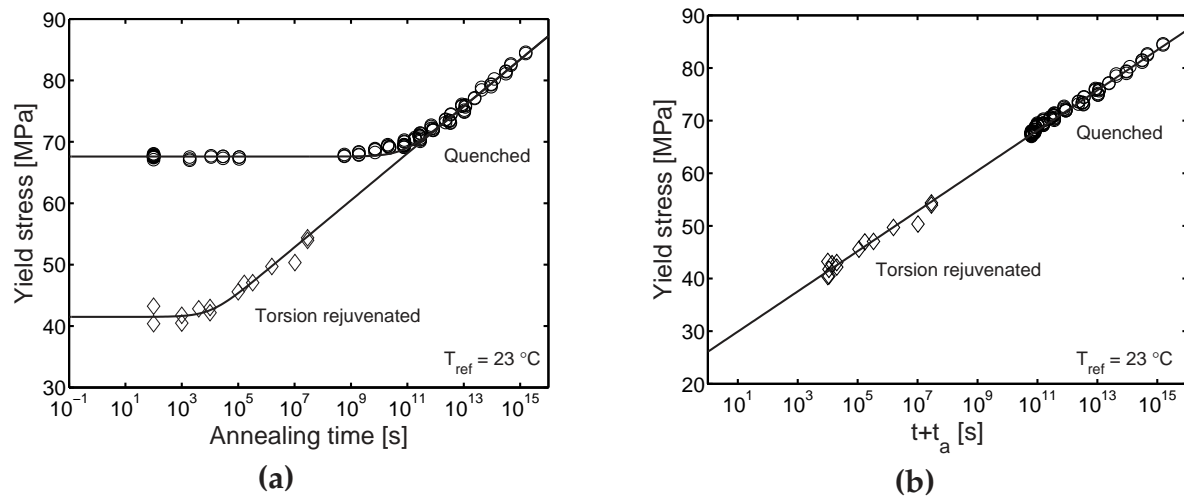


Figure 5.12: Evolution of yield stress of a mechanically rejuvenated material (\diamond), and quenched material (\circ) for a reference temperature of 23 °C . Solid lines are fits using Eq. (5.22).

3.87 MPa/decade. Furthermore, it also describes the annealing data obtained by Bauwens-Crowet and Bauwens [32] to a good approximation.

The large value for the initial age suggests that a change in yield stress can only be expected after several centuries. This agrees well with the observations by Bauwens [43], who saw no change in the yield stress of quenched polycarbonate that had aged for 3 years at room temperature. Further, LeGrand *et al.* [45] did not observe a change in the impact behaviour of polycarbonate that was stored for 35 years, tough still being tough.

In Figure 5.12(b) the time scale of the experiments is compensated for the initial age t_a of the different samples. It shows that both the rejuvenated and as-received samples age at the same rate, and can be described by the same kinetics. Further, the figure suggests that the rejuvenated material eventually will have the same yield stress as the as-received material. This, however, seems to contradict observations by Aboulfaraj *et al.* [35], on annealing a mechanically rejuvenated and as-received DGEBA diepoxy. Both types of samples showed the same aging kinetics, but differed approximately 5 MPa over the entire range of annealing times, including the equilibration plateau. No clear explanation for this difference seems at hand, except that Aboulfaraj *et al.* performed their experiments at the annealing temperature rather than cooling them to room temperature.

Considering the time scale of approximately 10^{11} seconds for the injection moulded samples one could argue that in such case neglecting ageing is a fair assumption. It is, however, also clearly demonstrated that both temperature and history have a significant effect on this time scale. Besides temperature, and history, also the

load applied has a profound influence on the development in time of the yield stress. The effect of stress, or deformation, is though more controversial than that of temperature, or thermal history, as it concerns the ongoing discussion on rejuvenation versus ageing. Whereas some authors claim that stress, or deformation, rejuvenates [29, 46, 47], there are others who claim that stress, or deformation, accelerates ageing similar to temperature [48–54]. Furthermore, there is an ongoing discussion whether either effect comprises a true structural change, or is merely a nonlinear viscoelastic effect [55].

To study the influence of stress on the evolution of the yield stress, a constant load was applied to injection moulded samples of Lexan 161R for different times at 80 °C. After the designated period, the sample was unloaded and allowed to cool to room temperature after which the yield stress was determined. The results are shown in Figure 5.13(a). From this figure it becomes evident that an applied load enhances the increase in yield stress, and that this effect is stronger for higher loads. It might be argued that the increase is due to flow induced orientational effects. Although there undoubtedly will be some orientation, the observed increase in yield stress is far greater than can be estimated on the basis of the plastic strain developed during the annealing periods.

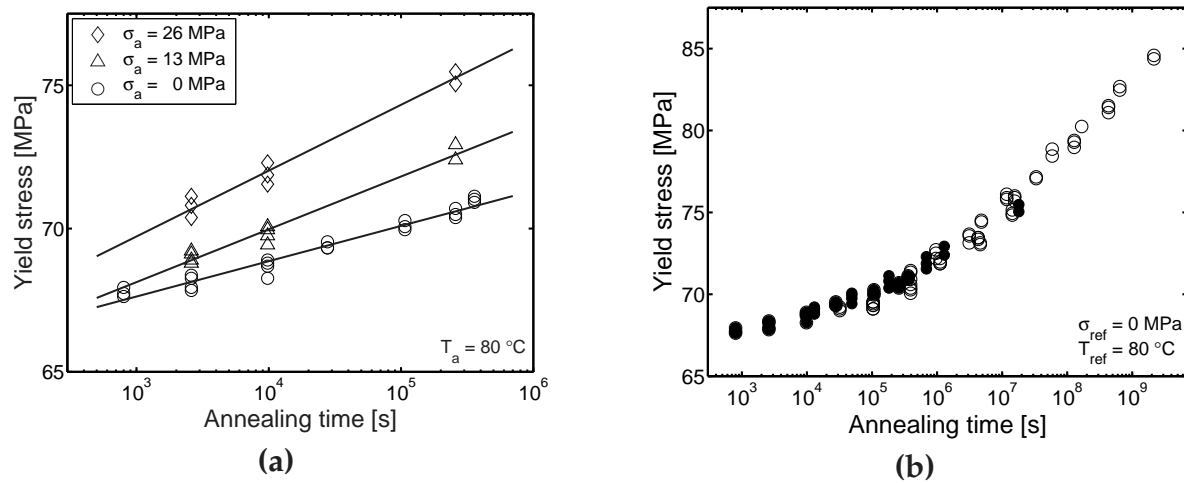


Figure 5.13: (a) Evolution of yield stress as a function of annealing time for different stresses at 80 °C. (b) Master curve constructed from the data in Figure 5.13(a) for a reference stress of 0 MPa and 80 °C (●), compared to the master curve obtained from temperature data only (○).

Similar to temperature, a master curve can be created using a stress activated shift of the Eyring type (annealing time-stress superposition [56]):

$$a_{\sigma}(\bar{\tau}) = \frac{\bar{\tau}/\tau_a}{\sinh(\bar{\tau}/\tau_a)} \quad \text{with:} \quad \tau_a = \frac{RT}{\bar{\nu}_a} \quad (5.24)$$

where an (ageing) activation volume $\bar{v}_a = 1.33 \cdot 10^{-3} \text{ m}^3/\text{mol}$ follows from fitting the shift data, and $\bar{\tau}$ is the equivalent stress applied. Figure 5.13(b) shows that these curves can indeed be superimposed to form a master curve. Moreover, this master curve coincides with that previously obtained for temperature annealing.

This result allows the description of a thermo-mechanical history using a single master curve, combined with a temperature and stress dependent shift function, which, for a constant strain rate $\dot{\epsilon}_0$, leads to the following equation for S_a (see Appendix 5.A):

$$S_a(t_{eff}) = c_0 + c_1 \log(t_{eff}(t, T, \bar{\tau}) + t_a) \quad (5.25)$$

where

$$c_0 = \frac{\sqrt{3} + \mu}{3\tau_0} \cdot \left(\sigma_{y,0}(\dot{\epsilon}_0) - \sigma_{rej}(\dot{\epsilon}_0) - \frac{\sqrt{3}}{\sqrt{3} + \mu} \sigma_r(\lambda_y) \right) \quad (5.26)$$

$$c_1 = \frac{\sqrt{3} + \mu}{3\tau_0} \cdot c \quad (5.27)$$

and the effective time, t_{eff} , is defined as:

$$t_{eff}(t, T, \bar{\tau}) = \int_0^t \frac{d\xi}{a_T(T(\xi)) \cdot a_\sigma(\bar{\tau}(\xi))} \quad (5.28)$$

where a_T and a_σ are given by Eqs. (5.23) and (5.24), respectively. For a reference temperature of 23 °C and strain rate $\dot{\epsilon}_0$ of 10^{-2} s^{-1} the values for c_0 and c_1 equal, -4.41 and 3.3, respectively.

To verify the applicability of these results to other grades, more specifically other molecular weights, the ageing kinetics of several different polycarbonate grades were studied at a temperature of 120 °C. From Figure 5.14 it is clear that the resulting annealing kinetics are independent of molecular weight.

This is according to expectation, since the evolution of yield stress is associated to segmental molecular motion and should, therefore, not be influenced by molecular weight. Similar results were found by Ryan [57] for annealing two polycarbonates with different molecular weights at 125 °C. Although there is a small vertical offset between the curves, which could be due to a difference in thermal history, the slope is the same.

To conclude this part we summarized all relevant parameters for polycarbonate in Table 5.3, with exception of values for the parameter S_a , the initial value for S , or, alternatively the initial age t_a , as these are determined for each material separately, using the yield stress at a reference strain-rate.

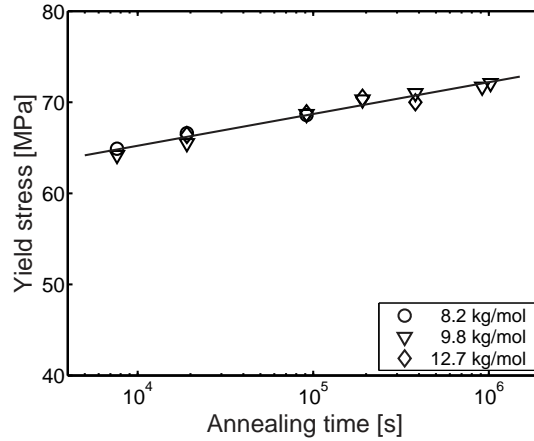


Figure 5.14: Yield stress versus annealing time for different grades of polycarbonate annealed at 120 °C, symbols indicate experimental data, the solid line is a guide to the eye.

E [MPa]	ν	$\eta_{0,r}$ [MPa s]	τ_0 [MPa]	μ	S_a	r_0	r_1	r_2	G_r [MPa]
900	0.4	$2.1 \cdot 10^{11}$	0.7	0.08	-	0.965	50	-5	26

c_0	c_1	t_a [s]	ΔU_a [kJ/mol/K]	\bar{v}_a [m ³ /mol]
-4.41	3.3	-	205	$1.33 \cdot 10^{-3}$

Table 5.3: Material parameters for polycarbonate at a reference temperature of 23 °C.

Validation of ageing kinetics

To validate the expressions determined for the ageing kinetics, the evolution of the yield stress of injection moulded Lexan 141R was studied for two different initial states, obtained by using two different mould temperatures, 25 and 140 °C. Subsequently, samples from both initial states were annealed at temperatures from 80 to 130 °C for increasing annealing times. Using the previously obtained temperature shift expression (Eq. (5.23)) and activation energy, two master curves were constructed which are shown in Figure 5.15(a). Finally, for both types the initial age t_a (rather than S_a , since we used Eq. (5.22)) was determined from a single tensile test at a strain rate of 10^{-2} s^{-1} , and substituted in Eq. (5.22).

Figure 5.15(a) clearly shows that the difference in mould temperature has led to a significant difference in the initial age and thus initial yield stress of the samples. The initial age (at 80 °C) of the samples from the hot mould (140 °C) is about 15 times higher than that of the samples from the cold mould (20 °C). Therefore, the yield stress of the latter samples starts to increase first, and finally coincides with the increasing yield stresses of the other samples. From the figure it is also clear that this behaviour is captured well by the model.

In a second type of validation experiment, injection moulded samples were subjected

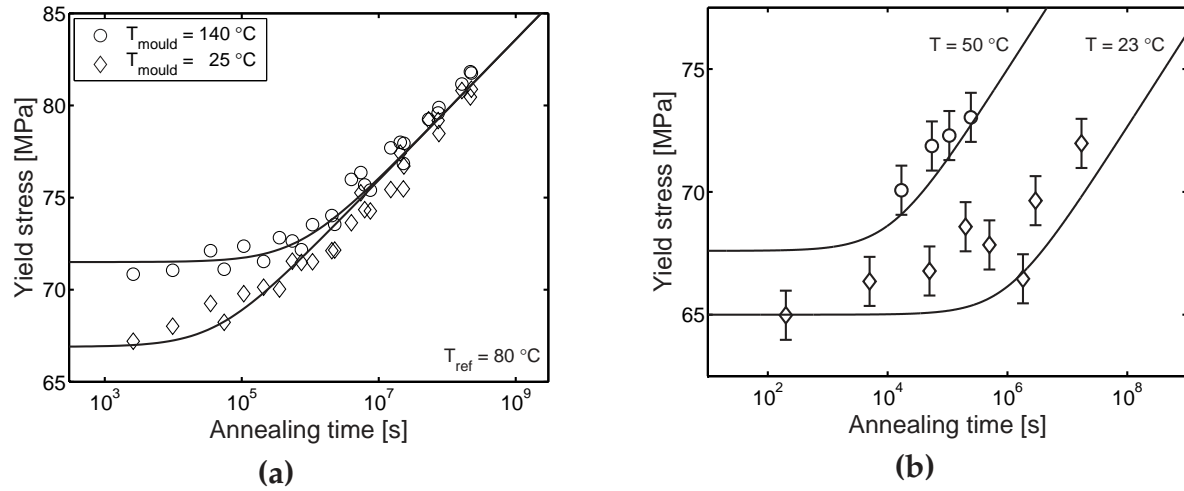


Figure 5.15: Evolution of yield stress as a function of time for: (a) PC Lexan 141R having two different initial ages, and (b) polycarbonate under the influence of combined temperature and stress (40 MPa). Symbols indicate experimental data and solid lines are model predictions.

to a constant load of 40 MPa at two different temperatures (23 and 50 °C) for different annealing times. For both combinations the evolution of the yield stress is shown in Figure 5.15(b), together with the prediction by the model. For both cases, the yield stress is constant at first and then evolves with time, the evolution starting at shorter times for the higher temperature. The model appears to capture the trend in the evolution fairly well, although for room temperature the time scale is slightly overpredicted. It should, however, be noted that the selected test conditions are far outside the experimental window used to determine the material parameters used for this prediction.

5.5 Conclusions

In this investigation a first attempt is made to introduce ageing kinetics in the existing 3D elasto-viscoplastic constitutive models. To achieve this, the driving stress was assumed to consist of a history independent rejuvenated stress, which acts as a reference level for the history dependent yield drop. The evolution of the yield drop, which is the increase in yield stress with time due to ageing, is determined by a single state parameter S that depends on time, temperature, stress, and plastic strain. To a first approximation the ageing and rejuvenation kinetics are represented by two decoupled expressions. Although this limits the applicability, it greatly facilitates the determination of the relevant kinetics.

The relevant softening kinetics could be extracted from the intrinsic deformation behaviour determined in uniaxial compression, and a suitable expression to de-

scribe the kinetics was selected. Some material parameters were obtained from the literature (like the strain hardening modulus and Poisson's ratio), the remainder was determined experimentally from compression tests at different strain rates. The resulting parameter set was shown to be able to correctly predict the strain rate dependence of yield stress, draw stress, and the draw ratio in the neck for a material with an arbitrary initial state, which was obtained from a single tensile test.

Ageing kinetics were determined by monitoring the evolution of the yield stress for mechanically rejuvenated, and quenched, polycarbonate samples. It was shown that, except for a pronounced difference in initial age, both types of samples had the same ageing kinetics. Moreover, the evolution of the yield stress of the rejuvenated samples appeared to coincide with that of the quenched samples for very long times. The resulting kinetics are described with a single expression with different initial ages. Furthermore it was shown that ageing kinetics are accelerated both by temperature, and stress. For each, appropriate shift functions were derived including the material parameters. In combination with the expression for the ageing kinetics it proved possible to describe the evolution of the yield stress of polycarbonate samples subjected to very different thermo-mechanical histories.

The influence of the molecular weight on the intrinsic deformation behaviour, ageing kinetics, and strength was shown. As expected, both the intrinsic deformation behaviour, and ageing kinetics were independent of molecular weight. This simplifies the characterization of different polymers tremendously, since almost all parameters in the constitutive model need to be determined once only, for every polymer. Only the tensile strength showed a clear dependence on molecular weight, which is important for the development of a final failure criterion.

References

- [1] Haward, R. and Thackray, G. (1968). The use of a mathematical model to describe isothermal stress-strain curves in glassy thermoplastics, *Proc. Roy. Soc. A*, **302**, 453–472.
- [2] Boyce, M.C., Parks, D.M., Argon, A.S. (1988). Large inelastic deformation of glassy polymers. Part I: Rate dependent constitutive model, *Mech. Mat.*, **7**, 15–33.
- [3] Wu, P.D. and van der Giessen, E. (1993). On improved network models for rubber elasticity and their applications to orientation hardening in glassy polymers, *J. Mech. Phys. Solids*, **41**, 427–456.
- [4] Buckley, C.P. and Jones, D.C. (1995). Glass-rubber constitutive model for amorphous polymers near the glass transition. *Polymer*, **36**, 3301–3312.

- [5] Govaert, L.E., Timmermans, P.H.M., Brekelmans, W.A.M. (2000). The influence of intrinsic strain softening on strain localization in polycarbonate: modeling and experimental validation, *J. Eng. Mat. Techn.*, **122**, 177–185.
- [6] Meijer, H.E.H. and Govaert, L.E. (2003). Multi-scale analysis of mechanical properties of amorphous polymer systems. *Macromol. Chem. Phys.*, **204**, 274–288.
- [7] Eyring, H. (1936). Viscosity, plasticity, and diffusion as examples of absolute reaction rates. *J. Chem. Phys.*, **4**, 283–295.
- [8] Treloar, L.R.G. (1975). *The Physics of Rubber Elasticity*. Clarendon Press, Oxford, third edition.
- [9] Argon, A.S. (1973). A theory for the low-temperature plastic deformation of glassy polymers, *Phil. Mag.*, **28**, 839–865.
- [10] Wang, M.C. and Guth, E.J. (1952). Statistical theory of networks of non-Gaussian flexible chains, *J. Chem. Phys.*, **20**, 1144–1157.
- [11] Arruda, E.M. and Boyce, M.C. (1993). Effects of initial anisotropy of the finite strain deformation behavior of glassy polymers, *Int. J. Plast.*, **9**, 783–811.
- [12] Tervoort, T.A., Smit, R.J.M., Brekelmans, W.A.M., Govaert, L.E. (1998). A constitutive equation for the elasto-viscoplastic deformation of glassy polymers, *Mech. Time-Dep. Mat.*, **1**, 269–291.
- [13] Leonov, A.I. (1976). Nonequilibrium thermodynamics and rheology of viscoelastic media, *Rheol. Acta*, **15**, 85–98.
- [14] Baaijens, F.P.T. (1991). Calculation of residual stresses in injection molded products, *Rheol. Acta*, **30**, 284–299.
- [15] Hasan, O.A., Boyce, M.C., Li, X.S., Berko, S. (1993). An investigation of the yield and postyield behavior and corresponding structure of poly(methyl methacrylate). *J. Pol. Sci.: Part B: Pol. Phys.*, **31**, 185–197.
- [16] Tervoort, T.A. and Govaert, L.E. (2000). Strain hardening behavior of polycarbonate in the glassy state, *J. Rheol.*, **44**, 1263–1277.
- [17] Wu, P.D. and van der Giessen, E. (1993). Analysis of shear band propagation in amorphous glassy polymers, *Int. J. Sol. Struct.*, **31**, 1493–1517.
- [18] Wu, P.D. and van der Giessen, E. (1993). On neck propagation in amorphous polymers under plane strain tension, *Int. J. Plast.*, **11**, 211–235.
- [19] Meijer, H.E.H., Govaert, L.E., Smit, R.J.M. (1999). A Multi-Level Finite Element Method for Modelling Rubber-Toughened Amorphous Polymers, In: R.A. Pearson, Ed., *Toughening of Plastics*, American Chemical Society, Boston, 50–70.
- [20] van Melick, H.G.H., Govaert, L.E., Meijer, H.E.H. (2003). Localisation phenomena in glassy polymers: influence of thermal and mechanical history. *Polymer*, **44**, 3579–3591.
- [21] Adam, G.A., Cross, A., Haward, R.N. (1975). The effect of thermal pretreatment on the mechanical properties of polycarbonate. *J. Mat. Sci.*, **10**, 1582–1590.
- [22] Cross, A., Haward, R.N. (1978). Orientation hardening in PVC. *Polymer*, **19**, 677–682.
- [23] G'Sell, C. (1986). Plastic deformation of glassy polymers: constitutive equations and macromolecular mechanisms, In: H.J. McQueen *et al.*, Eds., *Strength of metals and alloys*, Pergamon Press, Oxford, 1943–1982.

- [24] Bauwens, J.C. (1978). A new approach to describe the tensile stress-strain curve of a glassy polymer. *J. Mat. Sci.*, **13**, 1443–1448.
- [25] Govaert, L.E., van Melick, H.G.H., Meijer, H.E.H. (2001). Temporary toughening of polystyrene through mechanical pre-conditioning. *Polymer*, **42**, 1271–1274.
- [26] LeGrand, D.G. (1969). crazing, yielding, and fracture of polymers. I. Ductile-brittle transition in polycarbonate. *J. Appl. Pol. Sci.*, **13**, 2129–2147.
- [27] Hill, A.J., Heater, K.J., Agrawal, C.M. (1990). The effects of physical aging in polycarbonate. *J. Pol. Sci.: Part B: Pol. Phys.*, **28**, 387–405.
- [28] Bubeck, R.A., Bales, S.E., Lee, H.-D. (1984). Changes in yield and deformation of polycarbonates caused by physical aging. *Pol. Eng. Sci.*, **24**, 1142–1148.
- [29] Struik, L.C.E. (1978). *Physical aging in amorphous polymers and other materials*, Elsevier, Amsterdam.
- [30] Van Melick, H.G.H., Govaert, L.E., Raas, B., Nauta, W.J., Meijer, H.E.H. (2003). Kinetics of ageing and re-embrittlement of mechanically rejuvenated polystyrene. *Polymer*, **44**, 1171–1179.
- [31] Golden, J.H., Hammant, B.L., Hazell, E.A. (1967). The effect of thermal pretreatment on the strength of polycarbonate. *J. Appl. Pol. Sci.*, **11**, 1571–1579.
- [32] Bauwens-Crowet, C., Bauwens, J.-C. (1982). Annealing of polycarbonate below the glass transition: quantitative interpretation of the effect on yield stress and differential scanning calorimetry measurements. *Polymer*, **23**, 1599–1604.
- [33] Hutchinson, J.M., Smith, S., Horne, B., Gourlay, G.M. (1999). Physical aging of polycarbonate: enthalpy relaxation, creep response and yielding behavior. *Macromolecules*, **32**, 5046–5061.
- [34] Bauwens-Crowet, C., Bauwens, J.-C. (1988). Effect of annealing on the shear yield stress of rejuvenated polycarbonate. *Polymer*, **29**, 1985–1989.
- [35] Aboufaraj, M., G'Sell, C., Mangelinck, D., McKenna, G.B. (1994). Physical aging of epoxy networks after quenching and/or plastic cycling. *J. Non-Cryst. Solids*, **172-174**, 615–621.
- [36] G'Sell, C., Hiver, J.M., Dahoun, A., Souahi, A. (1992). Video-controlled tensile testing of polymers and metals beyond the necking point. *J. Mat. Sci.*, **27**, 5031–5039.
- [37] Macosko, C.W. (1994). *Rheology; Principles, Measurements, and Applications*. VCH Publishers, New York.
- [38] Bauwens-Crowet, C., Bauwens, J.-C., Homès, G. (1972). The temperature dependence of yield of polycarbonate in uniaxial compression and tensile tests. *J. Mat. Sci.*, **7**, 176–183.
- [39] Govaert, L.E., Schellens, H.J., Thomassen, H.J.M., Smit, R.J.M., Terzoli, L., Peijs, T. (2001). A micromechanical approach to time-dependent failure in off-axis loaded polymer composites. *Composites: Part A*, **32**, 1697–1711.
- [40] Sauer, J.A., Mears, D.R., Pae, K.D. (1970). Effects of hydrostatic pressure on the mechanical behaviour of polytetrafluoroethylene and polycarbonate. *Eur. Pol. J.*, **6**, 1015–1032.
- [41] Christiansen, A.W., Baer, E., Radcliffe, S.V. (1971). The mechanical behaviour of polymers under high pressure. *Phil. Mag.*, **24**, 451–467.

- [42] Spitzig, W.A., Richmond, O. (1979). Effect of hydrostatic pressure on the deformation behavior of polyethylene and polycarbonate in tension and compression. *Pol. Eng. Sci.*, **19**, 1129–1139.
- [43] Bauwens, J.-C. (1987). Differences between the effect of annealing and physical ageing on the mechanical behaviour of polycarbonate. *Plast. Rubber Proc. Appl.*, **7**, 143–147.
- [44] Lee, A., McKenna, G.B. (1988). Effect of crosslink density on physical ageing of epoxy networks. *Polymer*, **29**, 1812–1817.
- [45] LeGrand, D.G., Miller, S., McCloskey, P. (2002). Long term room temperature aging of polycarbonate resins, In: A. Co, Ed., *Abstract book 74th Annual Meeting Society of Rheology*, Minneapolis, October 13–17.
- [46] Ricco, T., Smith, T.L. (1985). Rejuvenation and physical aging of a polycarbonate film subjected to finite tensile strains. *Polymer*, **26**, 1979–1984.
- [47] Pixa, R., Le Dû, V., Wippler, C. (1988). Dilatometric study of deformation induced volume increase and recovery in rigid PVC. *Colloid Pol. Sci.*, **266**, 913–920.
- [48] Vincent, P.I. (1960). The necking and cold-drawing of rigid polymers. *Polymer*, **1**, 7–19.
- [49] Kramer, E.J. (1970). Stress aging in anhydrous Nylon 6-10. *J. Appl. Phys.*, **41**, 4327–4341.
- [50] Struik, L.C.E. (1980). The mechanical enhancement of physical aging. *Polymer*, **21**, 962–967.
- [51] Nanzai, Y., Miwa, A., Cui, S.Z. (2000). Aging in fully annealed and subsequently strained poly(methyl methacrylate). *Pol. J.*, **32**, 51–56.
- [52] Nanzai, Y., Cui, S.Z. (2001). Aging in quenched poly(methyl methacrylate) under inelastic tensile strain. *J. Pol. Sci.: Part B: Pol. Phys.*, **33**, 444–449.
- [53] Cui, S.Z., Nanzai, Y., Yoshioka, S. (2000). Aging in quenched polycarbonate under compressive strain. *Kobunshi Ronbunshu*, **57**, 37–44.
- [54] Sternstein, S.S. (1976). Homogeneous and inhomogeneous properties of glassy polymers. *Polym. Prepr.*, **17**, 136–141.
- [55] McKenna, G.B. (2003). Mechanical rejuvenation in polymer glasses: fact or fallacy? *J. Phys.: Condens. Matter*, **15**, 737–763.
- [56] Tervoort, T.A., Klompen, E.T.J., Govaert, L.E. (1996). A multi-mode approach to finite, three-dimensional, nonlinear viscoelastic behavior of polymer glasses, *J. Rheol.*, **40**, 779–797.
- [57] Ryan, J.T. (1978). Impact and yield properties of polycarbonate as a function of strain rate, molecular weight, thermal history, and temperature. *Pol. Eng. Sci.*, **18**, 264–267.

5.A Appendix: ageing kinetics

Under the assumption that at the yield point the material behaves incompressible, it is possible to derive a simple linear relationship between the tensile yield stress $\sigma_y(t)$ at a constant rate of deformation $\dot{\epsilon}_0$ and $S_a(t)$.

For incompressible behaviour the total stress σ can be described by:

$$\sigma = -p\mathbf{I} + 2\eta\mathbf{D}_p + G_r\mathbf{B}^d \quad (5.29)$$

where the unknown hydrostatic pressure p follows from the boundary conditions, the second term represents the flow contribution with viscosity η , defined by Eq. (5.16), and the last term representing the strain hardening contribution with modulus G_r .

For uniaxial deformation under a constant strain rate, we find for the resulting stress σ and hydrostatic pressure p :

$$\sigma = 3\eta\dot{\epsilon}_p + G_r(\lambda^2 - \lambda^{-1}) \quad (5.30)$$

$$p = -\eta\dot{\epsilon}_p - \frac{1}{3}G_r(\lambda^2 - \lambda^{-1}) = -\frac{1}{3}\sigma \quad (5.31)$$

where $\dot{\epsilon}_p$ is the plastic strain rate, and λ is the draw ratio.

It is assumed that at the yield point (λ_y, σ_y) :

- the plastic strain rate equals the applied strain rate $\dot{\epsilon}_0$,
- the softening expression $R_y = 1$ and, therefore, $S = S_a(t)$,
- the argument of the hyperbolic sine in the viscosity function is large, and therefore may be approximated by an exponential function

Incorporation of these considerations, and rewriting, yields for the viscosity:

$$\eta = \frac{\tau_0}{\sqrt{3}\dot{\epsilon}_0} \left[\ln \left(2\sqrt{3} \frac{\eta_{0,r}}{\tau_0} \dot{\epsilon}_0 \right) + S_a(t) + \frac{\mu p}{\tau_0} \right] \quad (5.32)$$

combined with Eqs. (5.30) and (5.31) this results in:

$$\sigma_y(t) = \sigma_{rej}(\dot{\epsilon}_0) + \frac{3\tau_0}{\sqrt{3} + \mu} S_a(t) + \frac{\sqrt{3}}{\sqrt{3} + \mu} \sigma_r(\lambda_y) \quad (5.33)$$

where

$$\sigma_{rej}(\dot{\epsilon}_0) = \frac{3\tau_0}{\sqrt{3} + \mu} \ln \left(2\sqrt{3} \frac{\eta_{0,r}}{\tau_0} \dot{\epsilon}_0 \right) \quad (5.34)$$

$$\sigma_r(\lambda_y) = G_r \left(\lambda_y^2 - \lambda_y^{-1} \right) \quad (5.35)$$

Together with the experimentally obtained evolution equation for the yield stress (Eq. (5.22)) this leads to:

$$S_a(t) = c_0 + c_1 \log(t + t_a) \quad (5.36)$$

with

$$c_0 = \frac{\sqrt{3} + \mu}{3\tau_0} \left[\sigma_{y,0} - \sigma_{rej}(\dot{\epsilon}_0) - \frac{\sqrt{3}}{\sqrt{3} + \mu} \sigma_r(\lambda_y) \right] \quad (5.37)$$

$$c_1 = \frac{\sqrt{3} + \mu}{3\tau_0} \cdot c \quad (5.38)$$

Quantitative prediction of long-term failure of polycarbonate¹

In Chapter 5 a constitutive relation was derived that can account for differences in the initial structural state, as well as the evolution of the structural state in terms of the yield stress. Here, this model is applied to predict the time-dependent ductile failure of polycarbonate under a constant load, which can involve long periods of time and is, therefore, susceptible to physical ageing.

6.1 Introduction

The viscoelastic nature of polymers has a big influence on their deformation and failure behaviour, since their response to different excitations strongly depends on the time-scale of the experiment. An implication is that a polymer loaded well below its tensile strength, as determined in a short-term test, may not sustain this load indefinitely. Classical examples are failure of polymers subjected to long-term static (creep) and dynamic (fatigue) loading [1,2].

The failure of polymers subjected to a long-term static load, generally referred to as creep rupture, is often accompanied by a significant amount of plastic deformation, including the formation of a neck [3,4]. Sometimes the actual failure, either ductile or brittle, is preceded by pre-rupture processes like stress-whitening, cracking, or

¹Reproduced from: Klompen, E.T.J., Engels, T.A.P., van Breemen, L.C.A., Schreurs, P.J.G., Govaert, L.E., Meijer, H.E.H., A 3-D viscoelastic approach to time-dependent failure of polycarbonate. *J. Rheol.*, submitted.

crazing [3–6] and, although these can play an important role in the final failure behaviour, particularly in active environments [7], they are not dealt with here.

Irrespective of the exact failure mode, the molecular mechanism(s) responsible for the long-term failure of polymers is generally accelerated by stress and temperature. With the exception of polyethylene, which sometimes shows a change in failure kinetics at intermediate stresses [8,9], the logarithm of the time-to-failure is observed to increase linearly with decreasing stress for the majority of polymers [3]. In some cases a lower stress limit is encountered below which no failure occurs, the so-called endurance limit [4, 10–12]. The effect of temperature is straightforward, reducing the time-to-failure as temperature increases [4,5,8,10,11]. Decreasing the molecular weight has a similar effect, although it only appears to influence the brittle failure mode [3,8,9]. Orientation [11,13] and structural evolution due to annealing [14], slow cooling [6,8,12], and physical ageing [15], are known to increase the time-to-failure. While most materials show either brittle or ductile failure [3], polyvinylchloride and polyethylene are known to display ductile-to-brittle transitions at intermediate stress levels [5,6,8,9], where the transition observed is accelerated by temperature [4,5,8]. The effect of the stress-state can point in different directions [16,17] and, while in laboratory tests the stress state is often uniaxial, in reality more complex stress states occur, showing different failure kinetics [16–19].

The importance of preventing failure under long-term static loading is evident. It is also clear that the necessity to perform real-time experiments, over the entire lifetime of a polymer structure or component, is highly impractical. This is particularly the case when the influence of all the different parameters, mentioned above, has to be verified. Consequently there is a need for the development of methods and techniques to predict the long-term durability of polymer materials, preferably from short-term tests, and it is, therefore, not surprising that a considerable number of studies has been dedicated to this goal. These studies can roughly be divided into two categories. The first category is that of the molecular theories, which consider failure of either primary [20,21], or secondary [22,23] molecular bonds as a stress activated process. Although these theories have been applied successfully to the failure of many polymers, they have their limitations since they, for instance, can not account for the previously mentioned occurrence of an endurance limit. The second category contains the approaches based on continuum mechanics theory. Most commonly they combine a proper constitutive equation, describing the polymer's (time-dependent) deformation with a suitable failure criterion, such as a critical level of strain [14,15], a deviatoric (free) stored energy [24–26], or a time-dependent yield stress [26]. In essence failure is regarded to occur instantaneously after initiation, which is the moment the failure criterion is met. In this second category we also find the fracture mechanics approaches that consider crack propagation to be the rate determining step. Using a modified linear elastic fracture theory it is possible to predict a time-to-failure under constant stress for both notched and homogeneous materials [27,28].

Although promising results have been obtained, there are reasons which prevent a more extensive use of these models. First, several models require the actual failure data to determine their model parameters and, as a consequence, they lack predictive capability. Second, the majority of the models is essentially one-dimensional, preventing them from being used in more realistic loading geometries. Finally, none of the models can account for the influence of thermal history (including processing). This implies that a change in processing history, or the application of a heat treatment, requires repeating the entire, often very laborious, characterization procedure. Consequently, all changes have to be validated in the actual product under operating conditions. The only remedy to these disadvantages is the development of a 3D constitutive equation (and failure criterion), which can account for differences in thermal history, and molecular weight. This is the objective of the present research.

The failure modes generally observed in long-term failure involve a plastic instability, particularly in ductile failure. For glassy polymers under a constant rate of deformation, the formation of such plastic instabilities is extensively studied, both experimentally [29] and numerically [30–32], for short-term failure. Using three-dimensional constitutive models to describe the intrinsic deformation behaviour, it was shown that the post-yield behaviour plays an essential role in the initiation and stabilization of strain localization in polymers [30–32]. To account for the influence of thermal history a modification and extension of these models was presented, and verified for different molecular weights in Chapter 5, [33]. This modification is based on the fully rejuvenated state that can be attained through application of a large plastic deformation erasing the initial state of the material. In time, the aged state is slowly recovered, a process that is accelerated by temperature and load applied.

In this chapter we show that long-term ductile failure is governed by the same process as short-term ductile failure and that the viscoelastic models developed for the second are therefore applicable for the first. To account for structural evolutions during the long-term loading we use the enhanced model presented in Chapter 5, [33]. First, the creep rupture response of the model is compared to experimentally obtained time-to-failure results on polycarbonate in different loading geometries. Second, the influence of thermal history is investigated experimentally for a high molecular weight polycarbonate, and compared to model predictions. Third, the influence of molecular weight is evaluated using a polycarbonate with a considerably lower molecular weight. Finally, all results are discussed and conclusions are drawn.

6.2 Experimental

Materials

Two different commercial grades of polycarbonate were used Bayer Makrolon CD2000 and General Electric Lexan 121R. In addition we used an extrusion grade of Lexan (General Electric, type unknown) supplied as 6 mm diameter extruded rod, as well as an extrusion grade of Makrolon (Bayer, type unknown) supplied as 3 mm thick extruded sheet. Molecular weight distributions were determined using gel permeation chromatography (GPC), the resulting number-averaged and weight-averaged molecular weights are listed in Table 6.1.

Grade	M_n [kg/mol]	M_w [kg/mol]
Makrolon CD2000	8.2	18.7
Lexan 121R	9.8	23.4
Makrolon sheet	13.3	29.4
Extruded rod	14.0	35.9

Table 6.1: *Weight-averaged and number-averaged molecular weights of the polycarbonate grades used in this study measured with respect to a PC-standard.*

For uniaxial compression tests, cylindrical samples ($\varnothing 6$ mm \times 6 mm) were machined from either the extruded rod, or from plates ($200 \times 200 \times 10$ mm³), that were compression moulded from granular material at a temperature of 250 °C. First the dried granulate was heated for 15 minutes and next compressed up to 300 kN in five subsequent intervals of 5 minutes. After each step the force was released to allow for degassing. Finally, the mould was placed in a cold press and cooled to room temperature (20 °C) under a moderate force (100 kN). Tensile samples were prepared either through injection moulding, or milled from compression moulded plates ($160 \times 160 \times 3$ mm³), moulded according to the procedure outlined above. The geometry of all tensile specimens was according to ISO 527.

A separate set of samples for three different loading geometries was prepared from the Makrolon sheet. For uniaxial tensile tests, samples according to ASTM D638 and a thickness of 1.7 mm were milled from this sheet. For planar extension tests, rectangular samples with a dogbone-shaped cross-section were milled from the sheet, see [34], with in the testing region a thickness of 1.7 mm over a length of 10 mm and a width of 50 mm. Due to the large width-to-length ratio the contraction of the material is constrained, creating a plane strain condition [35]. For simple shear tests, samples similar to those used in the planar tests were used, now with a width of 100 mm instead of 50 mm. With a gauge length of 10 mm this results in an aspect ratio of 10. To avoid any influence of orientation effects due to the extrusion process all samples were taken from the same direction.

Thermo-mechanical treatments

Annealing of some of the samples was performed for 120 hours in an air circulated oven at a temperature of 120 °C. Initial equilibration of the sample temperature was measured to take approximately 15 minutes. After a predefined ageing time the samples were removed from the oven and allowed to cool to room temperature in air before being tested.

Mechanical pre-conditioning under dead-weight loading was performed on either a Zwick Rel servo-hydraulic tensile tester equipped with a temperature chamber, or by using a long-term dead-weight setup at room temperature.

Mechanical testing

Uni-axial compression tests were performed on a servo-hydraulic MTS Elastomer Testing System 810. The specimens were cylindrical shaped and compressed under true strain control, at constant true strain-rates of 10^{-4} to 10^{-2} s⁻¹ between two parallel, flat steel plates. Friction between samples and plates was reduced by an empirically optimized method. Onto the sample ends a thin film of PTFE tape (3M 5480, PTFE skived film tape) was applied and the contact area between steel and tape was lubricated using a 1:1 mixture of liquid soap and water. During the test no bulging of the sample was observed, indicating that the friction was sufficiently reduced.

Uniaxial and planar tensile tests were performed on a Zwick Z010 tensile tester, at constant linear strain-rates of 10^{-5} to 10^{-1} s⁻¹. Shear tests were performed on a Zwick 1475 at shear rates from 10^{-5} to 10^{-2} s⁻¹. Stress-strain curves were recorded and, where appropriate true stresses were calculated assuming a constant sample volume.

Constant load tests at high loads in uniaxial and planar extension were performed on a Zwick Z010 tensile tester, and in shear on a Zwick 1475. The load was applied in approximately 10 seconds, both force and displacement were monitored. Uniaxial constant load tests at comparatively medium and low stresses were performed under dead-weight load on a static load setup. At long loading times electronic timers were used to detect failure of a sample.

6.3 Time-dependent ductile failure: relation to intrinsic behaviour

An example of long-term time-dependent deformation is shown in Figure 6.1(a). The evolution of creep strain for a polycarbonate sample subjected to a constant tensile load of 55 MPa is shown, as well as various marked stages of the macroscopic deformation. Initially, the sample deforms homogeneously at a decreasing rate until, after some time, a constant minimum creep rate is reached. Subsequent to this stage, the creep rate increases again, finally resulting in the formation of a sudden neck that

propagates rapidly along the length of the sample.

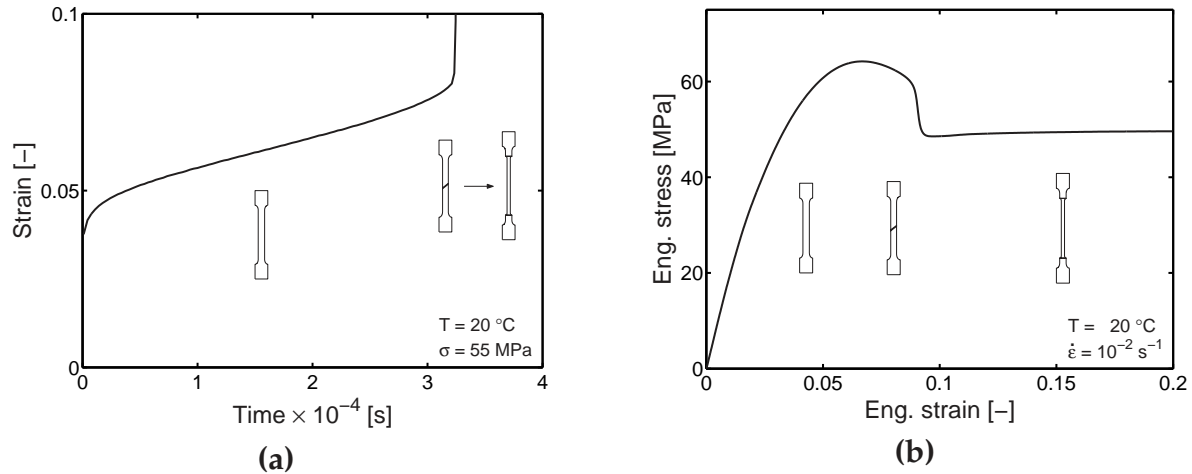


Figure 6.1: Deformation behaviour of polycarbonate in uniaxial tension (a) under a constant load of 55 MPa, and (b) at a constant strain-rate of 10^{-2} s^{-1} .

This typical pattern of homogeneous deformation, neck formation, and neck growth is also observed at a constant rate of deformation in a short term tensile test (Figure 6.1(b)). During the initial homogeneous deformation the stress rises until a maximum is reached, the yield stress. Shortly after the yield stress a neck is formed that propagates at a constant rate and stress along the sample.

From numerical investigations it has become evident that the occurrence of plastic instabilities such as neck formation, but also crazing, is closely related to the intrinsic deformation behaviour of polymer materials determined from constant true strain-rate compression experiments [30–32], see Figure 6.2(b). At relatively small deformations, the yield stress of the material is reached. With increasing strain the stress decreases, generally referred to as (true) strain softening. At even larger strains the stress rises again due to orientation of the polymer molecules: strain hardening. Both experimental and numerical studies showed that the post yield behaviour plays an important role in strain localization phenomena. Initiation of the instability is triggered by strain softening, whereas strain hardening stabilizes the localization allowing it to grow [29–32].

Now we can of course also compare this intrinsic behaviour in a *constant true strain-rate* compression test (Figure 6.2(b)), with that in a *constant true-stress* compression experiment, Figure 6.2(a). Upon loading, the strain increases at a decreasing rate, reaching a constant creep rate. After a long time of steady creep, the creep rate accelerates rapidly and the sample becomes compressed homogeneously in a relatively short time. At large strains this acceleration decreases strongly, and further creep proceeds at a strongly reduced rate. This behaviour of Figure 6.2(a) includes

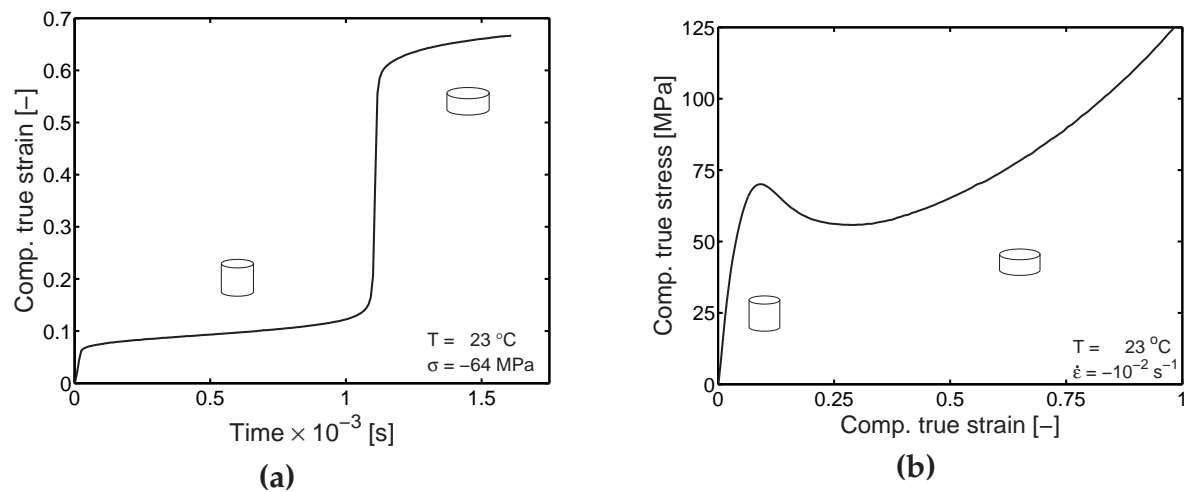


Figure 6.2: Intrinsic deformation behaviour of polycarbonate in uniaxial compression (a) under a constant true compressive stress of 64 MPa, and (b) at a constant true compressive strain rate of 10^{-2} s^{-1} .

the same features as described for the constant rate compression test, Figure 6.2(b): yield, (true) strain softening, and strain hardening. This is illustrated more clearly by using a so-called Sherby-Dorn plot [36], Figure 6.3, for different levels of applied stress.

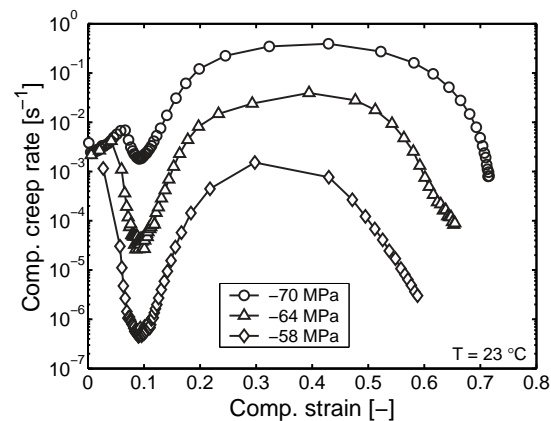


Figure 6.3: Sherby-Dorn plot for polycarbonate in uniaxial compression under three different compressive true stresses.

The graphs show that, after applying the initial load, the creep rate decreases to a minimum level. It was shown by Bauwens-Crowet *et al.* for polycarbonate [37], and by Nanzai for polymethylmethacrylate [38], that this point is identical to the yield point observed in a constant strain-rate test. After passing the yield point the material starts to soften which, due to the constant stress applied, results in a fast increase in creep rate and, therefore, creep strain. At sufficiently large strains, the orientation-induced strain hardening sets in, stabilizing the softening process and

strongly reducing the creep rate (the vertical axis is logarithmic).

From these results it is concluded that the intrinsic deformation under constant load already contains an inherent failure mechanism which is strain softening. While first deforming homogeneously, the onset of strain softening results in a sudden, large, increase of strain. Macroscopically, the strain softening phenomenon triggers a strain localization which manifests itself in the formation of a neck.

Due to the strong similarity between the intrinsic behaviour under constant stress and that under constant strain rate, it is suggested that the 3D constitutive models used for the latter are applicable to constant load tests as well. In view of the larger time scales involved, such models should, however, also account for structural evolution due to physical ageing. An example of such an approach was presented in Chapter 5, [33], and will be summarized below.

6.4 Constitutive modelling

All 3D constitutive models for solid polymers start with the split of the total stress in two main contributions, based on the original work of Haward and Thackray [39]:

$$\sigma = \sigma_s + \sigma_r \quad (6.1)$$

where σ_r denotes the strain hardening contribution that is attributed to molecular orientation and is described by neo-Hookean behaviour, and σ_s includes the contribution due to rate dependent plastic flow. This plastic flow process is represented by a nonlinear Maxwell model [40] as suggested by Baaijens [41]. Under isothermal conditions the nonlinearity of the model is completely governed by a stress, pressure, and state dependent viscosity η , which is defined as:

$$\eta(T, \bar{\tau}, p, S) = \eta_{0,r}(T) \underbrace{\frac{\bar{\tau}/\tau_0}{\sinh(\bar{\tau}/\tau_0)}}_{(I)} \underbrace{\exp\left(\frac{\mu p}{\tau_0}\right)}_{(II)} \underbrace{\exp(S(t, \bar{\gamma}_p))}_{(III)} \quad (6.2)$$

Here the part marked (I), where $\bar{\tau}$ is the equivalent stress, represents the stress dependence of the viscosity governed by the parameter τ_0 . Part (II) yields the pressure dependency governed by the parameter μ , and where p is the hydrostatic pressure. Part (III) represents the dependence of the viscosity on the state of the material expressed by the state parameter S . Finally $\eta_{0,r}(T)$ denotes the viscosity for the completely rejuvenated state.

The material state S is determined by two processes, physical ageing measured as an increase in yield stress, and mechanical rejuvenation during loading, mea-

sured as true strain softening. In the model, these two processes are decoupled: $S(t, \bar{\gamma}_p) = S_a(t) \cdot R_\gamma(\bar{\gamma}_p)$. In this expression the function R_γ describes the mechanical rejuvenation upon plastic deformation $\bar{\gamma}_p$ and is given by:

$$R_\gamma(\bar{\gamma}_p) = (1 + (r_0 \cdot \exp(\bar{\gamma}_p))^{r_1})^{\frac{r_2-1}{r_1}} \quad (6.3)$$

where $\bar{\gamma}_p$ denotes the equivalent plastic strain, and r_0 , r_1 , and r_2 are fitting parameters. The ageing contribution is $S_a(t)$:

$$S_a(t_{eff}) = c_0 + c_1 \log(t_{eff}(t, \bar{\tau}, T) + t_a) \quad (6.4)$$

where c_0 , c_1 are constants determined at a constant strain rate of 10^{-2} s^{-1} , t_a is the initial age, and t_{eff} is the effective time, defined as:

$$t_{eff}(t, \bar{\tau}, T) = \int_0^t \frac{d\xi}{a_\sigma(\bar{\tau}(\xi)) \cdot a_T(T(\xi))} \quad (6.5)$$

where a_σ a stress activation of the Eyring-type, and a_T is a temperature shift function of the Arrhenius-type.

In Chapter 5 the details of the model and all relevant material parameters were given, partly reproduced in Table 6.2. Values for the parameter S_a , the initial value for S at the initial age t_a , are not provided since they are determined for each material separately measuring the yield stress at a single strain-rate.

E [MPa]	ν	$\eta_{0,r}$ [MPa s]	τ_0 [MPa]	μ	S_a	r_0	r_1	r_2	G_r [MPa]										
900	0.4	$2.1 \cdot 10^{11}$	0.7	0.08	-	0.965	50	-5	26										
<table border="1"> <thead> <tr> <th>c_0</th> <th>c_1</th> <th>t_a [s]</th> <th>ΔU_a [kJ/mol/K]</th> <th>\bar{v}_a [m³/mol]</th> </tr> </thead> <tbody> <tr> <td>-4.41</td> <td>3.3</td> <td>-</td> <td>205</td> <td>$1.33 \cdot 10^{-3}$</td> </tr> </tbody> </table>										c_0	c_1	t_a [s]	ΔU_a [kJ/mol/K]	\bar{v}_a [m ³ /mol]	-4.41	3.3	-	205	$1.33 \cdot 10^{-3}$
c_0	c_1	t_a [s]	ΔU_a [kJ/mol/K]	\bar{v}_a [m ³ /mol]															
-4.41	3.3	-	205	$1.33 \cdot 10^{-3}$															

Table 6.2: Material parameters for polycarbonate at a reference temperature of 23 °C.

To demonstrate the model's capability, constant strain-rate compression tests were numerically simulated and compared to experimental results, see Figure 6.4(a) which shows an excellent description of the strain rate dependence of both the yield and post-yield behaviour. Due to the single mode representation, the pre-yield behaviour is not captured accurately. Employing a multi-mode representation will improve on this significantly.

Figure 6.4(b) shows that also for different initial ages the yield and post-yield behaviour is captured well by the model. At large strains the calculated stresses coincide, something which has also been observed in experiments on various polymers [29, 42, 43].

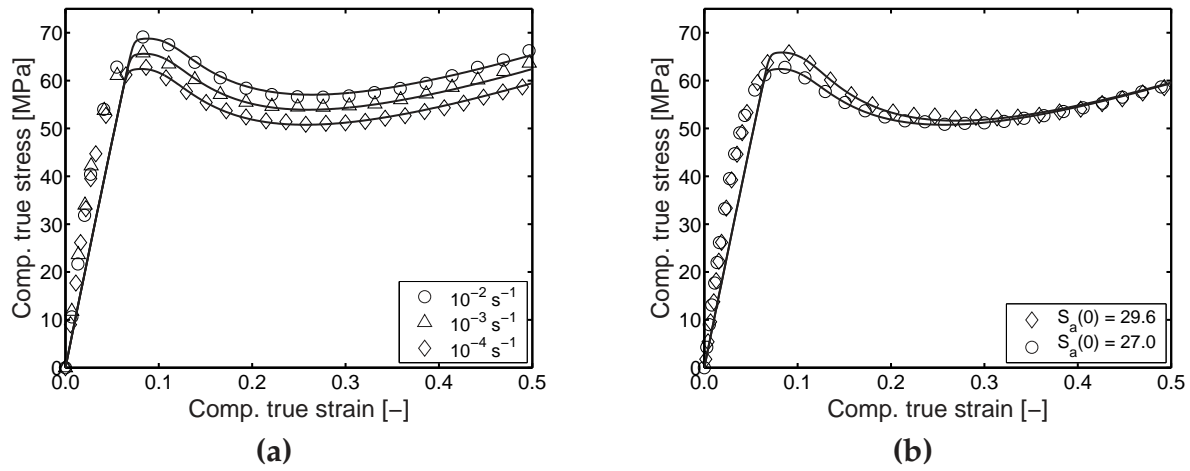


Figure 6.4: Comparison of model predictions (solid lines) to experimental results (symbols) for (a) different strain rates, and (b) quenched (○) and annealed (◇) samples.

6.5 Application to time-dependent ductile failure

Influence of loading geometry

The loading geometry is known to play an important role in deformation and failure. This is shown by the true yield stresses obtained for polycarbonate strained at different rates in three different loading geometries, Figure 6.5(a). The response is strongly geometry dependent in both the magnitude of the yield stress as well as its rate dependence. Identical trends can be observed in the time-to-failure of creep rupture experiments where a constant load is applied to the same material until either a neck or shear band is formed, Figure 6.5(b).

Finite element simulations were performed using full three-dimensional meshes of the uniaxial, planar, and shear samples used in the experiments, consisting of 2130, 3760, and 7520 eight-node linear brick elements, respectively. During the constant rate of deformation tests the samples were deformed at constant linear strain rates from 10^{-5} to 10^{-1} s^{-1} , similar to the actual experiments. Time-to-failure for different constant loads was predicted by applying a load to the samples in 10 seconds, conform the average experimental application time, and sustaining this load accordingly. For the constant load calculation, the time step is controlled by an adaptive time stepping scheme based on a critical strain increment. The actual failure time is defined as the time at which a strain localization, which can be either a neck or a shear band, is formed and starts propagating.

To enable numerical simulations, the initial value of the state parameter S was fitted using the experimental yield stress in uniaxial extension at a single strain rate of 10^{-3} s^{-1} as the reference point (see the single filled symbol in Figure 6.5(a)). This resulted in a value for $S_a(0)$ of 31.7, or, using Eq. (6.4), an initial age t_a of $8.76 \cdot 10^{10}$ seconds.

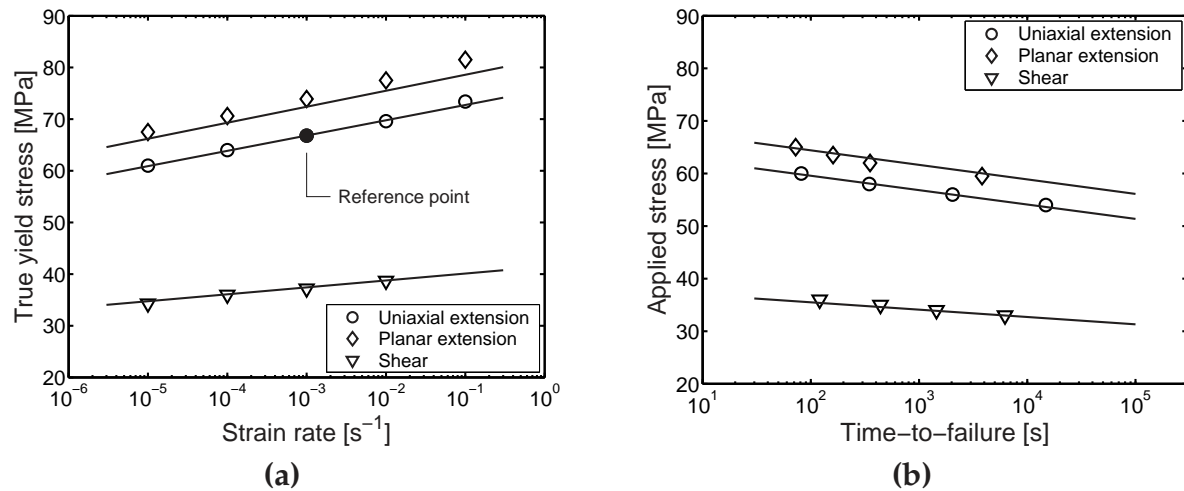


Figure 6.5: (a) True yield stress vs. strain rate for polycarbonate in three different loading geometries, and (b) applied stress vs. time-to-failure for polycarbonate in three different loading geometries. Symbols indicate experimental results, and solid lines represent model predictions.

Using the general parameter set of Table 6.2, and the fitted values for S_a or t_a , an excellent description of both the magnitude and rate dependence of the true yield stresses is found for each loading geometry, compare the solid lines (model predictions) and the symbols (experiments) in Figure 6.5(a). In the numerical calculations of the constant load experiments of Figure 6.5(b) ageing did not have to be taken into account, i.e. t_{eff} in Eq. (6.4) is set zero, given the relatively short experimental time scale. The results of the model predictions (solid lines) of the constant load experiments (symbols) are shown in Figure 6.5(b). From this figure it is clear that the model accurately predicts both the stress dependence as well as the magnitude of the times-to-failure for the three different loading geometries used in this investigation.

Influence of thermal history

Thermal history has a profound influence on the initial state of a polymeric material, and thus on its (macroscopic) deformation and failure. Therefore two different sets of samples were prepared, one via annealing. Tensile tests on these two sets revealed a significant increase in yield stress for the annealed specimens, whereas the strain rate dependence remained unaffected (Figure 6.6(a)), which corresponds to similar observations by Bauwens-Crowet and Bauwens [44].

Subsequently, creep rupture experiments were performed where samples are subjected to a constant load until either a neck is formed, or the sample breaks. Both sets of samples formed a neck, although the annealed samples fractured shortly after necking. The experimental results show a strong resemblance to the tensile results in that, for a given time, the annealed samples can sustain a higher load than the

quenched samples, and that the stress dependence is independent of the thermal history (Figure 6.6(b)). Similar to the experiments of Narisawa *et al.* [12], the quenched materials show what appears to be the onset of an endurance limit.

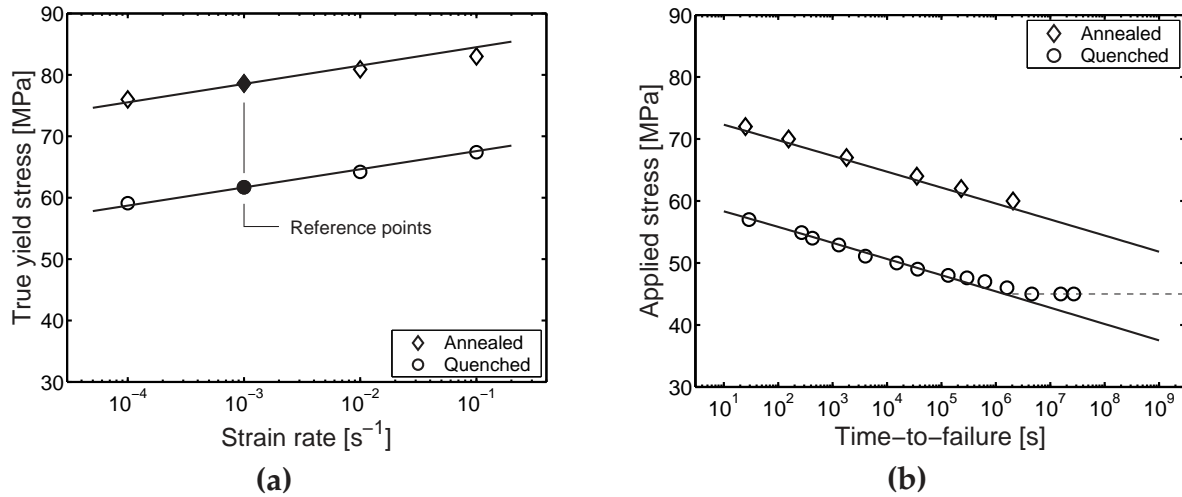


Figure 6.6: (a) Yield stress vs. strain rate for quenched and annealed polycarbonate, and (b) Applied stress vs. time-to-failure for quenched and annealed polycarbonate. Symbols indicate experimental results, and solid lines represent model predictions (ageing not taken into account).

Finite element simulations were performed using an axisymmetric model of a tensile bar with a small imperfection in the middle. This cylindrical tensile bar has a parallel length of 1 and a radius of 0.2. The circular imperfection has a radius of 0.02 and a maximum depth of 0.003, which is 1.5% of the bar's radius [29]. The finite element mesh consists of 537 8-node second-order elements [29]. Furthermore, the same procedure as in the previous section was applied for the prediction of tensile and creep rupture tests.

The resulting fitted values for $S_a(0)$ were 28.05 and 41.5, and the initial ages t_a were $6.86 \cdot 10^9$ and $8.17 \cdot 10^{13}$ seconds for the quenched and the annealed material, respectively. Using the general parameter set of Table 6.2, and the fitted values for S_a or t_a , an excellent description of magnitude and strain rate dependence of the yield stress is found, see Figure 6.6(a). When, to a first approximation, ageing is not taken into account in the constant load experiments, i.e. in Eq. (6.4) t_{eff} is again set zero, the results for the long term prediction shown in Figure 6.6(b) are obtained. Despite the limited range of strain rates used to characterize the kinetics, it is clear from this figure that the stress dependence of the failure times is predicted very well over a large range of stresses and times. The reasons for this successful extrapolation was demonstrated by Bauwens-Crowet *et al.* [37] who showed that for polycarbonate the yield behaviour in both tensile and creep loading is governed by a single process. In addition to the prediction of the stress dependence of

the times-to-failure, Figure 6.6(b) also shows that the difference in initial state is extremely well accounted for. In contrast to the experimental results, the model predicts, however, no endurance limit for the quenched material.

This changes, however, drastically when ageing is taken into account by including Eqs. (6.4) and (6.5) in the calculation, and relating, as a first approximation, the stress activated part of the effective time expression (Eq. (6.5)) to the applied stress rather than the local stress. From Figure 6.7(a) it can be seen that the incorporation of ageing leads to a considerable improvement of the prediction for the quenched material including an endurance limit at 44 MPa.

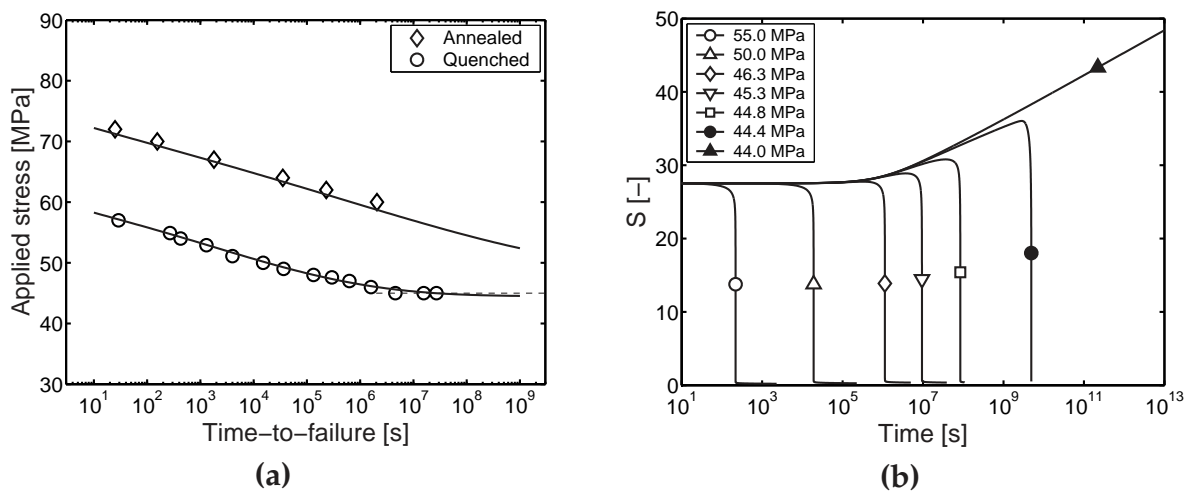


Figure 6.7: (a) Comparison of experimental results (symbols) with numerically predicted failure times using the model including ageing (solid lines) for both quenched and annealed material. (b) Evolution of the state parameter S as a function of time for the quenched material at different stress levels.

The origin of this improvement in prediction, and the existence of an endurance limit, is clarified in Figure 6.7(b), displaying the local evolution of the state parameter S with time for the quenched material at different applied loads in a representative node on the axis of symmetry below the imperfection. At high stresses and short failure times, the material rejuvenates (S goes to zero) since strain softening decreases the parameter S . With decreasing loads, and thus increasing loading times, the influence of the stress accelerated ageing process becomes noticeable. For small loads and long times this process becomes dominant resulting in an increase in S , and consequently an increase in the yield stress and a reduction in creep rate and thus the prevention of an accumulation of plastic strain. As a result, softening can no longer occur and the material no longer fails by necking.

Influence of molecular weight: a tough-to-brittle transition

Until now we only used a single polycarbonate grade (Lexan 121R) of relatively high molecular weight. In the introduction it was, however, already pointed out that failure is affected by molecular weight. A decrease in molecular weight can lead to a reduction of failure times sometimes accompanied by a change in failure mode [3,8,9].

In Chapter 5, [33], it was shown that, provided that the thermal history is the same, the intrinsic deformation behaviour of polycarbonate is independent of the molecular weight. This is confirmed once more in Figure 6.8 which shows the strain rate dependence of the yield stress for a high (Lexan 121R), and low molecular weight (Makrolon CD2000) polycarbonate having identical thermal histories.

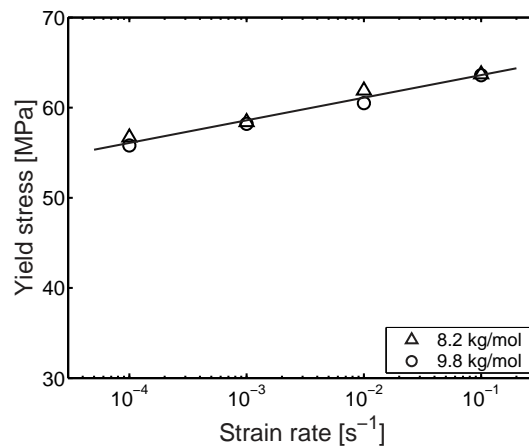


Figure 6.8: Comparison of the strain rate dependence of the yield stress for a low (CD2000), and high molecular weight polycarbonate (121R). Symbols indicate experimental results, and the solid line is a linear fit to guide the eye.

Based on this observation, and the results of the previous sections, it can be anticipated that creep rupture of the low molecular weight material is identical to that of the high molecular weight material and that, consequently, the numerical results obtained for the high molecular weight material also apply to the low molecular weight material.

Actual creep rupture experiments performed on the low molecular weight material show that this is only partially true, Figure 6.9(a). For high stresses the failure kinetics are indeed the same and, here, both grades fail ductile through neck-formation. With decreasing stress, the time to failure increases and the failure mode for the low molecular weight material gradually changes to brittle. In the transition zone, a neck is still formed, but fails shortly after initiation, see Figure 6.9(b). At this stage locally

fairly large strains can still be observed. With further decrease of the stress applied, the plastically deformed zone becomes smaller until finally the failure becomes completely brittle, see the filled symbols in Figure 6.9(a).

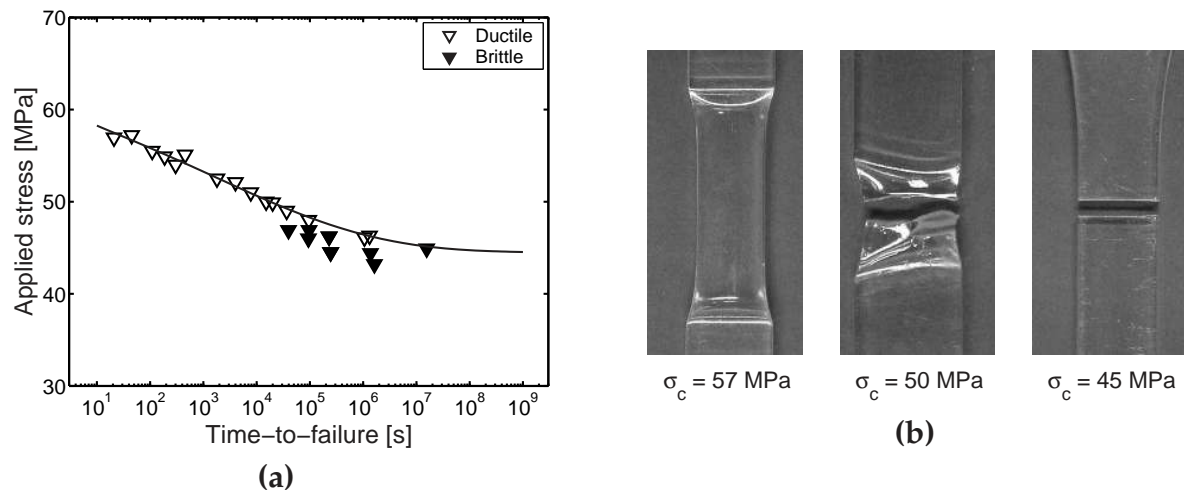


Figure 6.9: (a) Applied stress versus time-to-failure for the low molecular weight polycarbonate (CD2000), symbols indicate experimental results and the solid line is the model prediction from Figure 6.7(a). (b) Macroscopic failure behaviour of low molecular weight polycarbonate at different loads applied.

Despite the change in failure mode, Figure 6.9(a) clearly shows that the failure kinetics are not significantly influenced. This is in line with observations reported in literature for polyvinylchloride [5] and polyethylene [4, 6]. The change in failure kinetics observed for polyethylene at elevated temperatures [8, 9] was attributed to oxidative thermal degradation, reducing the molecular weight *during* the experiment, by Gedde *et al.* [45]. Results by Crissman and McKenna [14] on polymethylmethacrylate indicate that a decrease in molecular weight (caused by long term annealing *before* the creep test) reduces the time-to-failure, but does not influence the failure kinetics. This is consistent with the creep rupture behaviour observed by Gotham [3] for a low and high molecular weight polymethylmethacrylate. While the high molecular weight material failed ductile, the lower molecular weight material failed brittle. The failure kinetics of both materials were, however, identical. Combined with our results this suggests that, rather than two separate mechanisms, a single mechanism is responsible for both ductile and brittle failure in long-term loading.

The existence of a ductile-to-brittle transition is often explained by means of a critical strength above which the material fractures rather than showing ductile failure. If this approach is applied to creep rupture experiments it would predict a transition with *increasing* load, i.e. as the applied stress on the material is increased. In literature such a transition at high loads is known, and reported for several

materials [1]. However, using such a critical strength criterion for *decreasing* loads will not result in a transition, since a decreasing load implies decreasing stress levels, and a polymer material that fails ductile at a given stress will therefore fail ductile at any other lower stress.

An alternative explanation is provided by the combination of time and stress applied, rather than the stress level alone. It has been shown experimentally that applying a constant load for a given amount of time accelerates the ageing process, increasing the yield stress [33, 46–51]. From the numerical results in the previous section we concluded that ageing during testing induces a change in the macroscopic behaviour leading to an endurance limit. Associated with this endurance limit is an increase in the parameter S , which is equivalent to an increase in the yield stress.

To verify whether this change in the material leads to embrittlement in the case of a low molecular weight polycarbonate, an initially ductile sample (Figure 6.10(a), left) is subjected to a constant load of 45 MPa for 2 days. After this treatment the material failed brittle under the same testing conditions (middle). Bringing a sample with an identical history above the glass transition temperature for half an hour, followed by a quench to room temperature, restored the original ductile behaviour (right), indicating that the change observed in failure mode is thermo-reversible and therefore not caused by degradation.

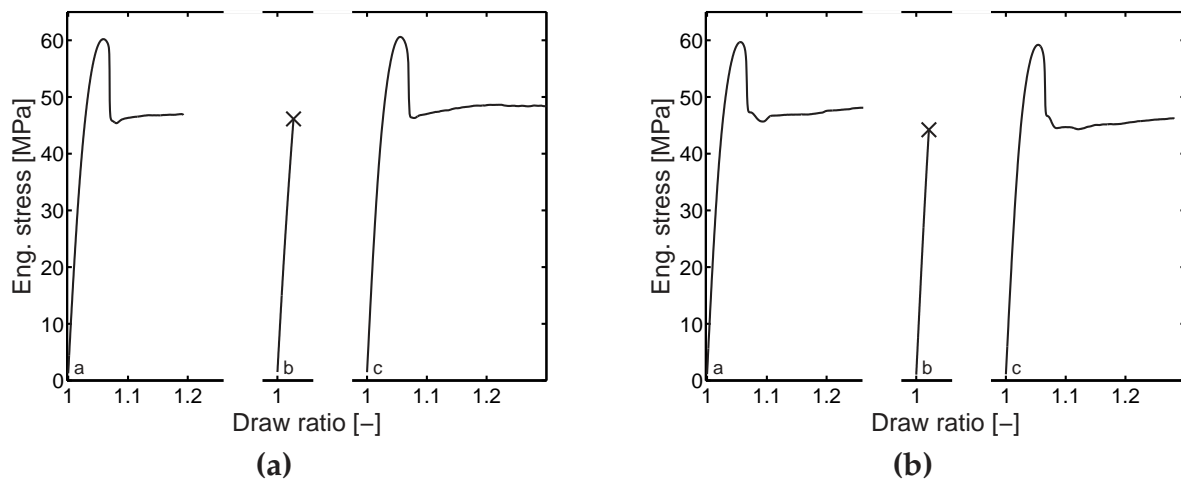


Figure 6.10: (a) Influence of mechanical history (constant load) on the macroscopic deformation behaviour of low molecular weight polycarbonate. (b) Influence of thermal history (annealing) on the macroscopic failure behaviour of low molecular weight polycarbonate [29].

A similar change in the macroscopic failure behaviour of polycarbonate was reported by van Melick *et al.* [29], who observed a ductile-brittle transition as a result of thermal history, annealing an initially ductile low molecular weight polycarbon-

ate (Figure 6.10(b), left) for 120 hours at 120 °C. After this thermal treatment the material failed brittle (middle), whereas heating an annealed sample again, now above the glass transition temperature for half an hour, and cooling rapidly to room temperature, restored the original ductile behaviour (right), indicating that the change observed in failure is again thermo-reversible and not caused by degradation due to long term annealing.

Van Melick *et al.* rationalized this change in macroscopic behaviour by comparing the intrinsic deformation behaviour of a quenched and annealed polycarbonate [29]. The thermal treatment causes an increase in yield stress and, consequently, an increase in the amount of strain softening upon mechanical rejuvenation during deformation. Strain hardening is, on the other hand, unaffected. The higher yield stress and enhanced strain softening require a higher draw ratio for the neck to stabilize, thus increasing the true stress in the necked region. When this stress exceeds the strength of the material, which is determined by the molecular weight, premature fracture rather than stable neck propagation occurs [29].

The approach by van Melick *et al.* provides a criterion which is essentially a molecular weight dependent critical strength above which a neck can not sustain the load it is subjected to. As stated previously, for creep tests such a criterion only predicts a transition for increasing stress levels. Despite the change in material properties with decreasing load and increasing time it follows from the analysis by van Melick *et al.* that still no transition will occur with decreasing load. This can be understood since for the latter the stress in the neck is dictated by the (decreasing) load applied, while for a constant rate of deformation test it is determined by the changing, state-dependent, yield stress. The prediction of a ductile-to-brittle transition with decreasing loads, therefore, requires a different approach.

The basic assumption of the analysis by van Melick *et al.* is that there already is a neck, and they only verify if this neck can exist (ductile), or not (brittle). The formation of a neck, however, involves the evolution of localized deformation zones, triggered by inhomogeneities in the local stress field, and is influenced by the amount of strain softening. The resulting concentration of deformation leads to changes in the local stress distribution enhancing any deviation from the macroscopical stress applied. If during this localization process some local failure criterion is exceeded this results in brittle failure, and no neck will be formed (and hence the analysis of van Melick *et al.* is not applicable). An example of such a local criterion is the critical hydrostatic stress which has been shown to be effective in predicting local craze initiation [52]. The fact that this failure process is preceded by local plastic deformation would also explain the observed similarity between the failure kinetics of the ductile and brittle failure mode.

The identification of the actual local failure criterion requires knowledge of the local state of the material and stress. Unfortunately, these are generally unknown. This can be solved by investigating the local stress state in well-defined stress concentrations (e.g. notches, microstructure, indentation) using numerical techniques [53, 54], but preferably in combination with an experimental verification [52, 55]. This requires further research and is outside the scope of this chapter.

6.6 Conclusions

The long-term failure behaviour of polycarbonate under constant static load was investigated. It is shown that ductile failure observed under these conditions is similar to that observed in short term tests under constant rate of deformation.

To model long-term failure, an elasto-viscoplastic model, incorporating ageing kinetics, was employed. The model was shown to accurately predict both magnitude and stress dependence of the time-to-failure of polycarbonate in three different loading geometries, using a single yield stress to determine the initial age. With similar accuracy the time-to-failure for two sets of materials with different thermal histories was predicted, again using a single yield stress to determine the initial age of each set. Furthermore, the endurance limit, observed for the quenched material, could be predicted quantitatively when the material was allowed to also numerically age during the experiment.

Reducing the molecular weight does not introduce changes in the short-term failure behaviour, neither under constant rate of deformation, nor under constant load. For reducing loads and increasing failure times, however, the structural evolution causes an increased localization due to which locally the strength of the material is exceeded. Although it is clear from the experiments that a suitable failure criterion enabling a quantitative prediction of brittle failure depends on molecular weight, the identification of an actual criterion requires further research.

References

- [1] Kausch, H.H. (1978). *Polymer Fracture*. Springer-Verlag, Berlin.
- [2] Kinloch, A.J., Young, R.J. (1985). *Fracture Behaviour of Polymers*. Elsevier Applied Science Publishers, London.
- [3] Gotham, K.V. (1972). Long-term strength of thermoplastics: the ductile-brittle transition in static fatigue, *Plast. Polym.*, **40**, 59–64.
- [4] Crissman, J.M., Zapas, L.J. (1979). Creep failure and fracture of polyethylene in uniaxial extension, *Pol. Eng. Sci.*, **19**, 99–103.

- [5] Niklas, H., Kausch von Schmeling, H.H. (1963). Molekularstruktur und mechanische Eigenschaften von Polyvinylchlorid. III. Mitteilung: Ursachen zeitabhängiger Festigkeitseigenschaften von PVC-Rohren, *Kunststoffe*, **53**, 886–891.
- [6] Teoh, S.H., Cherry, B.W. (1984). Creep rupture of a linear polyethylene: 1. Rupture and pre-rupture phenomena, *Polymer*, **25**, 727–734.
- [7] Lustiger, A. (1986). Environmental stress cracking: the phenomenon and its utility, In: W. Brostow and R.D. Corneliussen, Eds. *Failure of Plastics*, Hanser Publisher, New York, 305–329.
- [8] Cooney, J.L. (1964). Effect of morphology on biaxial stress rupture of polyethylene, *J. Appl. Pol. Sci.*, **3**, 1889–1901.
- [9] Richard, K., Gaube, E., Diedrich, G. (1959). Trinkwasserrohre aus Niederdruckpolyäthylen, *Kunststoffe*, **49**, 516–525.
- [10] Matz, D.J., Guldemon, W.G., Cooper, S.L. (1972). Delayed yielding in glassy polymers, *J. Pol. Sci.: Pol. Phys. Ed.*, **10**, 1917–1930.
- [11] Ender, D.H., Andrews, R.D. (1965). Cold drawing of glassy polystyrene under dead load, *J. Appl. Phys.*, **36**, 3057–3062.
- [12] Narisawa, I., Ishikawa, M., Ogawa, H. (1978). Delayed yielding in polycarbonate under constant load, *J. Pol. Sci.: Pol. Phys. Ed.*, **16**, 1459–1470.
- [13] Richard, K., Diedrich, G., Gaube, E. (1960). Verfestigte Rohre aus Zieglerpolyäthylen, *Kunststoffe*, **50**, 371–375.
- [14] Crissman, J.M., McKenna, G.B. (1990). Physical and chemical aging in PMMA and their effects on creep and creep rupture behavior, *J. Pol. Sci.: Part B: Pol. Phys.*, **28**, 1463–1473.
- [15] Crissman, J.M., McKenna, G.B. (1987). Relating creep and creep rupture in PMMA using a reduced variable approach, *J. Pol. Sci.: Part B: Pol. Phys.*, **25**, 1667–1677.
- [16] Crawford, R.J., Benham, P.P. (1975). A note on creep rupture of thermoplastics under triaxial stress conditions, *Plast. Pol.*, **8**, 140–142.
- [17] Gisolf, J.H., van Goudoever, H. (1959). Dauerbeständigkeitsversuche an Rohren aus Weichpolyäthylen, *Kunststoffe*, **49**, 264–268.
- [18] Ogorkiewicz, R.M., Sayigh, A.A.M. (1967). The strength of rigid PVC, *Brit. Plast.*, **7**, 126–128.
- [19] Gaube, E. (1959). Zeitstandfestigkeit und Spannungsrißbildung von Niederdruckpolyäthylen, *Kunststoffe*, **49**, 446–454.
- [20] Zhurkov, S.N. (1965). Kinetic concept of the strength of solids, *Int. J. Frac. Mech.*, **1**, 311–323.
- [21] Bueche, F. (1957). Tensile strength of plastics below the glass temperature, *J. Appl. Phys.*, **28**, 784–787.
- [22] Tobolsky, A., Eyring, H. (1943). Mechanical properties of polymeric materials, *J. Chem. Phys.*, **11**, 125–134.
- [23] Coleman, B.D. (1956). Application of the theory of absolute reaction rates to the creep failure of polymeric filaments, *J. Pol. Sci.*, **20**, 447–455.
- [24] Teoh, S.H., Cherry, B.W., Kausch, H.H. (1992). Creep rupture modelling of polymers, *Int. J. Damage Mech.*, **1**, 245–256.

- [25] Raghavan, J., Meshii, M. (1995). Prediction of creep rupture of unidirectional carbon fibre reinforced polymer composites, *Mat. Sci. Eng.*, **A197**, 237–249.
- [26] Brinson, H.F. (1999). Matrix dominated time dependent failure predictions in polymer matrix composites, *Comp. Struct.*, **47**, 445–456.
- [27] Beaumont, P.W.R., Young, R.J. (1975). Failure of brittle polymers by slow crack growth. Part 1: Crack propagation in polymethylmethacrylate and time-to-failure predictions, *J. Mat. Sci.*, **10**, 1334–1342.
- [28] Young, R.J., Beaumont, P.W.R. (1976). Time-dependent failure of poly(methyl methacrylate), *Polymer*, **17**, 717–722.
- [29] van Melick, H.G.H., Govaert, L.E., Meijer, H.E.H. (2003). Localisation phenomena in glassy polymers: influence of thermal and mechanical history. *Polymer*, **44**, 3579–3591.
- [30] Govaert, L.E., Timmermans, P.H.M., Brekelmans, W.A.M. (2000). The influence of intrinsic strain softening on strain localization in polycarbonate: modeling and experimental validation, *J. Eng. Mat. Techn.*, **122**, 177–185.
- [31] Wu, P.D. and van der Giessen, E. (1993). Analysis of shear band propagation in amorphous glassy polymers, *Int. J. Sol. Struct.*, **31**, 1493–1517.
- [32] Wu, P.D. and van der Giessen, E. (1993). On neck propagation in amorphous polymers under plane strain tension, *Int. J. Plast.*, **11**, 211–235.
- [33] Klompen, E.T.J., Engels, T.A.P., Govaert, L.E., Meijer, H.E.H. (2004). Elasto-viscoplastic modelling of large strain deformation of glassy polymers: influence of thermomechanical history, *J. Rheol.*, Submitted.
- [34] Govaert, L.E., Schellens, H.J., Thomassen, H.J.M., Smit, R.J.M., Terzoli, L., Peijs, T. (2001). A micromechanical approach to time-dependent failure in off-axis loaded polymer composites, *Composites: Part A*, **32**, 1697–1711.
- [35] Whitney, W., Andrews, R.D. (1967). Yielding of glassy polymers: volume effects, *J. Pol. Sci., Pol. Symp.*, **16**, 2981–2990.
- [36] Sherby, O.D., Dorn, J.E. (1954). Anelastic creep of polymethyl methacrylate, *J. Mech. Phys. Solids*, **6**, 145–162.
- [37] Bauwens-Crowet, C., Ots, J.-M., Bauwens, J.-C. (1974). The strain-rate and temperature dependence of yield of polycarbonate in tension, tensile creep and impact tests, *J. Mat. Sci. Lett.*, **9**, 1197–1201.
- [38] Nanzai, Y. (1994). Plastic deformation mechanism in PMMA under creep stress, *JSME Int. J. Series A*, **37**, 149–154.
- [39] Haward, R. and Thackray, G. (1968). The use of a mathematical model to describe isothermal stress-strain curves in glassy thermoplastics, *Proc. Roy. Soc. A*, **302**, 453–472.
- [40] Tervoort, T.A., Smit, R.J.M., Brekelmans, W.A.M., Govaert, L.E. (1998). A constitutive equation for the elasto-viscoplastic deformation of glassy polymers, *Mech. Time-Dep. Mat.*, **1**, 269–291.
- [41] Baaijens, F.P.T. (1991). Calculation of residual stresses in injection molded products, *Rheol. Acta*, **30**, 284–299.
- [42] Adam, G.A., Cross, A., Haward, R.N. (1975). The effect of thermal pretreatment on the mechanical properties of polycarbonate. *J. Mat. Sci.*, **10**, 1582–1590.

- [43] Hasan, O.A., Boyce, M.C., Li, X.S., Berko, S. (1993). An investigation of the yield and postyield behavior and corresponding structure of poly(methyl methacrylate). *J. Pol. Sci.: Part B: Pol. Phys.*, **31**, 185–197.
- [44] Bauwens-Crowet, C., Bauwens, J.-C. (1982). Annealing of polycarbonate below the glass transition: quantitative interpretation of the effect on yield stress and differential scanning calorimetry measurements. *Polymer*, **23**, 1599–1604.
- [45] Gedde, U.W., Viebke, J., Leijström, H., Ifwarson, M. (1994). Long-term properties of hot-water polyolefine pipes - A review. *Pol. Eng. Sci.*, **34**, 1773–1787.
- [46] Vincent, P.I. (1960). The necking and cold-drawing of rigid polymers. *Polymer*, **1**, 7–19.
- [47] Kramer, E.J. (1970). Stress aging in anhydrous Nylon 6-10. *J. Appl. Phys.*, **41**, 4327–4341.
- [48] Struik, L.C.E. (1980). The mechanical enhancement of physical aging. *Polymer*, **21**, 962–967.
- [49] Nanzai, Y., Miwa, A., Cui, S.Z. (2000). Aging in fully annealed and subsequently strained poly(methyl methacrylate). *Pol. J.*, **32**, 51–56.
- [50] Nanzai, Y., Cui, S.Z. (2001). Aging in quenched poly(methyl methacrylate) under inelastic tensile strain. *J. Pol. Sci.: Part B: Pol. Phys.*, **33**, 444–449.
- [51] Cui, S.Z., Nanzai, Y., Yoshioka, S. (2000). Aging in quenched polycarbonate under compressive strain. *Kobunshi Ronbunshu*, **57**, 37–44.
- [52] van Melick, H.G.H., Bressers, O.F.J.T., den Toonder, J.M.J., Govaert, L.E., Meijer, H.E.H. (2003). A micro-indentation method for probing the craze-initiation stress in glassy polymers. *Polymer*, **44**, 2481–2491.
- [53] Smit, R.J.M., Brekelmans, W.A.M., Meijer (2000). Predictive modelling of properties and toughness of polymeric materials. Part I *Why is polystyrene brittle and polycarbonate tough?* *Polymer*, **44**, 2481–2491.
- [54] Smit, R.J.M., Brekelmans, W.A.M., Meijer (2000). Predictive modelling of properties and toughness of polymeric materials. Part II *Effect of microstructural properties on the macroscopic response of rubber-modified polymers.* *J. Mat. Sci.*, **35**, 2869–2879.
- [55] van Melick, H.G.H., Govaert, L.E., Meijer, H.E.H. (2003). Prediction of brittle-to-ductile transitions in polystyrene. *Polymer*, **44**, 457–465.

Conclusions and recommendations

7.1 Main conclusions

The mechanical response of a polymer is determined by its intrinsic behaviour (true stress-strain), which depends on the molecular structure, and is influenced by the thermal and mechanical history. On a molecular level specific molecular motions exist, the so-called relaxation mechanisms, that determine the macroscopic deformation. In this thesis it was attempted to account for the presence of these mechanisms, as well as for the influence of processing history, in the constitutive modelling process.

In Chapter 2 it was shown that for a thermorheological simple material, i.e. a material with only a single molecular relaxation mechanism, time-stress superposition is applicable, analogous to time-temperature superposition. The shift function is of the Eyring-type, and also applies to the yield stress. Consequently, the deformation up to and including the yield point is described by a single stress-activated spectrum of relaxation times.

When there are multiple relaxation mechanisms, a polymer material behaves thermorheological complex. For two relaxation mechanisms, it is shown in Chapter 3 that a straightforward extension of the model from Chapter 2 based on stress additivity is possible. This approach leads to a parallel arrangement of two stress-activated spectra of relaxation times, each with a different stress-dependence, that is no longer related to the total stress, but only to a part of the total stress. Results from numerical creep predictions at different loads show a good qualitative agreement with experimental data reported in literature. Furthermore, the calculations show that the observed increase in the so-called relaxed β -compliance with temperature should be attributed to the primary α -process instead.

The approach used in Chapters 2 and 3 is restricted to the yield and the pre-yield range. Therefore, Chapter 4 addressed the deformation in the post-yield range, and investigates how this might be affected by the presence of multiple relaxation mechanisms. For a thermorheological simple material, like polycarbonate, the post-yield deformation is proportionally influenced by strain rate, i.e. the yield drop is constant. This can be described using a parallel arrangement of a single nonlinear Maxwell element, and a rubber elastic modulus. A thermorheological complex material, like polymethylmethacrylate, on the other hand shows a pronounced influence of strain rate, leading to an increasing yield drop. Using a model extended in analogy to Chapter 3, two mechanisms are identified leading to the observed strain rate dependence. Introduction of a secondary process leads to an enhanced thermal softening, and this contribution leads to an intrinsic strain-rate dependent softening.

So far only the relationship between deformation and the underlying relaxation mechanisms was considered, which leaves one important aspect uncovered: the influence of changes in the structural state. A polymer glass is generally in a non-equilibrium state and, as a consequence strives to establish equilibrium. As a result the thermal history of the material will have an influence on the molecular mobility and hence on the intrinsic properties. To account for this structural evolution, an elasto-viscoplastic model was proposed where the momentary structural state, as well as its further evolution with time (physical ageing), is characterized by a single parameter S_a . The evolution of S_a is fully decoupled from the mechanical rejuvenation (strain softening), the erasure of prior thermal history with plastic deformation. For polycarbonate both the softening and ageing kinetics were determined and shown to be independent of the molecular weight.

In Chapter 6, the model proposed in Chapter 5 was used to predict ductile failure under long-term static loading. The applicability of the model follows from a comparison of both the intrinsic and macroscopic response of polycarbonate at a constant rate of deformation and for a constant stress. Under both conditions a plastic strain instability is initiated by softening due to the accumulation of plastic strain. From this it can be concluded that, for failure, this mechanism is more important than the actual viscoelastic response. The failure kinetics depend on the loading geometry, but are independent of thermal history and molecular weight. For a quenched material an endurance limit is observed that originates from stress-induced ageing, reducing the plastic strain rate. A change in failure mode from ductile to brittle for a low molecular weight material is also associated with this ageing process, but a quantitative prediction thereof requires an additional failure criterion.

7.2 Recommendations

In Chapters 4 to 6, a single mode approximation was used, which led to an underestimate of the pre-yield response. It was, however, also indicated that this could be improved by using a representation with multiple relaxation times, analogous to that presented in Chapters 2 and 3. Although a 3D version of such an approach is available [1], this currently lacks several relevant features such as pressure dependence, strain softening and strain hardening. Under the assumption that all relaxation times are equally affected by the hydrostatic stress, the pressure dependence can easily be included as a pressure-dependent shift. A similar approach would allow for a simple incorporation of strain softening as well, using a single evolution equation for all relaxation times, which is driven by an equivalent global plastic strain. Finally, it was already shown in Chapters 4–6 that strain hardening is regarded as a separate contribution, and can, therefore, easily be included.

The use of a spectrum of relaxation times also requires the experimental determination of additional material parameters representing the linear relaxation time spectrum. In Chapter 2, these parameters were obtained from time-stress superposition of a set of creep curves at different loads. Since a different thermal history leads to a change in the mechanical response, these experiments would have to be repeated for each thermal history. Therefore, it would be beneficial to have a procedure that requires less experiments (preferably even a single). A potential candidate for this would be the tensile test, as it was shown in Chapter 2 that this covers the entire spectrum of relaxation times. Another alternative would be the use of time-temperature superposition in the linear viscoelastic range as was done by e.g. Wu and Buckley [2].

In Chapter 4 it was shown that the post-yield deformation is influenced by the presence of a secondary relaxation mechanism. Although a model was proposed that captured the observed strain-rate dependence of the yield drop, this model was not validated in other loading geometries. Performing this validation in tensile at different strain-rates, it immediately can be investigated to what extent the observed change in post-yield deformation leads to changes in the macroscopic failure behaviour.

The kinetics proposed in Chapter 5 to describe the structural evolution due to physical ageing and mechanical rejuvenation, assume that these processes are decoupled. As a result of this, one of these processes eventually becomes dominant, and the material either ages or rejuvenates. In reality both processes depend on the momentary state of the material, i.e. they are coupled. Implementation of this coupling ensures that a material, which has been mechanically rejuvenated, will show the proper ageing behaviour. Since the material will eventually attain equilibrium at long times, or high temperatures, the expression for the ageing

kinetics should also include a temperature dependent equilibrium state.

In both Chapters 5 and 6 a single tensile test was used to establish the initial state of the material. Although this is a fairly simple test, the samples require a certain amount of material, which might not always be available, and have to behave ductile in tension. The latter does not apply for a compression test, but compression samples still require a discrete amount of material. An interesting alternative might, therefore, be (micro)indentation. This technique requires much less material, and was shown to be capable of detecting differences in thermal history [3]. It should be investigated if this technique is also capable of monitoring the evolution of the structural state under load. While all these techniques are used for materials with an *unknown* history, for a *known* history the material state could be predicted, provided information regarding the evolution of the state parameter through the glass transition range is available.

In Chapter 6 it was argued that the ductile-to-brittle transition observed at decreasing loads for a low molecular weight polycarbonate is governed by a local failure criterion. To identify this failure criterion, the local stress state has to be investigated for well-defined stress concentrations using either numerical techniques, or a combination of numerical and experimental techniques. This investigation could also include the role of temperature, since this influences both the failure and ageing kinetics.

In both stress- and strain-controlled fatigue experiments on polymer materials, ductile failure phenomena are reported, similar to those observed under a constant load, or strain rate [4]. In comparison to static loads, failure in a stress-controlled dynamic experiment appears to be accelerated, while in strain-controlled tension-compression tests with fixed strain limits cyclic softening is observed, reducing the initial stress amplitude. When such a softened sample is subsequently tested in tensile, it deforms homogeneously, very similar to a sample that is rejuvenated in torsion. This suggests that for dynamic loading softening related mechanisms are active as well, and that, therefore, the approach used for long-term static loading in Chapter 6 is also applicable. Preliminary calculations in both stress and strain-controlled fatigue, already showed promising results.

References

- [1] Tervoort, T.A., Klompen, E.T.J., Govaert, L.E. (1996). A multi-mode approach to finite, three-dimensional, nonlinear viscoelastic behavior of polymer glasses. *J. Rheol.*, **40**, 779–797.
- [2] Wu, J.J., Buckley, C.P. (2004). Plastic deformation of glassy polystyrene: a unified model of yield and the role of chain length. *J. Pol. Sci.: Part B: Pol. Phys.*, **42**,

- 2027–2040.
- [3] van Melick, H.G.H., Bressers, O.F.J.T., den Toonder, J.M.J., Govaert, L.E., Meijer, H.E.H. (2003). A micro-indentation method for probing the craze-initiation stress in glassy polymers. *Polymer*, **44**, 2481–2491.
- [4] Hertzberg, R.W., Manson, J.A. (1980). *Fatigue of Engineering Plastics*. Academic Press Inc., New York.

Samenvatting

Het gebruik van numerieke technieken voor het analyseren en optimaliseren van het mechanisch gedrag van polymere materialen en producten kan een efficiënt en goedkoop alternatief zijn voor een vaak tijdrovende en dus dure experimentele procedure. Eén van de voorwaarden voor een betrouwbare numerieke analyse is een goede constitutieve relatie, die het ware spanning-rek verloop van het materiaal correct beschrijft. Dit intrinsieke deformatiegedrag is echter afhankelijk van de moleculaire structuur van het polymeer, alsmede van de verwerkingsgeschiedenis (thermisch en mechanisch). Dit betekent dat een constitutieve relatie die wordt gebruikt voor een polymeer met een bepaalde geschiedenis, niet bruikbaar hoeft te zijn voor een ander polymer met dezelfde of een andere geschiedenis. In dit proefschrift is een poging gedaan om hierin verandering te brengen door relaties te leggen tussen de intrinsieke deformatie aan de ene kant, en de moleculaire structuur en de verwerkingsgeschiedenis aan de andere.

Het vermogen van een polymeer om te vervormen wordt bepaald door de mobiliteit van diens moleculen. Dit leidt tot specifieke moleculaire bewegingen, die worden versneld door temperatuur en spanning. Deze zogeheten moleculaire overgangen zullen hier worden gebruikt om een verband te leggen tussen de mechanische respons en de moleculaire structuur. Doorgaans bezit een polymeer meerdere van dergelijke overgangen, waarbij de experimentele omstandigheden bepalend zijn of deze al dan niet een bijdrage leveren aan de respons van het materiaal. Het veranderen van de moleculaire structuur, of het beïnvloeden van de mobiliteit van een transitie leidt tot veranderingen in de intrinsieke en macroscopische deformatie.

In hoofdstuk 2 wordt als modelmateriaal polycarbonaat onderzocht waarin bij kamertemperatuur slechts één relaxatiemechanisme een actieve rol speelt. Voor dit zogenaamde thermoreologisch eenvoudige materiaal wordt een constitutieve relatie afgeleid op basis van tijd-spanning-superpositie. Dit principe veronderstelt dat alle relaxatietijden in gelijke mate worden beïnvloed door de opgelegde spanning. Deze situatie is vergelijkbaar met tijd-temperatuur-superpositie, waar alle relaxatietijden een zelfde functie zijn van de temperatuur. De invloed van

spanning wordt beschreven door een niet-lineaire Eyring relatie. Door middel van experimenten wordt aangetoond dat de voorgestelde tijd-spanning-superpositie geldig is voor het gebruikte modelmateriaal. De hierbij verkregen waarde voor de karakteristieke spanning blijkt goed overeen te komen met de waarde die is bepaald aan de hand van vloeispanningen gemeten bij verschillende reksnelheden. Verder wordt aangetoond dat het hele deformatiegedrag tot en met vloeit wordt bepaald door het lineaire spectrum van relaxatietijden in combinatie met de karakteristieke spanning die afhangt van het activeringsvolume.

Aangezien in vrijwel alle polymeren minstens twee van dergelijke moleculaire processen actief zijn, wordt de voorgaande aanpak uitgebreid met een extra bijdrage in hoofdstuk 3. Op basis van de lineair viscoelastische theorie kan deze extra bijdrage zowel parallel als in serie worden gezet met de reeds bestaande. Resultaten van vloeispanningsmetingen wijzen echter in de richting van het optellen van spanningen, dus het parallel schakelen van twee processen. Voor het niet-lineair viscoelastische gebied resulteert dit in een constitutief model bestaande uit twee parallele spectra van relaxatietijden met ieder een eigen spannings- en temperatuurafhankelijkheid. Terwijl de invloeden van temperatuur en spanning voor een thermoreologisch eenvoudig materiaal vergelijkbaar waren, geldt dit niet meer voor een thermoreologisch complex materiaal. In plaats van de totale spanning hangen de spectra af van dat deel van spanning dat wordt gedragen door het betreffende spectrum. Gebruikmakend van het uitgebreide model laten numerieke voorspellingen zien dat experimenteel gemeten vloeipunten goed worden beschreven. Verder komen voorspellingen van kruipexperimenten bij verschillende spanningen en temperaturen goed overeen met in de literatuur gerapporteerde experimentele resultaten.

De voorgaande beschrijvingen beperkten zich uitsluitend tot het gebied tot en met het vloeipunt. Voor het gebied na het vloeipunt voorspellen ze een constante vloeispanning, terwijl in realiteit de spanning in eerste instantie afneemt als gevolg van "softening" en bij verdere deformatie weer toeneemt als gevolg van moleculaire oriëntatie ("hardening"). Aangezien van deze twee fenomenen bekend is dat ze een cruciale rol spelen bij de vorming en de ontwikkeling van rek-lokalisatie, en het macroscopisch faalgedrag, wordt het "post-yield"-gedrag nader beschouwd in hoofdstuk 4. Voor een thermoreologisch eenvoudig materiaal, polycarbonaat, wordt het gedrag na het vloeipunt niet beïnvloed door reksnelheid hetgeen tot uitdrukking komt in een constante waarde van de daling van de spanning na het vloeipunt ("yield drop"). Voor een thermoreologisch complex materiaal zoals polymethylmethacrylaat blijkt daarentegen dat er een sterke invloed van de reksnelheid op het "post-yield" gedrag bestaat. Het vóórkomen van deze reksnelheidsafhankelijkheid valt samen met het optreden van de secundaire transitie, en leidt tevens tot een brosser macroscopisch gedrag. Ofschoon er een duidelijk waarneembare relatie bestaat tussen deze secundaire transitie en de reksnelheidsafhankelijkheid in de "yield-drop", kon niet eenduidig worden vastgesteld of dit effect wordt veroorzaakt

door thermische effecten, of dat dit een intrinsieke eigenschap van het materiaal betreft.

Tot zover werd alleen aandacht besteed aan de relatie met de moleculaire structuur middels de moleculaire overgangen. Hierbij werd steeds aangenomen dat de verkregen materiaalparameters constant zijn. Doorgaans bevinden polymeren zich op moleculaire schaal niet in evenwicht, maar proberen dit in de loop van de tijd te herstellen. Deze zogenaamde fysische veroudering hangt sterk samen met de thermische geschiedenis van het materiaal, en kan ongedaan worden gemaakt door het aanbrengen van een grote (plastische) deformatie, of het verhogen van de temperatuur tot boven de glasovergangstemperatuur. In hoofdstuk 5 zijn deze invloeden experimenteel onderzocht en geïmplementeerd in een bestaande constitutieve relatie. Deze is vervolgens gevalideerd voor een reeks van polycarbonaten met verschillende molecuulgewichten. De deformatie van al deze verschillende grades kan worden beschreven met één enkele parameterset, waarbij de thermische geschiedenis is samengevat in één parameter, S_a , die uit een eenvoudige trekproef kan worden bepaald.

Een toepassingsgebied waar kan worden verwacht dat fysische veroudering een rol speelt is dat van kruip onder statische of dynamische belasting. Voor statische belastingen wordt de tijd tot falen en het faalgedrag beïnvloed door de aangelegde spanning, de temperatuur, de thermische geschiedenis en het molecuulgewicht. In hoofdstuk 6 wordt aannemelijk gemaakt dat hetzelfde proces verantwoordelijk is voor zowel ductiel falen onder een constante belasting, als ook onder een constante reksnelheid, en dat dit zijn oorsprong vindt in het intrinsieke gedrag van het materiaal met name in de "strain softening". Dit geeft indirect aan dat het in hoofdstuk 5 gepresenteerde constitutieve model, ook toepasbaar is voor het voorspellen van plastische instabiliteiten onder constante belastingen. Met dit model wordt de tijd tot falen voorspeld als functie van de aangelegde spanning voor achtereenvolgens, verschillende belastingstoestanden, verschillende thermische geschiedenissen en molecuulgewichten. Voor alle gevallen wordt de faalkinetiek goed beschreven, alsmede de grootte van de tijd tot falen. Ook wordt er een "endurance limit", zoals geobserveerd voor snelafgekoeld materiaal onderworpen aan relatief lage spanningen, correct voorspeld. Het optreden van deze "endurance limit" kan worden verklaard met het optreden van fysische veroudering tijdens de (langdurige) belasting. Alleen de taai-bros overgang in het laag moleculaire polycarbonaat kan niet worden voorspeld door het ontbreken van een geschikt faalcriterium.

Tot slot worden in hoofdstuk 7 de belangrijkste conclusies en aanbevelingen voor verder onderzoek gepresenteerd.

Dankwoord

Graag wil ik hier iedereen bedanken die een bijdrage heeft geleverd aan het tot stand komen van dit proefschrift. Een speciaal woord van dank gaat uit naar Leon Govaert voor de begeleiding tijdens de voorbije periode. Zijn aanstekelijk enthousiasme en geduld zijn van onschatbare waarde geweest. Ook Han Meijer wil ik bedanken voor het vertrouwen en voor de mogelijkheid die hij geboden heeft om dit onderzoek te verrichten.

Theo Tervoort en Piet Schreurs dank ik voor de vele discussies in de loop der jaren, en voor het uiteindelijk nauwgezet doorlezen van het manuscript.

Een groot deel van de beschreven experimentele resultaten is te danken aan de inzet van de volgende stagiaires en afstudeerders: Peter Toonsen, Marcel van Mensvoort, François Bardinnet, Rene Leenaars, Martijn Wubbolts, Paul Goessens, Roel Janssen, Chris van Haag, Helle Baselmans, Bas Raas, Tom Engels en Lambert van Breemen, waarbij Tom en Lambert tevens een deel van de numerieke simulaties voor hun rekening hebben genomen.

Voor de GPC-metingen ben ik Ilse van Casteren en Jules Kierkels van de groep SKT de nodige dank verschuldigd.

Warner Nauta van TNO-Industrie ben ik erkentelijk voor het beschikbaar stellen van de lange duur meetfaciliteiten.

Voor goed numeriek en experimenteel werk is een vakkundige technische ondersteuning onontbeerlijk. Voor alle ondersteuning gedurende de voorbije jaren ben ik veel dank verschuldigd aan Leo Wouters, Patrick van Brakel, Johan Boekholt, Ab Kneppers, Rob van de Berg, Toon van Gils en Sjef Garenfeld.

Verder wil ik alle (ex-)collega's van de Materials Technology groep, en met name mijn (ex-)kamergenoten Harold, Varja, Jesus, Katja, Ceren, Müge en Linda, bedanken voor de prettige samenwerking en de gezellige sfeer.

Tot slot, wil ik vrienden en familie bedanken voor hun steun en belangstelling gedurende de afgelopen jaren. De meeste dank gaat echter uit naar mijn ouders, die me altijd onvoorwaardelijk hun steun en vertrouwen hebben gegeven.

Curriculum Vitae

Edwin Klompen (Roggel, July 3rd 1969) graduated from secondary school in 1987 at Sg. St. Ursula, Horn. Upon finishing secondary school, he enrolled at Eindhoven University of Technology, Eindhoven, where he received his Master degree in Mechanical Engineering in 1993. Subsequently, he entered the designer's course on Computational Mechanics at the Stan Ackermans Institute, Eindhoven, from which he graduated in 1996. He went on to work for the TNO Road-Vehicles Research Institute as a research assistant developing tests for, and testing, crash-test-dummy materials and components under crash conditions. In the fall of 1998 he returned to Eindhoven University of Technology to work with Ton Peijs on the development of a new single-polymer composite (PURE), as well as the development of natural fibre reinforced thermoplastics (FlaxCraft). In 2001 he was offered the opportunity to pursue a PhD-degree within the Materials Technology group. The results of this work are presented in this thesis.